

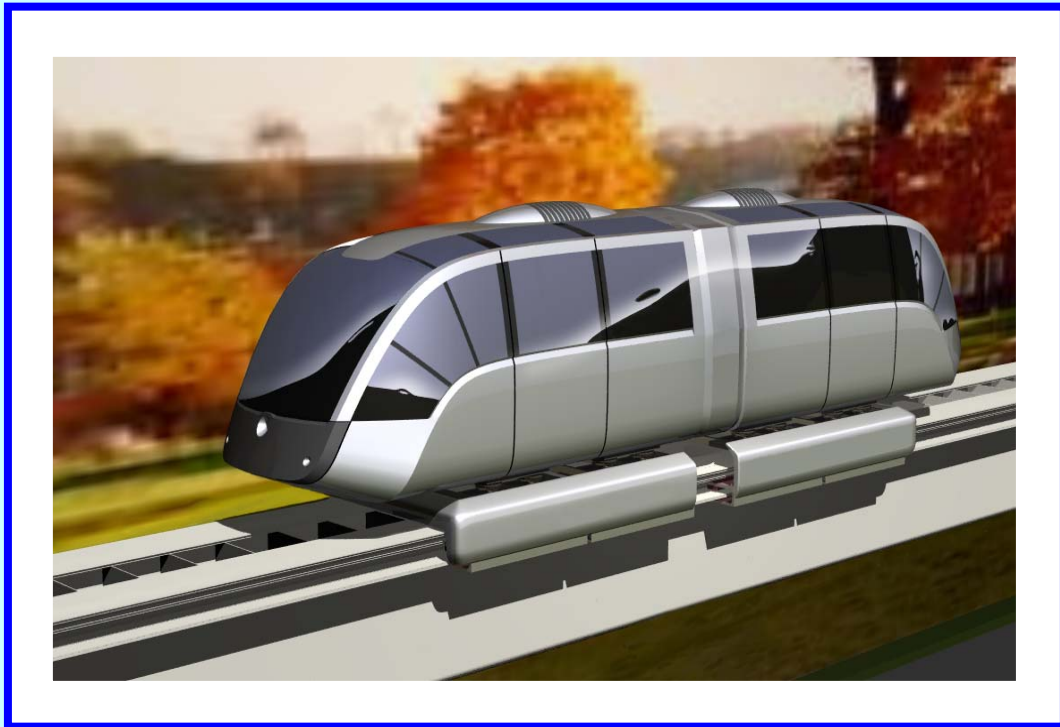


General Atomics Low Speed Maglev Technology Development Program (Supplemental #3)

U.S. Department
of Transportation

**Federal Transit
Administration**

**May 2005
Final Report**



**Federal Transit
Administration**

OFFICE OF RESEARCH, DEMONSTRATION, AND INNOVATION

NOTICE

This document is disseminated under the sponsorship of the U.S. Department of Transportation in the interest of information exchange. The United States Government assumes no liability for its contents or use thereof.

The United States Government does not endorse products of manufacturers. Trade or manufacturers' names appear herein solely because they are considered essential to the objective of this report.

Low Speed Maglev Technology Development Program

Final Report

May 2005

Prepared by:

**General Atomics
3550 General Atomics Court
San Diego, CA 92121**

Prepared for:

**Federal Transit Administration
400 7th Street, SW
Washington, DC 20590**

Report Number:

**FTA-CA-26-7025.2005
GA-A24920**

This page intentionally left blank

REPORT DOCUMENTATION PAGEForm Approved
OMB No. 0704-0188

Public reporting burden for this collection of information is estimated to average 1 hour per response, including the time for reviewing instructions, searching existing data sources, gathering and maintaining the data needed, and completing and reviewing the collection of information. Send comments regarding this burden estimate or any other aspect of this collection of information, including suggestions for reducing this burden, to Washington Headquarters Services, Directorate for Information Operations and Reports, 1215 Jefferson Davis Highway, Suite 1204, Arlington, VA 22202-4302, and to the Office of Management and Budget, Paperwork Reduction Project (0704-0188), Washington, DC 20503.

1. AGENCY USE ONLY (Leave blank)		2. REPORT DATE Mat 2005	3. REPORT TYPE AND DATES COVERED Final Report Sept 2003 – Dec 2004	
4. TITLE AND SUBTITLE General Atomics Low Speed Maglev Technology Development Program (Supplemental #3)			5. FUNDING NUMBERS	
6. AUTHOR(S) Husam Gurol, Robert Baldi, Phillip Jeter, In-Kun Kim, Daryl Bever				
7. PERFORMING ORGANIZATION NAME(S) AND ADDRESS(ES) General Atomics 3550 General Atomics Court San Diego, CA 92121-1122			8. PERFORMING ORGANIZATION REPORT NUMBER GA-A24920	
9. SPONSORING/MONITORING AGENCY NAME(S) AND ADDRESS(ES) U.S. Department of Transportation, Federal Transit Administration, Office of Technology, 400 Seventh Street, SW, Washington, DC 20590			10. SPONSORING/MONITORING AGENCY REPORT NUMBER FTA-CA-26-7025.2005	
11. SUPPLEMENTARY NOTES This is a Web Document, available on FTA website (http://www.fta.dot.gov)				
12a. DISTRIBUTION/AVAILABILITY STATEMENT Available From: National Technical Information Service/NTIS, Springfield, Virginia, 22161. Phone 703.605.6000, Fax 703.605.6900, Email [orders@ntis.fedworld.gov]			12b. DISTRIBUTION CODE	
13. ABSTRACT (Maximum 200 words) This report addresses the accomplishments of Supplemental #3. The four major tasks included: guideway foundation construction, fabrication and installation of seven guideway modules, system integration and testing, and laminated track development. The test track construction was completed in September 2004, and testing commenced to validate the vehicle dynamics and ride quality. Testing included evaluation of the propulsion and control systems, and initial levitation. Additional future testing will validate the ride dynamics involving the levitation, propulsion, and guidance systems.				
14. SUBJECT TERMS Maglev, Magnetic Levitation, Low-Speed, Urban			15. NUMBER OF PAGES	
			16. PRICE CODE	
17. SECURITY CLASSIFICATION OF REPORT Unclassified	18. SECURITY CLASSIFICATION OF THIS PAGE Unclassified	19. SECURITY CLASSIFICATION OF ABSTRACT Unclassified	20. LIMITATION OF ABSTRACT	

This page intentionally left blank

Acknowledgment

This report presents the results of a research effort undertaken by General Atomics under Cooperative Agreement No CA-26-7025 to the Office of Research, Demonstration, and Innovation, Federal Transit Administration (FTA). This work was funded by the U. S. Department of Transportation, Federal Transit Administration's Office of Technology. The interest, insight, and advice of Ms. Mary Anderson and Mr. Walt Kulyk of the Federal Transit Administration are gratefully acknowledged.

The valuable comments provided by the representatives of transit agencies, research institutes, and other independent organizations are gratefully acknowledged. Special thanks are due to Mr. Roger Hoopengardner of SAIC and Dr. Gopal Samavedam of Foster-Miller for their valuable comments during the period of this effort.

General Atomics also acknowledges the support of a number of subcontractor corporations and other entities, who are team members in this activity. They include Booz-Allen Hamilton, Carnegie Mellon University, Hall Industries, Lawrence Livermore National Laboratory, Mackin Engineering, P.J. Dick, Union Switch and Signal, U.S. Maglev Development Corporation, and the Pennsylvania Department of Transportation.

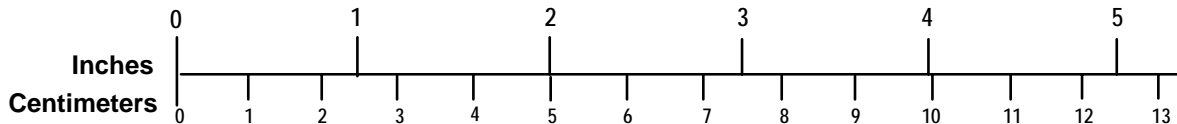
Metric/English Conversion Factors

English To Metric

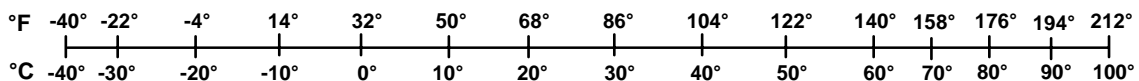
Metric To English

<p>LENGTH (APPROXIMATE)</p> <p>1 inch (in) = 2.5 centimeters (cm) 1 foot (ft) = 30 centimeters (cm) 1 yard (yd) = 0.9 meter (m) 1 mile (mi) = 1.6 kilometers (km)</p>	<p>LENGTH (APPROXIMATE)</p> <p>1 millimeter (mm) = 0.04 inch (in) 1 centimeter (cm) = 0.4 inch (in) 1 meter (m) = 3.3 feet (ft) 1 meter (m) = 1.1 yards (yd) 1 kilometer (km) = 0.6 mile (mi)</p>
<p>AREA (APPROXIMATE)</p> <p>1 square inch (sq in, in²) = 6.5 square centimeters (cm²) 1 square foot (sq ft, ft²) = 0.09 square meter (m²) 1 square yard (sq yd, yd²) = 0.8 square meter (m²) 1 square mile (sq mi, mi²) = 2.6 square kilometers (km²) 1 acre = 0.4 hectare (he) = 4,000 square meters (m²)</p>	<p>AREA (APPROXIMATE)</p> <p>1 square centimeter (cm²) = 0.16 square inch (sq in, in²) 1 square meter (m²) = 1.2 square yards (sq yd, yd²) 1 square kilometer (km²) = 0.4 square mile (sq mi, mi²) 10,000 square meters (m²) = 1 hectare (ha) = 2.5 acres</p>
<p>MASS - WEIGHT (APPROXIMATE)</p> <p>1 ounce (oz) = 28 grams (gm) 1 pound (lb) = 0.45 kilogram (kg) 1 short ton = 2,000 pounds (lb) = 0.9 tonne (t)</p>	<p>MASS - WEIGHT (APPROXIMATE)</p> <p>1 gram (gm) = 0.036 ounce (oz) 1 kilogram (kg) = 2.2 pounds (lb) 1 tonne (t) = 1,000 kilograms (kg) = 1.1 short tons</p>
<p>VOLUME (APPROXIMATE)</p> <p>1 teaspoon (tsp) = 5 milliliters (ml) 1 tablespoon (tbsp) = 15 milliliters (ml) 1 fluid ounce (fl oz) = 30 milliliters (ml) 1 cup (c) = 0.24 liter (l) 1 pint (pt) = 0.47 liter (l) 1 quart (qt) = 0.96 liter (l) 1 gallon (gal) = 3.8 liters (l) 1 cubic foot (cu ft, ft³) = 0.03 cubic meter (m³) 1 cubic yard (cu yd, yd³) = 0.76 cubic meter (m³)</p>	<p>VOLUME (APPROXIMATE)</p> <p>1 milliliter (ml) = 0.03 fluid ounce (fl oz) 1 liter (l) = 2.1 pints (pt) 1 liter (l) = 1.06 quarts (qt) 1 liter (l) = 0.26 gallon (gal) 1 cubic meter (m³) = 36 cubic feet (cu ft, ft³) 1 cubic meter (m³) = 1.3 cubic yards (cu yd, yd³)</p>
<p>TEMPERATURE (EXACT)</p> <p>$[(x-32)(5/9)] \text{ } ^\circ\text{F} = y \text{ } ^\circ\text{C}$</p>	<p>TEMPERATURE (EXACT)</p> <p>$[(9/5)y + 32] \text{ } ^\circ\text{C} = x \text{ } ^\circ\text{F}$</p>

QUICK INCH - CENTIMETER LENGTH CONVERSION



QUICK FAHRENHEIT - CELSIUS TEMPERATURE CONVERSION



For more exact and or other conversion factors, see NIST Miscellaneous Publication 286, Units of Weights and Measures. Price \$2.50 SD Catalog No. C13 10286

Updated 6/17/98

Table of Contents

	Page
1. EXECUTIVE SUMMARY AND PROGRAM OVERVIEW	1-1
2. INTRODUCTION.....	2-1
2.1 Tasks Status	2-1
2.2 Lessons Learned	2-2
3. SYSTEM DESIGN.....	3-1
3.1 Guideway Foundation.....	3-1
3.1.1 Design.....	3-1
3.1.2 Design Basis	3-3
3.1.3 Test Track Foundation Construction	3-5
3.2 Guideway Module Manufacturing.....	3-10
3.2.1 Engineering.....	3-10
3.2.2 Manufacturing.....	3-11
3.3 System Integration and Testing	3-17
3.3.1 Control System Description.....	3-17
3.3.2 Test Results.....	3-22
3.4 Laminated Track Development.....	3-39
3.4.1 Laminated Track Test Rig.	3-40
3.4.2 Test Results.....	3-42
4. CONCLUSIONS	4-1
5. REFERENCES.....	5-1
APPENDIX A – FINAL TEST PLAN.....	A-1
APPENDIX B – LINEAR SYNCHRONOUS MOTOR CONTROL FOR AN URBAN MAGLEV	B-1
APPENDIX C – A LAMINATED TRACK FOR THE INDUCTRACK SYSTEM: THEORY AND EXPERIMENT	C-1
APPENDIX D – ATP AND SPEED/POSITION SENSING SYSTEM.....	D-1

List of Tables

Page

Table 2-1 Measures of Sufficient Confidence..... 2-3

List of Figures

		Page
Figure 1-1	General Atomics Urban Maglev vehicle uses permanent magnets arranged in a Halbach array configuration for levitation and propulsion	1-2
Figure 1-2	Double Halbach Array Levitation Magnets result in improved lift-to-drag ratio, and a stiffer primary suspension system.....	1-2
Figure 1-3	Aerial view of Test Track Site	1-3
Figure 1-4	Completed 120-m test track foundation, and first 15-m guideway weldment (left). Right picture shows completed guideway module ready for turning over.....	1-4
Figure 1-5	Completed test chassis on first section of track	1-4
Figure 1-6	Vehicle levitation, propulsion, and guidance systems	1-5
Figure 1-7	Semi-automated soldering process for the litz track enables consistent joint resistance	1-5
Figure 1-8	View of electrical room, which houses the rectifiers, variable frequency inverter, and train protection equipment	1-6
Figure 1-9	Typical gap and speed profiles during testing will allow vehicle dynamics evaluation	1-6
Figure 3.1-1	Foundation excavation and compaction in progress	3-5
Figure 3.1-2	Set-up patio (F-9) and segment F-1 formwork and rebar installed.....	3-6
Figure 3.1-3	South spiral (F-4) foundation slab and pedestal rebar installed.....	3-6
Figure 3.1-4	Typical slab segment separation expansion joint.....	3-7
Figure 3.1-5	Cut-out in segment F-8 for vehicle service access.....	3-7
Figure 3.1-6	All segments F-1 thru F-8 and F-9 south set-up patio completed.....	3-8
Figure 3.1-7	Design modification to segment F-8	3-9
Figure 3.2-1	The new guideway module design weighs 8,850 kg versus 9,213 kg for the old design used for the first guideway module.....	3-10
Figure 3.2-2	Guideway module weldment being delivered to General Atomics.....	3-11
Figure 3.2-3	Completed LSM laminations prior to being installed on the guideway weldment.....	3-12
Figure 3.2-4	LSM propulsion coils are assembled onto the weldment while it is upside down.....	3-13
Figure 3.2-5	Litz track sections positioned for soldering and final inspection.....	3-13
Figure 3.2-6	The guideway module is rolled over using the specially design rigging	3-14
Figure 3.2-7	Straight guideway module being positioned on the foundation.....	3-14
Figure 3.2-8	View from North end of track, showing “maintenance pit” and in the distance the straight guideway modules 1, 2, and 3	3-15

Figure 3.2-9	Curved guideway module being installed on the foundation	3-15
Figure 3.2-10	Completed test track	3-16
Figure 3.2-11	Control and electrical rooms provide excellent views and access during test track operations.....	3-16
Figure 3.2-12	Electrical equipment room, showing the AC-DC rectifier, which converts incoming AC to DC, and the inverter which converts the DC power to a variable frequency voltage applied to the LSM propulsion coils.....	3-17
Figure 3.3-1	Magnet polarity and LSM winding relationship	3-19
Figure 3.3-2	Thrust command block diagram.....	3-21
Figure 3.3-3	Vertical force balance block diagram.....	3-22
Figure 3.3-4	Urban maglev control panel	3-23
Figure 3.3-5	Control computer.....	3-23
Figure 3.3-6	DC rectifier (left) and inverter (right)	3-24
Figure 3.3-7	PWM waveform	3-24
Figure 3.3-8	Actual PWM waveform.....	3-25
Figure 3.3-9	Optical position sensor	3-26
Figure 3.3-10	Predicted position sensor data	3-27
Figure 3.3-11	Actual position sensor data	3-27
Figure 3.3-12	Data acquisition system architecture.....	3-28
Figure 3.3-13	PXI data acquisition system	3-28
Figure 3.3-14	Monitoring inverter temperatures.....	3-30
Figure 3.3-15	Monitoring LSM cable temperatures	3-30
Figure 3.3-16	Data acquisition computer station	3-31
Figure 3.3-17	Actual vehicle velocity vs. “Iq” current command	3-32
Figure 3.3-18	Actual vehicle “Id” current value.....	3-33
Figure 3.3-19	“Id” and “Iq” current value comparisons with velocity	3-33
Figure 3.3-20	“Id” and “Iq” current value comparisons with velocity	3-34
Figure 3.3-21	Gap sensor data for NW corner of vehicle	3-35
Figure 3.3-22	Gap sensor data for NE corner of vehicle	3-35
Figure 3.3-23	Gap sensor data for SE corner of vehicle	3-36
Figure 3.3-24	Gap sensor data for SW corner of vehicle.....	3-36
Figure 3.3-25	“Id” current command set to zero.....	3-37
Figure 3.3-26	“Id” current command set to +500 A	3-38
Figure 3.3-27	Actual vehicle velocity vs. “Iq” current command	3-39
Figure 3.4-1	Schematic drawing of laminated track configuration.....	3-40

Figure 3.4-2	Photograph of test rig, showing assembly within which Halbach arrays are mounted, vertical force sensor, and movable carrier for the laminated track	3-41
Figure 3.4-3	Lift force versus speed for the “5x4” magnet array, compared with theoretical predictions	3-43
Figure 3.4-4	Magnetic drag force versus speed for the “5x4” magnet array, compared with theoretical predictions	3-43

This page intentionally left blank

1. Executive Summary and Program Overview

This report covers the activities administered by the Federal Transit Administration under the Transportation Equity Act for the 21st Century (TEA-21) to complete the construction of a 120-meter long test track at General Atomics in San Diego, California. The General Atomics Urban Maglev team was funded in four increments since program inception in March 2000: base program - concept development, Supplemental #1 - testing of full-scale prototype components, Supplemental #2: construction of a full-scale vehicle chassis, control/electrical rooms, electrical power systems, and the first 15 m of track, which constitutes the 1st of 8 guideway modules and foundation, and Supplemental #3: fabrication of the remaining 7 guideway modules and foundation to complete the 120-meter test track. This report addresses the accomplishments of Supplemental #3. The test track construction was completed in September 2004, and testing commenced to validate the vehicle dynamics and ride quality. Only very limited testing was performed, and additional future testing will validate the ride dynamics involving the levitation, propulsion, and guidance systems. A general project overview is discussed in the following paragraphs of this section.

The Urban Maglev team led by General Atomics has developed an innovative approach using a passive, permanent magnet levitation system with a linear synchronous motor powering the guideway to provide propulsion and guidance. Among the advantages are simplicity, safe and quiet operation, ability to climb steep grades (up to 10%), negotiate tight turns, large operating air gap (25mm), and all-weather operation. The system is designed to be driverless, with a throughput capacity of 12,000 passengers per hour per direction, based on two-minute headway between vehicles. It is envisioned to be elevated, which when combined with the enabling features of maglev technology results in a system which can serve many established urban centers. One of maglev's most significant attributes is its quiet operation, which eliminates the need to tunnel underground for noise abatement as required for conventional wheeled transportation systems. This provides urban planners great flexibility, with potentially large savings in capital and maintenance costs.

The overall vehicle design, seen conceptually in Figure 1-1, consists of two chassis units connected with an articulation unit. Nominal vehicle length is 12 m, although the basic chassis units can be connected to produce a train of longer length. Levitation and propulsion magnets are in the vehicle "wrap-around" structure, resulting in a safe vehicle, which cannot derail under operational conditions. The vehicles have no active control systems; all the control and train protection systems are in the wayside control room.



Figure 1-1
General Atomics Urban Maglev vehicle uses permanent magnets arranged in a Halbach array configuration for levitation and propulsion

The levitation technology referred to as “Inductrack”, was developed by Dr. Richard Post of Lawrence Livermore National Laboratory (LLNL), and uses high field (1.4 Tesla) NdFeB permanent magnet cubes ($\sim 5 \times 5 \times 5 \text{ cm}^3$) arranged in a double “Halbach” array configuration, as seen in Figure 1-2. One of the notable characteristics of the Inductrack maglev system is that levitation and drag parameters can be analyzed theoretically and evaluated with high confidence through computer codes. Such levitation codes have been developed at General Atomics, at Carnegie-Mellon University, and at Lawrence Livermore National Laboratory, using both analytical and finite-element computational approaches. Cross-checked against each other, and bench-marked against the results of measurements made with the General Atomics test wheel and the Livermore Laminated Track Test Rig, these tools have proved to be of high value in designing the test track at General Atomics and in optimizing the design of future systems.

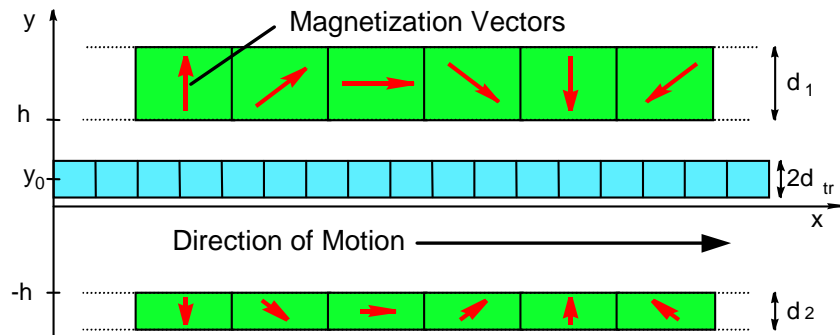


Figure 1-2
Double Halbach Array Levitation Magnets result in improved lift-to-drag ratio, and a stiffer primary suspension system

One of the advantages of this configuration is that the field is “focused” on the track, and tends to cancel on the passenger side. In fact, the magnetic field strengths in the passenger compartment are well within recommended allowable values for public safety and below those in existing rail systems without the need for shielding. In addition, because of the nature of the linear synchronous motor operation, all the fields on the vehicle are static. The array has been configured to provide a nominal air gap of 25 mm, providing the potential for less stringent guideway tolerance requirements. Since this is an Electrodynamics levitation system, the vehicles initially ride on wheels and start levitating at a speed of 3–4 m/s, depending on the weight. With a peak acceleration of 1.6 m/s^2 the vehicles are levitated by the time they exit a station.

In November 2002, construction of a 120-m long test track at the General Atomics Electromagnetics Systems facility in San Diego, California was initiated. The test track consists of eight guideway modules, each 15-m in length. It has a 50-m radius curve to demonstrate vehicle guidance. To save cost for testing, the track is built at grade, and consists of a loading ramp for the vehicle, a small test chassis access pit, electrical room, and control room. Figure 1-3 shows an aerial view of the laboratory, and indicates (in red) the test track site.



Figure 1-3
Aerial view of Test Track Site

Groundbreaking for the guideway foundation occurred in March 2003, followed by trenching, grading, installation of electrical conduits, and pouring the concrete foundation. The completed 120-m foundation, with the first guideway weldment (prior to turning over) is seen in Figure 1-4.

The completed chassis unit on the first guideway module is seen in Figure 1-5. The test chassis has many unique features, specifically focused at being able to vary magnet configurations and gaps, and making changes in the secondary suspension spring constant and damping rates. Variable level water tanks can be mounted on the chassis to simulate the correct center of gravity corresponding to a passenger-carrying vehicle, and the associated shifts in passenger loading.



Figure 1-4
Completed 120-m test track foundation, and first 15-m guideway weldment (left). Right picture shows completed guideway module ready for turning over



Figure 1-5
Completed test chassis on first section of track

The levitation, propulsion, and guidance systems are seen in the end-view of the vehicle and guideway module in Figure 1-6. The linear synchronous motor (LSM) windings are three-phase and interact with the field generated by the permanent magnet propulsion magnets on the vehicle, with a peak force capability of ~ 50 kN for a complete vehicle system (~ 25 kN for the test chassis, which represents half the length of a full vehicle). The propulsion magnets also provide guidance by interacting with the LSM iron lamination rails.

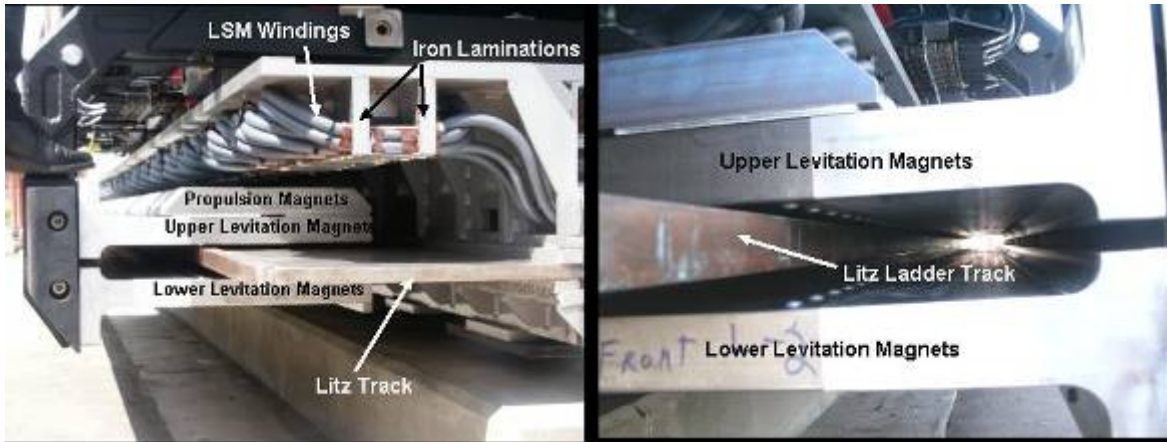


Figure 1-6
Vehicle levitation, propulsion, and guidance systems

The right side of Figure 1-6 shows the 3.6-m long levitation magnets and their relation to the cantilevered track, which is a ladder track design consisting of litz cable shorted on the ends with copper. This double-Halbach array combined with the use of litz cable results in significantly reduced magnetic drag forces, for a given lift force. The assembly used for the semi-automated soldering of the litz cable to copper shorting bars is shown in Figure 1-7.



Figure 1-7
Semi-automated soldering process for the litz track enables consistent joint resistance

Power to the test track is based on advanced power electronics designated as Insulated Gated Bipolar Transistor (IGBT). The three-phase inverter shown in a view of the electrical room in Figure 1-8 underwent significant reliability testing during the Spring of 2004. It is sized to be capable of full-scale system operation beyond the test track phase.



Figure 1-8
View of electrical room, which houses the rectifiers, variable frequency inverter, and train protection equipment

During a normal testing sequence, the vehicle starts at one end of the test track, accelerates to a maximum speed up to 10 m/s, and decelerates back to zero speed at the other end of the track. The vehicle levitates at 3-4 m/s. The testing verifies the dynamic performance of the system including levitation, propulsion and guidance. The vehicle motion along the curve and transition section allows assessment of the curve negotiation and guidance characteristics of the vehicle. Test chassis weights between 6,000 kg and 10,500 kg will be tested. Typical gap, speed and force profiles are shown in the simulations in Figure 1-9.

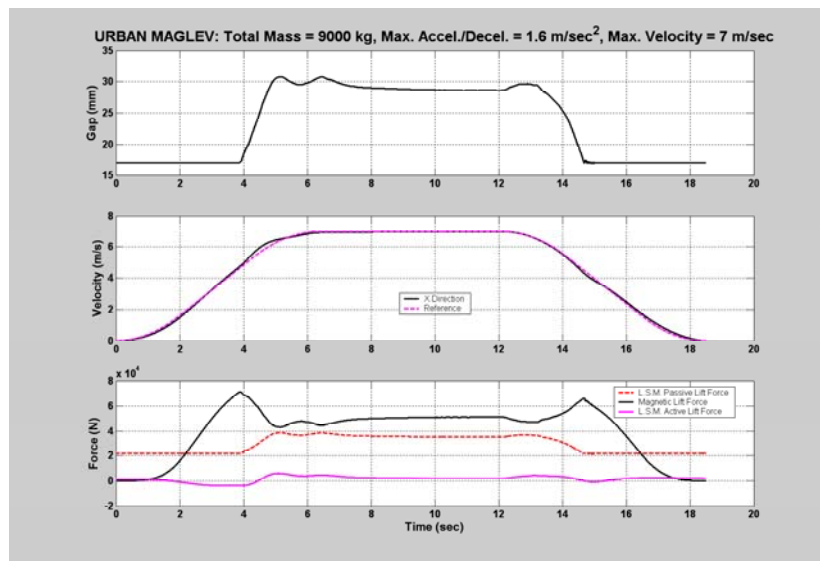


Figure 1-9
Typical gap and speed profiles during testing will allow vehicle dynamics evaluation

We expect the test track to be extremely valuable in detailed evaluations of ride dynamics, refining the key technology components, testing components required for the demonstration system planned for California University of Pennsylvania, and in verifying the reliability of

power and control system components. The following introduction will summarize the work performed under Supplemental #3 funding, including lessons learned during the construction of the test track, as well as during the limited testing performed to date.

This page intentionally left blank

2. Introduction

This report addresses the work performed on Supplemental #3 funding as part of the General Atomics Urban Maglev Technology Development program. There are four main tasks in this activity. These are:

- **Task 1. Guideway Foundation Construction.** The goal of this task was to construct all additional sections of the concrete slab foundation, in addition to the existing 15-m slab constructed under Supplemental #2 funding.
- **Task 2. Guideway Module Manufacturing.** The goal of this task was to fabricate seven additional guideway modules, and add them to the initial 15-m segment manufactured under Supplemental #2 funding. The resulting test track consists of three additional “straight”, two additional “transition”, and one 50-meter radius “curved” guideway module.
- **Task 3. System Integration and Testing.** This task is associated with (a) the final integration of all the test track hardware, including the attachment of guideway modules to the test track, the electrical connections, the data acquisition systems, and speed and location detection equipment, (b) development of a test and safety plan, and (c) testing and evaluation of the maglev test chassis on the guideway at varying speeds to demonstrate levitation, propulsion, and guidance.
- **Task 4. Laminated Track Development.** This goals of this task were: (a) to complete the development of an electromagnetics computational tool to calculate the effects of induced currents on lift and drag of a laminated track and (b) to test a 5x4 Halbach magnet array using the test set-up constructed under Supplemental #2 funding at Lawrence Livermore National Laboratory to validate the model.

2.1 Tasks Status

The specific status of each of these tasks is described below.

Task 1. Guideway Foundation Construction. The construction of 105 m of the concrete guideway foundation, and all associated underground electrical cabling was completed. This task was performed using at-risk GA funding during the performance of Supplemental #2 tasks (later reimbursed during Supplemental #3), to facilitate construction efficiency, and reduce overall costs.

Task 2. Guideway Module Manufacturing. This task was initiated by hosting a “bidder’s” conference at General Atomics. Prospective manufacturers of the large guideway module weldments were invited to participate to ensure the lowest cost/highest quality product. We selected two manufacturers: one in California, the other in Pennsylvania, and split the order by

awarding all curved sections to the California company and all straight sections to the Pennsylvania company. We have completed the construction of all seven guideway modules, and fitted them with the levitation litz track, and the linear synchronous motor (LSM) windings.

Task 3. System Integration and Testing. (a) The GA Team completed the attachment of the of the guideway modules to the concrete guideway foundation, all the electrical connections between the guideway modules and the power inverter, and the integration of the data acquisition, speed and location detection, and automatic train protection (ATP) equipment; (b) a test plan and a safety plan were completed and reviewed to ensure that all testing would be accomplished in a safe and orderly manner; (c) under Supplemental #3 funding, we completed all static testing of the vehicle propulsion and levitation systems. While construction estimates proved to be quite accurate, we did experience some cost growth in two main areas, namely the guideway weldment engineering, and the control system. As such, less funding was available for testing than originally planned. Because of this funding limitation, all dynamic testing was performed under reprogrammed “Port Authority” funding (Agreement No. 62T122). The testing which was completed is preliminary, and requires more testing to fully validate the levitation, propulsion, and guidance systems. To quantify the testing achievements, listed in the Table 2-1 are the measures of “sufficient confidence” in the technology from the Supplemental #3 proposal (page 1-1). Also listed is the associated achievement.

Task 4. Laminated Track Development. (a) The GA Team completed the development of an electromagnetics computational tool to calculate the effects of induced currents on the lift and drag forces of a laminated track. The tool is very unique in its ability to accurately predict these forces for a variety of track and magnet geometries. The code was benchmarked against other tools used by the team. The results predicted theoretically were compared with laminated track experiments performed during previous Supplemental #2 work, as well as Supplemental #3 work on a 5x4 magnet array. (b) Testing was performed on a 5x4 Halbach magnet array using the test set-up constructed under Supplemental #2 funding at Lawrence Livermore National Laboratory. The data was compared with the theoretical predictions made in (a), and were found to be in good agreement.

2.2 Lessons Learned

In the performance of these tasks, a number of lessons were learned, which will be used to guide future work on the project. Below, the major lessons are summarized, organized by the 4 major tasks.

- **Task 1. Guideway Foundation Construction Lessons Learned.** The entire guideway foundation was built at one time, instead of building the first 15 m under Supplemental #2, and the remaining 105 m at a later time under Supplemental #3. This was accomplished using about \$100K of GA at-risk funding, saving the program about \$25K.

**Table 2-1
Measures of Sufficient Confidence**

Desired Result – Measures of “Sufficient Confidence”	Performance Achieved
<i>Demonstrate a nominal operating gap of 20-25mm.</i>	Between the lift generated by the litz track and the LSM, we in fact generate more lift than desired. We have achieved greater than 30 mm. While this is better than not achieving sufficient lift, this results in the chassis in-board wheels hitting the steel top plate, and inducing dynamic oscillations. Our plan for the future is to remove/replace the in-board wheels to provide greater physical clearances, increase the space between the upper and lower magnets again for increased clearances, use the LSM control system to damp out oscillations, and test heavier chassis weights (more in line with actual vehicle weights).
<i>Demonstrate lift-off speed below 5m/s.</i>	Our lift-off is better than predicted with measured lift-off speeds below 5 m/s for chassis weights up to 8,500 kg.
<i>Demonstrate the propulsion and control system by accelerating the chassis at a rate of up to 1.6 m/s².</i>	During preliminary testing, we have accelerated significantly above 1.6 m/s ² (~2.5 m/s ²).
<i>Demonstrate the braking and control system by decelerating the chassis at a rate up to 1.6 m/s².</i>	We have tested decelerations of about 1 m/s ² . All indications are that more rapid decelerations are easily achievable, since we have significantly exceeded goal of acceleration up to above 1.6 m/s ² . We have demonstrated accelerations of 2.5 m/s ² .
<i>Demonstrate stable guidance of chassis going through a 50-meter radius curve and transition section. Stable guidance means that lateral motions do not grow in time.</i>	During preliminary testing, the guidance appears to be stable and not subject to growing oscillations. However, currently some of the guidance may be aided by the lateral wheels. These wheels will be withdrawn, and the guidance system more fully investigated in future testing.
<i>Assess ride quality by measuring vertical and lateral accelerations and jerk. Success will be to demonstrate that the chassis will exhibit stable dynamic behavior, and will be capable of being fine-tuned for a future operating demonstration system.</i>	We have diagnostics in place to measure the ride quality. Since the in-board wheels contact the guideway module top plate, as noted in point 1 above, the vehicle dynamics is affected significantly. Hence, there is insufficient data to draw conclusions regarding ride quality. During future testing, detailed accelerometer data will be collected to evaluate and fine-tune the ride quality.

- ***Task 2. Guideway Module Manufacturing Lessons Learned.*** The guideway modules, as they are currently designed, consist of large steel structures. During the fabrication process

both vendors used had some problems with weld distortions, making it difficult to maintain the required tolerances. This led to significantly more labor, resulting in higher costs. In the future, the GA Team plans to use a “hybrid” girder design, which consists of advanced high strength concrete, with built-in attachment points for the track and the LSM windings. Based on initial investigations, it is believed that this approach can reduce costs significantly, and also result in a slimmer structure

- **Task 3. System Integration and Testing Lessons Learned.** Since the system integration and testing occurred as part of this task, there are a significant number of lessons learned, listed below.
 - a. Test track clearances with the current chassis configuration are not sufficient, resulting in the chassis interfering with the underside of the top plate during trial runs. Mechanical adjustments on the chassis and the magnets will be made to correct this. In addition, we plan to change the position of the propulsion magnets relative to the iron laminations of the LSM. This will result in significantly reducing the passive lift force of the LSM, while affecting the peak propulsion force capability by a much smaller amount (~10-20%). This change will significantly increase the effective stiffness of the levitation system to ~4kN/mm, resulting in smaller amplitude oscillations.
 - b. The speed and location detection equipment requires an on-board instrument to read the position of the vehicle on the track and relay that information to the inverter control module. The original design used a “wiggly wire” on the track, which was hard-wired to the inverter. This design has interference from the high currents in the LSM windings, resulting in poor signal quality. The GA Team adopted instead an optical laser sensor, which relays the information remotely to the wayside. This system appears to work reasonably well, except that rain drops can potentially disperse the laser beam, resulting in loss of signal. To ensure all-weather system operation, the GA Team will install and test a non-optical “eddy-current” sensor on the test track in the future.
 - c. The control system used to provide propulsion power to the LSM windings, works reasonably well, except for two items. First, it does not track the programmed speed profile as closely as desired, which results in velocity overshooting as steady-state speed is approached. Second, the way the control software is currently written, there is no control of the component of current, which produces LSM lift forces (so-called “ I_d ”). This results in poor control of vertical and longitudinal oscillations. During the next phase of testing, we will improve the software to implement I_d control, and also adjust the control system gains to avoid overshooting the steady-state speed profile. Most of these are expected to require software changes. If testing indicates that the “Gold Box” controller is not fast enough, we may need to consider a faster processor. The optical encoder will be replaced with a non-optical system, which should improve reliability. More data is required to fully assess required modifications to the control system.

- ***Task 4. Laminated Track Development Lessons Learned.*** The litz track currently being used on the test track is very labor intensive to fabricate, resulting in higher costs than desired for future deployment. The laminated track testing performed both during Supplemental #2 and Supplemental #3, indicate that the laminated track design works very well magnetically, and because of the simplicity of the design, is potentially much cheaper to manufacture. Hence, we plan to investigate the manufacturability of the laminated track, and test the structural integrity of the structure in the future. We will also re-visit analyses which were performed during 2001 on a solid ladder track with transverse slots, and compare its losses and cost relative to the laminated track (sub-scale tests were performed at that time on a solid copper track without slots; no testing was performed on a solid track with slots).

The following sections discuss in greater detail the work performed under tasks 1 through 4. Appendix A contains the test plan, Appendix B contains a paper on motor control published at the Maglev 2004 conference, Appendix C discusses the theoretical underpinnings developed for analyzing the laminated track system (also presented at the Maglev 2004 conference), and Appendix D summarizes the automatic train protection and speed positioning system. Appendix A contains the test plan, Appendix B contains a paper on motor control published at the Maglev 2004 Conference, Appendix C discusses the theoretical underpinnings developed for analyzing the laminated track system (also presented at the Maglev 2004 Conference), and Appendix D summarizes the automatic train protection and speed/positioning system.

This page intentionally left blank

3. SYSTEM DESIGN

3.1 Guideway Foundation

3.1.1 Design

The design of the foundations for the maglev test track at General Atomics' Building 37 occurred during Supplemental Funding #1. The design complies with the Uniform Building Code 1997 requirements and local San Diego City codes and regulations. Initially, fourteen drawings were issued for construction on March 3, 2003. The design was modified during Supplemental Funding #2 and #3. Subsequently, all of the original drawings were revised and then re-released and four new drawings were issued for construction on April 14, 2003. Since the guideway foundation for the sections of track corresponding to the locations of guideway modules 2-7 are a Supplemental #3 task, the discussion regarding that task is reproduced here for completeness from the Supplemental #2 completion report.

The overall length of the test track is 120.96 m (see drawing A1^{*}). The track consists of eight 15.10 m long foundations separated by 20 mm expansion joints. The first three foundation segments are straight, the next three are curved, and the last two are straight totaling to eight segments (F-1 to F-8). The curved foundations consist of south and north spirals that transition into and out of a circular arc that has a 50 m radius (see drawing S1.) To simplify the installation (by reducing the geometric complexity of the formwork and the reinforcement schedule) and thereby decrease the cost, the spirals and the arc were approximately formed by eight chords each rather than exactly formed by continuous smooth curves (see drawings S5, S6, S7, and S8).

All of the foundations consist of two composite sections, a base slab and a pedestal. The base slabs and their pedestals were poured separately but were tied and bonded together with steel reinforcement and an epoxy bonding agent. Because of short height of the pedestal, the base slab and pedestal of segment F-1 were poured monolithic.

The foundations are tied together at each expansion joint using steel dowel bars and plastic speed dowels. The joints are protected by polyethylene Backer Rods and an elastomeric sealant. The dowel bars transfer shear across the joint, but not moment, and force the foundations to deflect and/or settle together instead separately. The speed dowels allow the foundations to thermally expand and contract (see drawings S5, S6, S7, S8).

The top of the base slab roughly follows the slope of the existing terrain along the southern half of the test track; the top of the base slab is level over the northern half. The top of the pedestal is

* All drawings located at the end of the section.

level for the entire length of the test track. The pedestals of the curved foundations are not superelevated because that was designed into the curved guideway modules (see drawing S2).

Every foundation has a 2000 mm wide by 350 mm thick base slab and a 1220-mm wide pedestal. However, no two foundations have a pedestal with the same depth. The depth of the first three straight foundations linearly varies from a minimum of 250 mm to a maximum of 940 mm. The depth of the three curved foundations and the last two straight foundations is a constant 940 mm. The minimum depth equals the standard thickness of the decks that will compositely attached to the prestressed box beams of an elevated maglev guideway. The maximum depth established an economic balance between the construction costs of the two design alternatives by roughly equalizing the cost of installing the additional formwork, reinforcement and concrete required by the deeper pedestals and the cost of compacting the additional backfill required by the shallower (constant depth) pedestals (see drawing S2).

The northern most foundation was originally designed for a 2000 mm wide by 350 mm thick base slab a 1220 mm wide by 940 mm deep solid pedestal over the entire length. The foundation was modified in April 2003 to provide a passageway sufficient in size to permit access to the underside of the maglev vehicle (see drawing S13).

The design of the south setup slab and the disconnect switch pad occurred during Supplemental Funding #2. Its drawing was issued for construction on April 14, 2003. The north setup slab was eliminated before the design was completed and the drawing was released. The north slab was designated "Optional"; as such it can be designed and constructed at a later date if required (see drawing S1).

The south setup slab is located immediately south of the first guideway foundation. It is 7300 mm long by 3600 mm wide by 150 mm thick (actually constructed to 7320 mm long by 3660 mm wide by 150). The south slab supports the weldment that is used to allow the maglev vehicle to be rolled on the guideway module (see drawing S15).

The disconnect switch pad is located roughly 10,000 mm north of Hub 'C' on the test track alignment and approximately 2850 mm west of the third guideway foundation. It is an 1100 mm square that is 150 mm thick. The pad supports the disconnect switch, a component of the power distribution system (see drawing S15).

The guideway foundations, the setup slab and the disconnect switch pad were constructed using concrete with a 28-day minimum compressive strength of 4,000 psi (27.6 MPa) and a unit weight of 150 pcf (2400 kg/m³). The steel reinforcement conformed to ASTM A615, Grade 60 (A615M, Grade 420).

3.1.2 Design Basis

The design of the test track foundations was based on ASD (allowable stress design) in lieu of LRFD (load and resistance factor design) using the following loading criteria, geotechnical investigations, chassis interface control drawings, guideway weldment layout and guideway module drawings as well as the guideway alignment and foundation drawings. The design complies with the Uniform Building Code 1997 and San Diego City local code and regulations. The design of the test track foundation also complies with California Coastal Commission height limitations.

Loading Criteria

- Dead Loads:
 - The mass of the concrete foundation
 - The 15,100 kg mass of the guideway module
- Live Loads:
 - The 20,000 kg mass of a full commercial maglev vehicle
 - The 12,500 kg mass of an empty commercial maglev vehicle
 - The 7,500 kg mass of a full passenger load in a commercial maglev vehicle
 - Based on the “ASCE 21-98, Automated People Mover Standards, Part 2”
 - The 50% impact factor
- Centrifugal Forces:
 - The 9.55 m/s allowable velocity of the test track maglev vehicle
- Lateral Acceleration Forces:
 - The 0.16 g allowable acceleration of a commercial maglev vehicle
 - Based on the “ASCE 21-98, Automated People Mover Standards, Part 2”
- Wind Loads:
 - The 70 mph (113 km/h) minimum basic wind speed
 - The 12.6 psf (603 Pa) wind stagnation pressure
 - Based on the “1997 Uniform Building Code, Volume 2, Structural Engineering Design Provisions, Chapter 16, Division III, Section 1615”
- Seismic Loads:
 - The seismic zone factor of 4
 - The stiff Soil profile type of S_D

- Based on the “1997 Uniform Building Code, Volume 2, Structural Engineering Design Provisions, Chapter 16, Division IV, Section 1626”
- The distance to the closest seismic source, Rose Canyon Fault of ± 4 km
- Defined by the “1998 Maps of Known Active Fault Near-Source Zones in California and Adjacent Portions of Nevada”
- Load Combinations:
 - Basic load combinations for allowable stress design
 - Alternate basic load combination for allowable stress design
 - Defined by the “1997 Uniform Building Code, Volume 2, Structural Design Provisions, Chapter 16, Division I, Section 1612”

Geotechnical Investigations

- “Final Report of Testing and Observation During Site Improvements, Building 39 Demolition,” General Atomics, San Diego, CA, dated December 7, 1999, prepared by GEOCON, Inc., San Diego, CA.
- “Geotechnical Investigation, Building 37 Addition, Newport Project,” General Atomics, San Diego, CA, dated April 27, 2000, prepared by GEOCON, Inc., San Diego, CA.
- “Limited Geotechnical Investigation, Building 37, Newport Project,” General Atomics, San Diego, CA, dated June 29, 2001, prepared by GEOCON, Inc., San Diego, CA.
- “Updated Geotechnical Investigation, Buildings 37 and 38, Urban Maglev Test Track Project,” General Atomics, San Diego, CA, dated November 1, 2002, prepared by GEOCON, Inc., San Diego, CA.
- “General Atomics MAGLEV Design Recommendations,” dated November 13, 2002, prepared by GEOCON, Inc., San Diego, CA.
- “Updated Geotechnical Investigation, Building 37, Magnetic Track Project,” General Atomics, San Diego, CA, dated July 23, 2002, prepared by GEOCON, Inc., San Diego, CA.

Chassis Interface Control Drawings

- Drawings 21-211 100-A through 100-D, prepared by Hall Industries, Elwood City, PA.

Guideway Weldment Layout Drawings

- Drawings 390430-FT-310, Sheets 1 through 8, prepared by General Atomics, San Diego, CA.

MAGLEV Guideway Module Drawings

- Drawings 4150-002-1-01 through –14, prepared by Mackin Engineering, Pittsburgh, PA.

MAGLEV Test Track Alignment Drawing

- Drawing 4150-002-0-03, prepared by Mackin Engineering, Pittsburgh, PA.

MAGLEV Guideway Foundation Drawings:

- Drawings 4150-002-02-00 through –13, prepared by Mackin Engineering, Pittsburgh, PA.

South Setup Slab and Disconnect Switch Pad Drawing

- Drawing 4150-002-02-14, prepared by Mackin Engineering, Pittsburgh, PA.

3.1.3 Test Track Foundation Construction

The test track foundation was laid out, surveyed and constructed as per above described Mackin Engineering drawings except for some minor modifications.

The foundation construction was started in mid March 2003 and all the eight segments F-1 through F-8 and the south set-up patio F-9 (12 ft wide x 24 ft long x 6 in. thick slab) were formed, rebar installed and concrete cast and completed in mid June 2003. Figures 3.1-1 through 3.1-6 show various stages of construction.



Figure 3.1-1
Foundation excavation and compaction in progress



Figure 3.1-2
Set-up patio (F-9) and segment F-1 formwork and rebar installed



Figure 3.1-3
South spiral (F-4) foundation slab and pedestal rebar installed



Figure 3.1-4
Typical slab segment separation
expansion joint

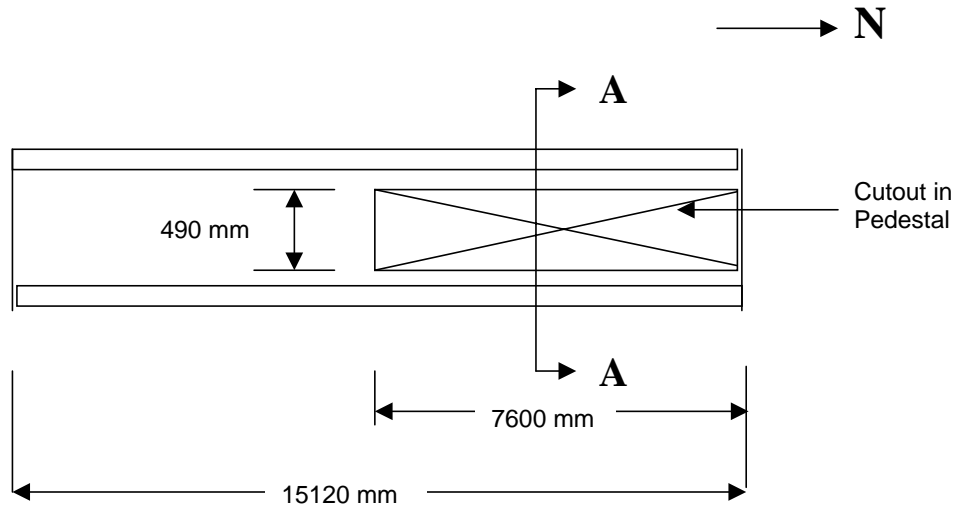


Figure 3.1-5
Cut-out in segment F-8 for vehicle
service access

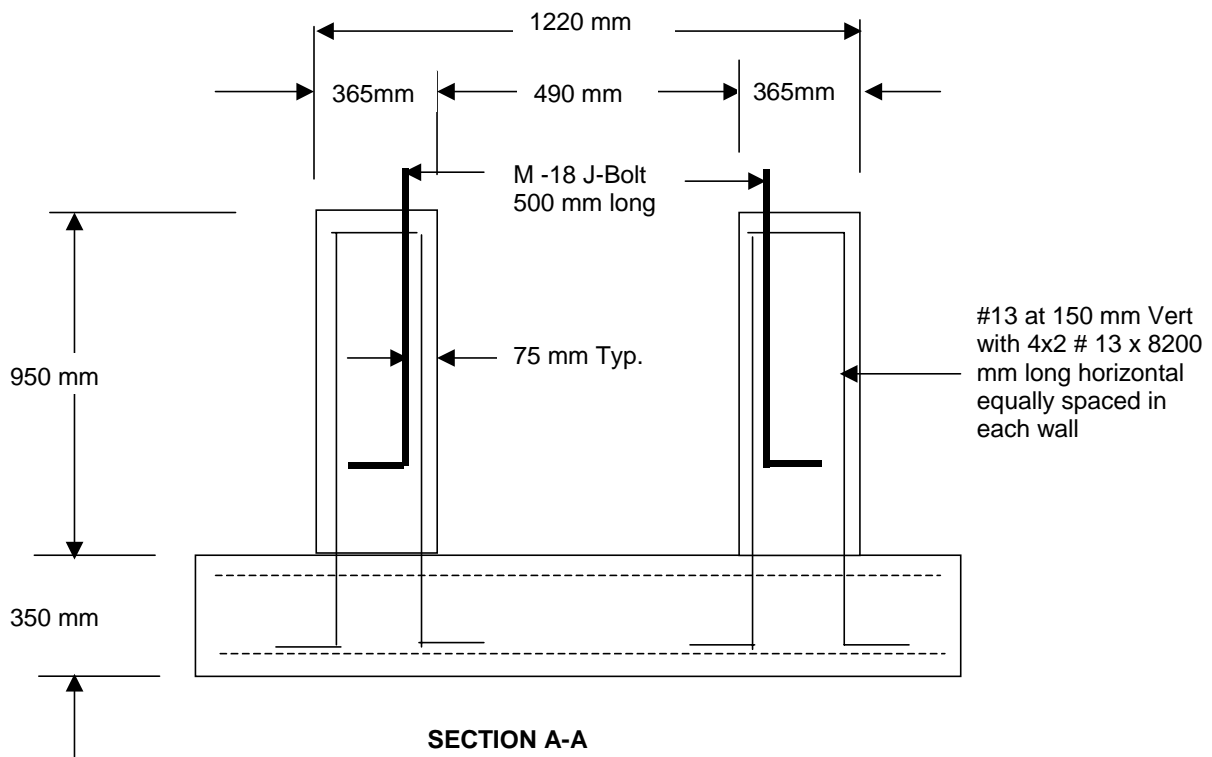


Figure 3.1-6
All segments F-1 thru F-8 and F-9 south set-up patio completed

In order to make efficient use of the forms, the pedestals of varying heights of every other segment were poured first and the rest completed later. Anchor bolts were provided as shown in the Mackin Engineering drawing (S-10). The Mackin Engineering drawing S-13 shows the segment F-8 splayed and foundation slab deepened and stepped. GA made a design modification (see Figure 3.1-7) to maintain the same anchor bolt configuration and the segment F-8 was constructed similar to other segments except that a cutout for the vehicle service access was provided (see Figure 3.1-5 photo). Also, Mackin Engineering drawing S-1 shows a optional north patio slab F-10. This is not necessary at this time and was not included in the construction.



PLAN OF SEGMENT F-8



SECTION A-A

**Figure 3.1-7
Design modification to segment F-8**

3.2 Guideway Module Manufacturing

3.2.1 Engineering

The guideway module designs for the 120-m test track include five straight 15-m segments, two spiral segments and one curved (50-m radius) guideway segment. The guideway modules consist of: the guideway module weldment, Litz track assembly, and LSM motor windings. The engineering tasks associated with Supplemental #3 included using lessons learned from manufacturing of the first guideway module to perform detail engineering design of these components. A very key element of this activity was to think about producibility improvements of the seven guideway modules to be built. Producibility considerations led to certain design improvements in each of the guideway module design areas. These included iron laminations, LSM coils, Litz track modules and guideway weldment modules. After a number of producibility meetings were held, decisions were made regarding which improvements to incorporate. The changes were reflected in the revised detail design drawings. The largest single improvement was a significant reduction in the number of weldment parts used in the first guideway module, and subsequent modules, due to improved manufacturing approaches and more refined analyses. Figure 3.2-1 shows the significant reduction in parts in the new design, when compared with the first guideway module built under Supplemental #2.

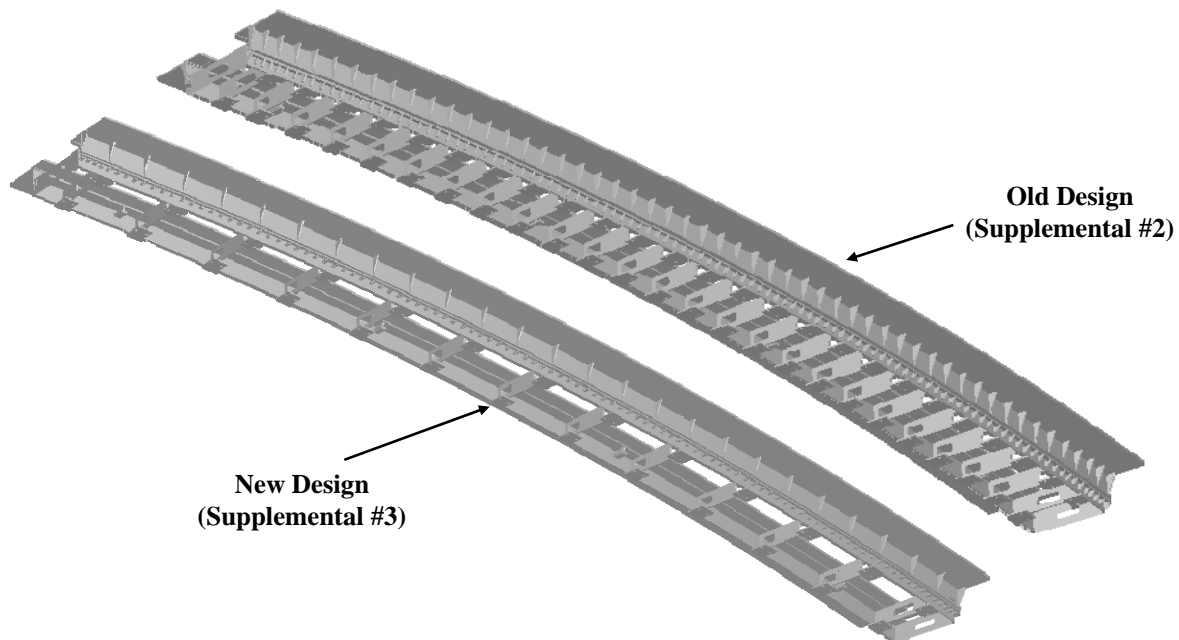


Figure 3.2-1
The new guideway module design weighs 8,850 kg versus 9,213 kg for the old design used for the first guideway module

Since the guideway module weldment was the largest procurement during this phase, a bidder's conference was held on the September 25, 2003 at General Atomics in preparation for the procurement of the seven guideway module weldments. At this conference the details of the guideway modules were discussed, including the critical dimensions and tolerances, and lessons learned during the assembly of components to the first weldment. We also answered a significant number of bidder questions. The procurement included the purchase of four additional straight guideway module weldments, similar to the one that was purchased during supplemental #2. In addition, three new types of guideway module weldments were purchased, two of them spiral modules which transition the maglev vehicle into a banked turn, and one curved guideway module which turns the vehicle around a 50-m radius. Like the original straight module, the running length of each of these modules was 15,100 mm. In the end, the lowest cost and lowest risk option selected was to use two vendors, one in California for all the transition and curved weldments, and one in Pennsylvania for all the straight weldments.

3.2.2 Manufacturing

The guideway module weldments were fabricated in three equal segments and the three segments were welded together to complete the structure. When completed and painted, they were shipped by truck to GA, as shown in Figure 3.2-2.



Figure 3.2-2
Guideway module weldment being delivered to General Atomics

Once the weldment was delivered to GA, the iron laminations, the LSM coils and litz track sections were attached. The first step is to assemble and install the LSM iron laminations (which form a part of the LSM motor). The laminations are made from a Silicon grade steel and are coated with an organic varnish insulation. The slots and attachment holes are cut into each of the 0.635-mm thick lamination using a laser cutting process. After the laminations were received,

they were stacked and bonded together. Tooling is very simple for the stack-up assembly. Twenty-foot long structural steel W-beams are used as lay-up platens, and a 0.25-in. thick plate with the same width as a lamination is used as a cover plate on top of the lamination lay-up. After the laminations have cured, the clamps are removed and the assemblies are prepared for the next step in the assembly. Finally the lamination stack-ups are bolted together with a spacer to form the lamination assembly. They are bolted together in their final configuration before being attached to the guideway weldment. The final configuration is seen in Figure 3.2-3.



Figure 3.2-3
Completed LSM laminations prior to being installed on the guideway weldment

The next step in the manufacturing process is to attach the LSM windings as shown in Figure 3.2-4 while it is in the upside down position. While the LSM coils are being wound, the litz track sections were being manufactured in parallel. The first step in process of fabricating the Litz track was to manufacture the Litz wire. Litz wire is a bundle of multiple insulated strands, which minimizes the power losses in the track system. After the Litz wire was received, it was installed in the stainless steel case, and the case was swaged around the wire. Then the rungs were precision cut to length. The next step was to place the ends of each rung into a solder pot and pre-tin the Litz wire. After the pre-tinning operation, the rungs were arranged in the track assembly tooling with the copper shorting bars positioned at each end along the track. Then the track, along with its tooling, was positioned vertically for the soldering operation, as shown in Figure 3.2-5. After final inspection the track sections were shipped to GA for installation on the guideway module weldment.



Figure 3.2-4

LSM propulsion coils are assembled onto the weldment while it is upside down



Figure 3.2-5

Litz track sections positioned for soldering and final inspection

With the installation of the Litz track segments, the guideway module is ready to be flipped over and positioned upright on the guideway foundation. The first step in the rollover process was to install the guideway module rigging. Figure 3.2-6 shows the rollover rigging installed on the guideway module performing the roll-over function on the first straight guideway module manufactured under Supplemental #3.



Figure 3.2-6

The guideway module is rolled over using the specially design rigging

Finally, after the module is rotated, it is placed on the foundation and aligned to the anchor bolts. In Figure 3.2-7 the module is shown being lowered onto the foundation. The final step in the process was to position and level the guideway module using the slotted sole and foot pad plates. Figure 3.2-8 shows a view from the North end of the track, after installing guideway modules 2 and 3. Figure 3.2-9 shows the same process being repeated for the installation of the curved guideway modules.



Figure 3.2-7

Straight guideway module being positioned on the foundation

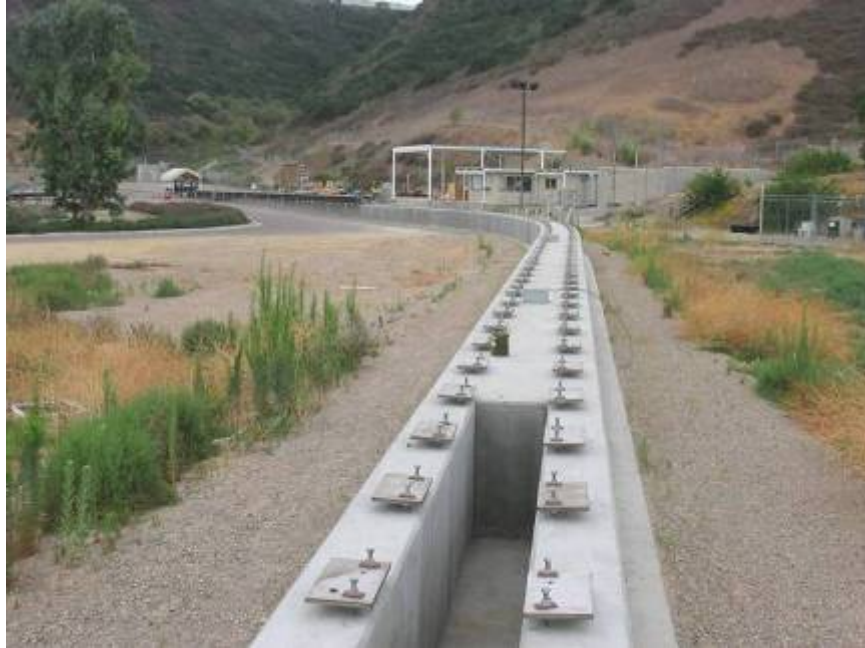


Figure 3.2-8
View from North end of track, showing “maintenance pit”
and in the distance the straight guideway modules 1, 2, and 3



Figure 3.2-9
Curved guideway module being installed on the foundation

The final step in the process is to connect the guideway modules electrically. The completed test track is shown in Figure 3.2-10, with team members who contributed to its successful construction.



Figure 3.2-10
Completed test track

While they were completed under Supplemental #2 funding, for completeness we also show below views of the electrical/control center, as well as the inside view of the electrical room (Figures 3.2-11 and 3.2-12).

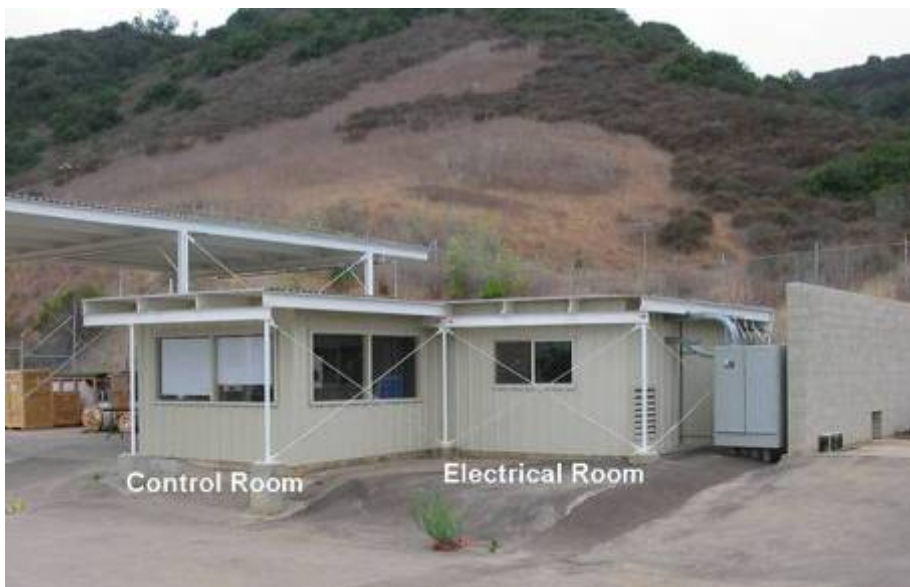


Figure 3.2-11
Control and electrical rooms provide excellent views and access during test track operations



Figure 3.2-12

Electrical equipment room, showing the AC-DC rectifier, which converts incoming AC to DC, and the inverter which converts the DC power to a variable frequency voltage applied to the LSM propulsion coils

3.3 System Integration and Testing

Prior to test track operations, we developed detailed test and safety plans to ensure safe and orderly testing. The test plan, published June 30, 2004 (Report # 39343-OO-001) was a deliverable under Supplemental #3, and includes discussion of the test system, component and subsystem testing, test parameters, analyses and simulations, and description of the three phases of testing. The safety plan develops safe operating procedures, including a daily safety checklist prior to starting testing. The test plan is published in Appendix A of this report. The safety plan is available upon request. In Sections 3.3.1 and 3.3.2, we discuss the control system architecture which is an integral part of successful testing, and the testing performed to date, respectively. The dynamic testing (Section 3.3.2) was completed under reprogrammed “Port Authority” funding (Agreement No. 62T122), and is reproduced here for completeness.

3.3.1 Control System Description

The maglev control system is designed to provide currents that are synchronous with the position of the magnets attached to the vehicle. The phase and amplitude of the currents are adjusted to provide the thrust required while minimizing disturbances in the vertical force created by the motor. The method adopted is a type of vector control using a position sensor to detect the

position of the vehicle. The position information is transmitted to the inverter on the wayside, which then provides the desired thrust, and normal force commands.

The inverter output is a three phase voltage applied to the linear synchronous motor (LSM) in the guide way. The amplitude, phase, and frequency of the ac voltage are adjusted to produce the desired current. The inverter current is measured and compared to the current commands. The error is used to vary the voltage to obtain the desired current. The position sensor is used to provide a reference position to the inverter to which the voltage and current signals are referenced.

The current commands are created by the vehicle control system using the commanded speed, estimates of the drag, and possibly predictions of the magnetic gap. A gap sensor is not presently used in the control but may be used in the future.

The command inputs to the control are the desired thrust and a value of “ I_d ” (see Section 3.3.1.2), which is used to control the attraction of the LSM to the vehicle magnets. This value is adjusted for the load weight in the vehicle. For the test track, this is a constant value, which is manually set.

The thrust control consists of a velocity regulator, which adjusts the thrust to maintain smooth acceleration through the drag peak. To aid the velocity regulator, an estimate of the vehicle drag is made using the speed signal and the estimated drag added to the output of the velocity regulator.

The feedback signals used by the control to establish the motor operating point consist of:

- AC voltage at the inverter terminals
- AC current at the inverter terminals
- A position sensor signal, which is processed to yield position, velocity, and acceleration
- DC link voltage at the inverter
- AC power output of the inverter

The control software to provide the necessary inputs to the vector control processes these feedback signals. Additionally, the feedback signals allow the operation of the system to be monitored and documented during test runs. This information is used to refine the vehicle operation and to document the test results.

The position sensing system provides the angle information showing the position of the magnets on the vehicle relative to the track within a precision determined by the position sensor resolution. The spatial resolution of the sensor is 18 mm. The wavelength of the motor is 432 mm, resulting in an angular resolution of 15 degrees.

The vehicle magnets are positioned so that magnet #9 from the south end of the vehicle is aligned with the center of phase A (start end of winding). The magnet polarity is away from the LSM winding. A drawing illustrating the magnet position in relationship to the back emf and the D-Q reference is shown in Figure 3.3-1.

$$\Theta = (\text{Inverter angle}) - 90 \text{ degrees}$$

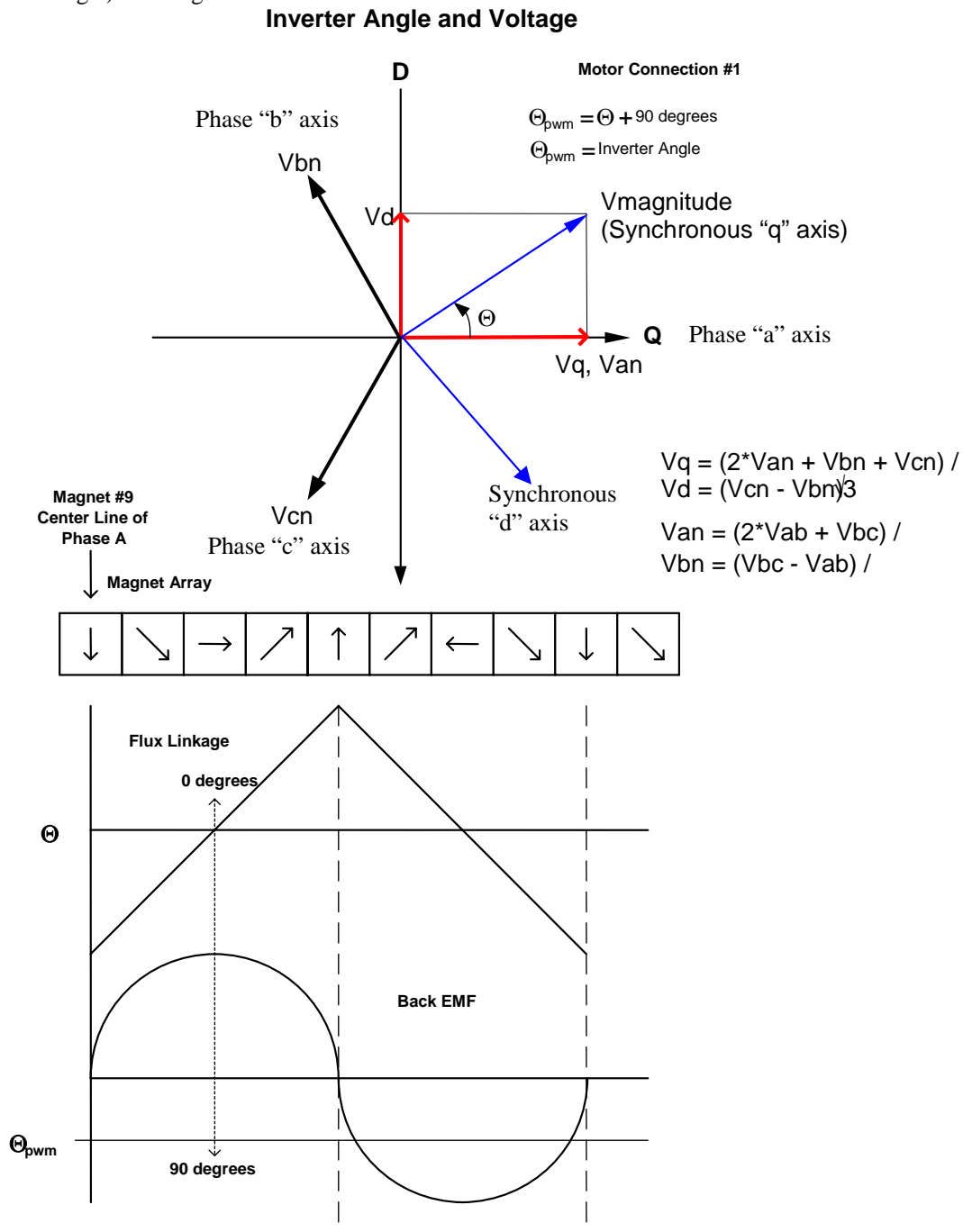


Figure 3.3-1
Magnet polarity and LSM winding relationship

Note that the power with modulation (pwm) angle (or inverter angle) is shifted 90 degrees from the Θ in the figure.

The primary control of the linear motor is a current control, which is aligned with the position of the vehicle magnets. The regulation of the current is accomplished in the synchronously rotating reference frame aligned with the vehicle magnets.

Field-oriented control is based on the transformation of the time-dependent three-phase stator system into a time-invariant D-Q reference frame. This rotating system has two orthogonal current vectors: one parallel and one orthogonal to the rotor field.

The alignment is chosen so that the Q (quadrature) axis current provides only thrust and the D (direct) axis current only affects the net magnetic field strength. The D axis current then affects the attraction force between the vehicle magnets and the motor iron. This method of control is used to minimize the effect of changes in vehicle position coupling into vertical force changes causing vertical oscillations of the vehicle position. The current regulator outputs are the voltage command to the inverter. There is a voltage feed forward used to estimate the value of the required steady state voltage as a function of speed and motor current so that the current regulator need only compensate for transient effects.

3.3.1.1 Vehicle Thrust Command – “Iq” Command

A speed regulator develops the “Iq” command. Usually a transit vehicle control is a thrust control, which approximately controls the acceleration of the vehicle. In the case of the maglev vehicle, the drag is highly nonlinear which causes large variations in vehicle acceleration and consequent unpleasant effects on the passengers. To solve this problem, the maglev vehicle uses a speed regulator, which varies the thrust to maintain a desired velocity profile. This control works well (by simulation) on the test track, which is level, i.e., without grades. For grade effects, there will need to be some correction for the track profile or a current limit function that controls the thrust at cruising speed to prevent overloads due to grades.

The block diagram (see Figure 3.3-2) shows the method of thrust (Iq cmd) command generation using a speed regulator. The speed regulator command input is generated by a velocity profile generator, which varies the speed command as a function of position along the track. The velocity command is compared to the actual speed and a thrust signal is produced. To help produce smooth vehicle acceleration, a feed forward estimate of the magnetic drag of the vehicle is added to the speed regulator output. An estimate of the force required to accelerate the vehicle is added to the speed regulator output to give an additional feed forward of the required thrust. The thrust command is converted to a current command and sent to the vector control. The LSM thrust/amp is affected by the gap so that a feed forward is used to compensate the current command. In the case that an actual gap estimate is not available, the normal cruising speed gap is used.

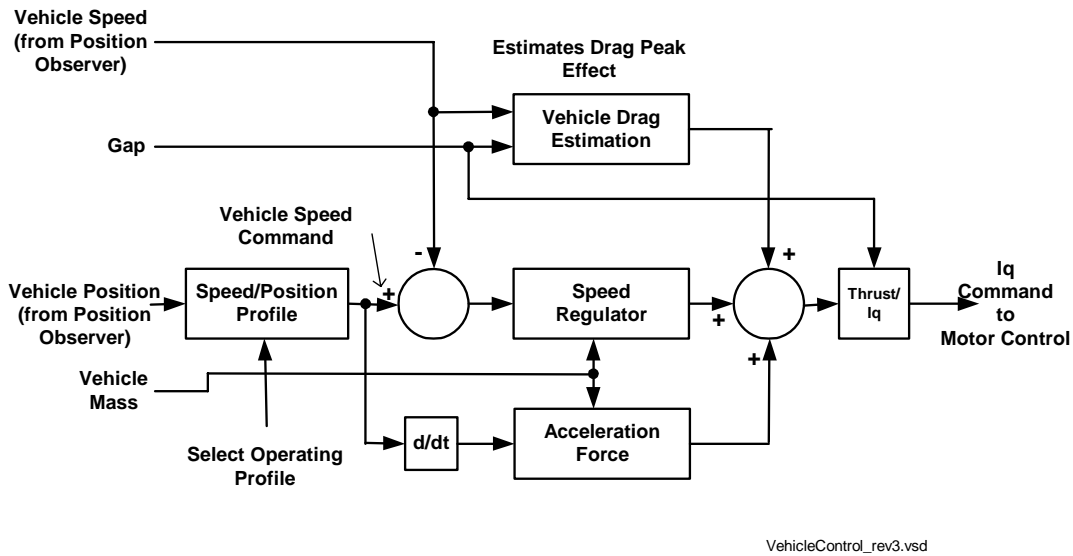


Figure 3.3-2
Thrust command block diagram

3.3.1.2 Vertical Force Balance – “Id” Command

There are several factors that affect the levitation of the vehicle. The LSM creates lift by passive attraction between the vehicle magnets and the LSM iron. The LSM adds or subtracts from this lift by the magnitude of the motor current that creates flux aligned with the magnets, effectively adding or subtracting from the magnet flux. The main levitation Halbach array creates lift.

The vehicle weight and the load weight combined must balance this lift force exactly; otherwise the vehicle either will not levitate or will hit the upper wheels due to excessive levitation. The motor “Id” command effectively varies the LSM lift. The relationship is (LSM Passive Lift) + (LSM Active Lift) + (Levitation Magnets Lift) - (Vehicle Weight + Load) = 0. An “Id” command of zero equates to a phase angle of 0 degrees. When the motor phase angle (Θ) is set to zero, as shown in Figure 3.3-1, the LSM flux is aligned with the horizontally aligned magnet cubes. At this phase angle the active lift force component of the LSM is equal to zero. A positive “Id” command equates to a positive phase angle. In this case the LSM flux is aligned with magnet cubes, which have their magnetic poles aligned upward, generating an active LSM force component pushing down. A negative “Id” command equates to a negative phase angle. In this case, the LSM flux is aligned with magnet cubes, which have their magnetic poles aligned downward, generating an active LSM force component pulling the vehicle upwards.

For normal operation, the LSM lift increases with ride height and the Halbach lift decreases with ride height. At the nominal operating gap of 25 mm, the Halbach array lift will decrease faster than the LSM lift increases leading to a statically stable vehicle ride height. If the vehicle should ride higher, there is a possibility that the LSM lift will increase faster than the Halbach lift leading to running at the upper stops. To prevent this, the value of “Id” command is adjusted by

measuring the passenger load with a load weight system similar in function to that used on a more conventional transit vehicle to provide the 25 mm ride height (see Figure 3.3-3 block diagram).

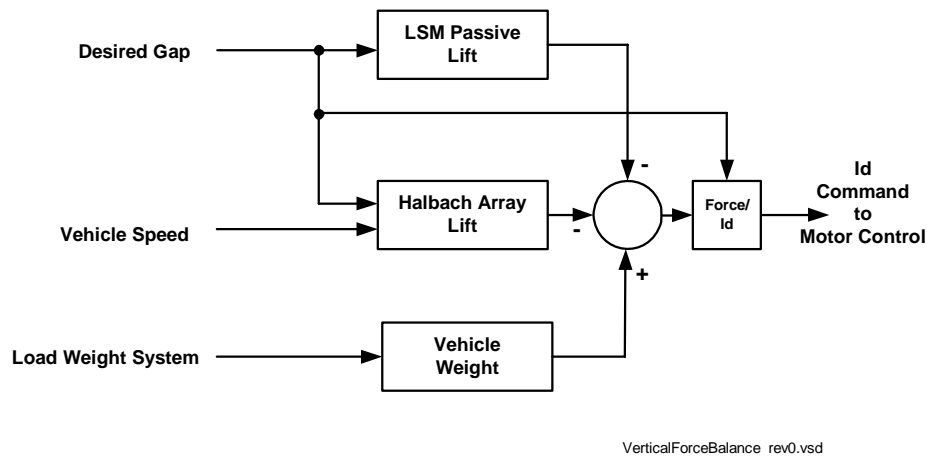


Figure 3.3-3
Vertical force balance block diagram

3.3.2 Test Results

During this project, initial testing of the vehicle levitation, propulsion/control systems were performed. While much still needs to be accomplished before the system is ready to be deployed, we are pleased with the progress to date. Testing was performed in two of the planned three phases of the test program, as described in the following sections.

3.3.2.1 Phase 1 Testing

The objective of the phase 1 testing was to perform a checkout of the (1) variable voltage variable frequency (VVVF) inverter and LSM motor control system and (2) the data acquisition system. These tests were performed before the high-speed levitation tests to validate and correct any problems with the systems.

Inverter and LSM Motor Control System. The key elements of the control system are the integration of the control program with the control system hardware and the maglev control screen interface (see Figures 3.3-4 and 3.3-5), initial operational checkouts of the control system outputs, such as the inverter PWM waveforms, and the interface with the position observer sensor system.

In order to merge the control screen of the control computer with the control program, a number of debug operations were required. These operations tested the ability of the control screen to set key parameters, display the status, the vehicle state, the vehicle position on the track, to display the actual dynamic speed and thrust values and to start and stop the vehicle.



Figure 3.3-4
Urban maglev control panel



Figure 3.3-5
Control computer

Next, the feedback signals used by the control to establish the motor operating point were validated. These consist of AC Voltage at the inverter, AC current at the inverter, position sensor signal (which is processed to yield position, velocity and acceleration), DC link voltage and AC power output of the inverter. As was mentioned in Section 3.3.1, these feed back signals are processed in the control to provide the necessary inputs to the vector control.

General Atomics specifically built the propulsion system inverter for the test track. It is based on advanced power electronics using insulated gated bi-polar transistor (IGBT) technology. Figure 3.3-6 shows the DC rectifier and inverter as installed in the power equipment room of the maglev test track control building. This inverter was originally designed for Electromagnetic Aircraft Launch System (EMALS) but was modified for the maglev application. It is configured to deliver three-phase power using a single pulsed width modulation card (PWMC) with an output power capability of 2.5 MW rms. With PWM techniques waveforms are synthesized by a sequence of pulses with a progressive width adjustment. Those pulses result from appropriate commutation of semiconductor switches (see Figure 3.3-7).



Figure 3.3-6
DC rectifier (left) and inverter (right)

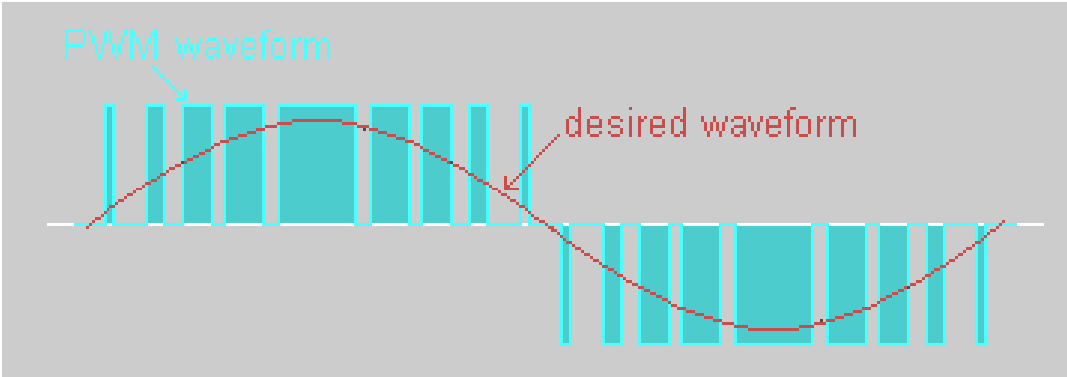


Figure 3.3-7
PWM waveform

An example of the current waveforms output from the inverter is shown in Figure 3.3-8 below.

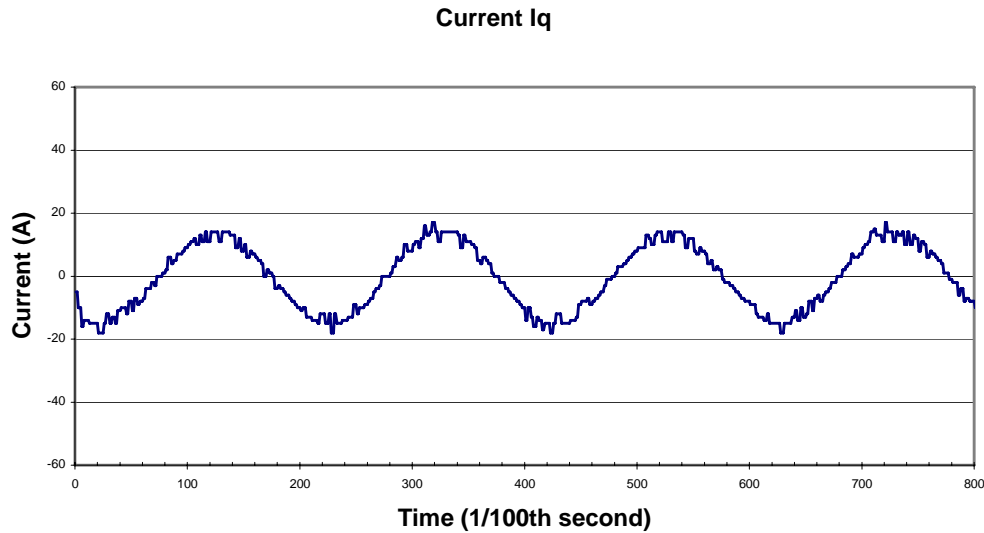


Figure 3.3-8
Actual PWM waveform

The LASER monitors the black and white transitions of the optical tape (see Figure 3.3-9). These transitions are transmitted back to the central control room via a modulated 450 MHz, NBFM radio. In the control room, a special controller counts these pulses and processes them. The information calculated represents angle and location, using the leading edge of the lead magnet as a reference point. This information is passed on to the Inverter Controller by a high-speed optical serial link. The spacing between the black bands is 18 mm; therefore, the resolution of the sensor is 18 mm. The wavelength of the motor is 432 mm giving an angular resolution of 15 degrees.

The data from the position sensor is a discrete signal, which is updated only when the sensor passes a black band on the optical tape. In between the steps of the position sensor data, the signal is held at a constant value. The effect is to have the average position lag the actual position as illustrated in the diagram shown in Figure 3.3-10.

An example of typical position data is given in the following Figure 3.3-11. The black line represents the command position and the red line is the actual position sensor output. At the top of the figure is a representation of the optical tape, which is placed along the track.

The wavelength of the LSM motor is 432 mm. At the start of each wavelength a double black bar is placed on the tape for the sensor system to detect. As it detects this reset position, the position system starts counting the next 24 black, 18 mm spaced bars, until it reaches the next double black bar reset point. This process continues as the vehicle travels along the track.

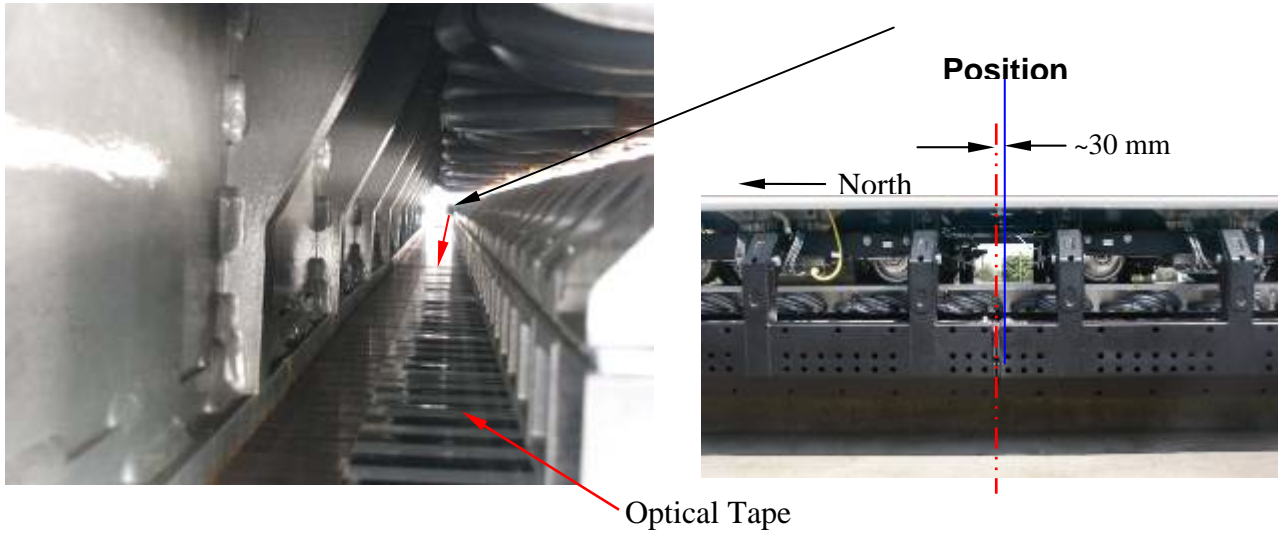
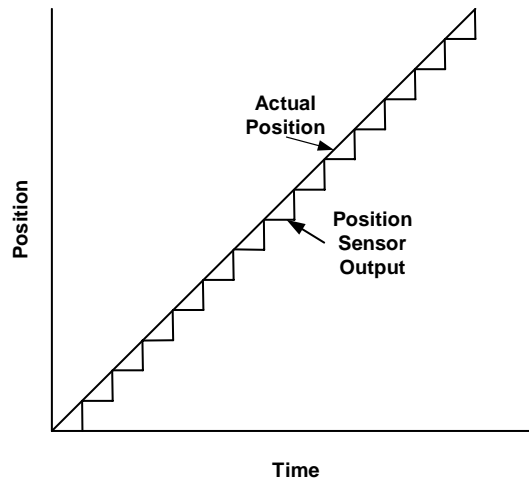


Figure 3.3-9
Optical position sensor

**Position Sensing
Quantization of Position**



**Figure 3.3-10
Predicted position sensor data**

Position Sensing

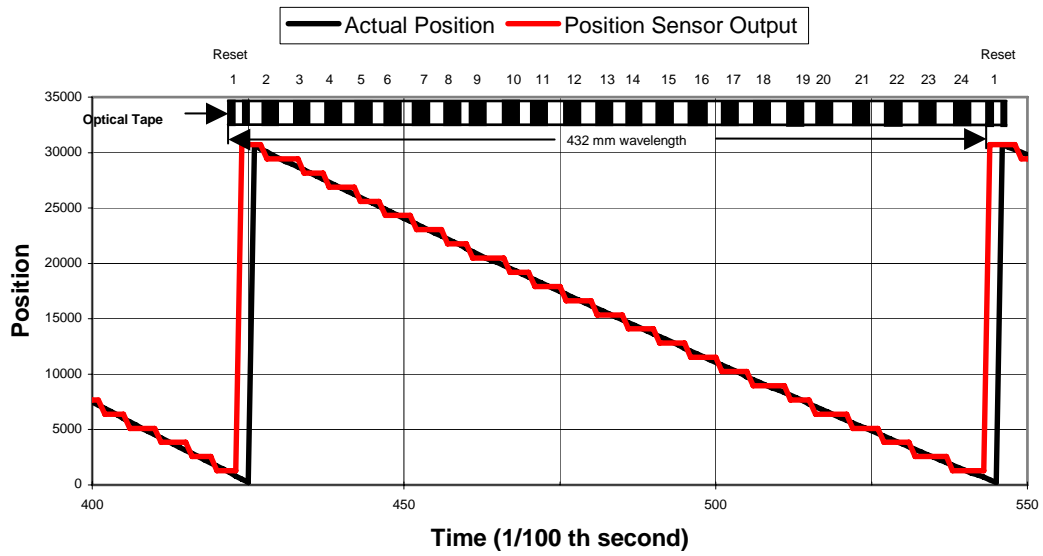


**Figure 3.3-11
Actual position sensor data**

Data Acquisition System. A schematic diagram of the data acquisition system is shown in Figure 3.3-12. As shown, instrumentation is provided both on the vehicle and the wayside.

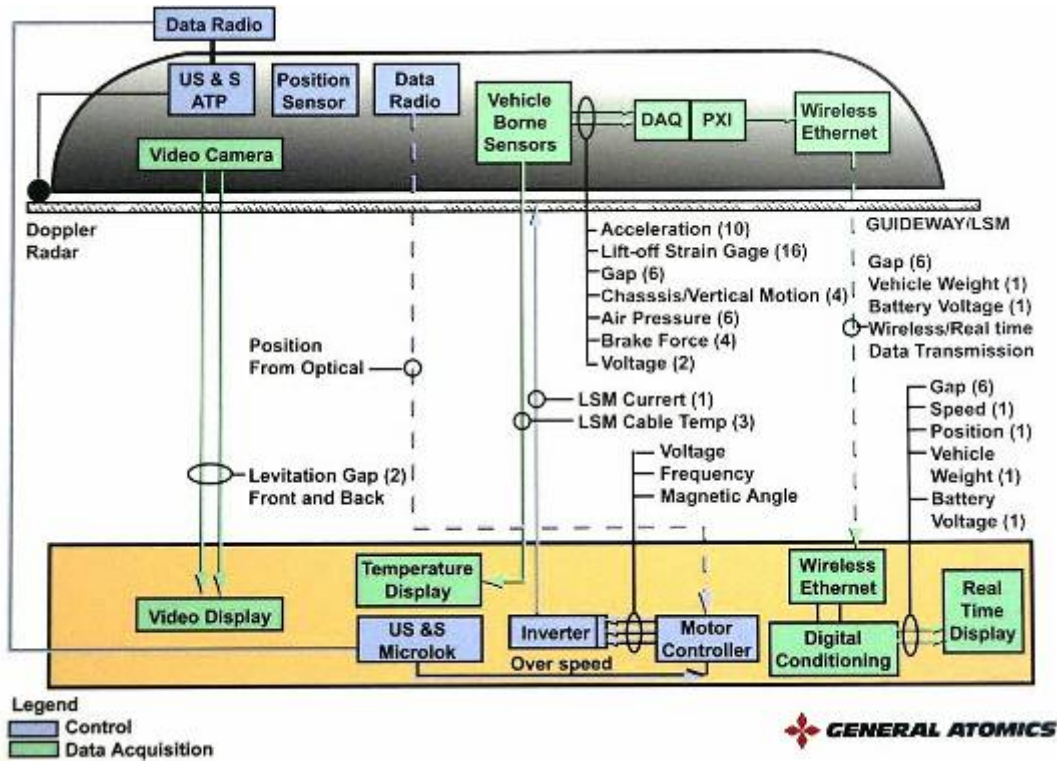


Figure 3.3-12
Data acquisition system architecture

On board the vehicle is a National Instruments PXI data acquisition module. PXI is a modular instrumentation platform designed specifically for measurement and automation applications. With the PXI, we were able to select the modules that we need to integrate into a single system. The PXI monitors the sensor channels for all of the on board sensors. It stores all of the data runs on its hard drive for recovery at a later date (see Figure 3.3-13).



Figure 3.3-13
PXI data acquisition system

The data acquisition system on the vehicle can collect and store up to 64 sensor signals. At present, a total of 51 sensors on the vehicle have been assigned. Ten of these signals are wirelessly transmitted for real time monitoring and are displayed in the control room on the data acquisition computer. The signals that are displayed include:

- 4 levitation gaps
- 2 lateral gaps
- Vehicle speed
- Accelerations (vertical, lateral and longitudinal)
- Vehicle position
- Vehicle weight (16 strain gauges mounted on landing wheels)
- Vehicle battery voltage

The remainder of the data is hard-wired from within or to the control room and is displayed on the data acquisition system. These channels include the following:

- 3 LSM cable temperatures
- 6 inverter power electronics temperatures
- Output inverter currents (“Id” and “Iq”)
- Output inverter voltages (“Vd” and “Vq”)
- Inverter power

A number of phase 1 tests were performed to checkout the data acquisition system. In addition to monitoring and recording the data, a number of refinements and adjustments were required for both the instrumentation hardware and software.

An example of one of the data acquisition channels, which can be displayed, is the inverter and LSM track temperature as shown in Figures 3.3-14 and 3.3-15. For reference, the maximum LSM winding temperature allowed is 125°C, and the maximum desirable inverter temperature is about 60°C; as seen in these figures, our operating temperatures are significantly below these values.

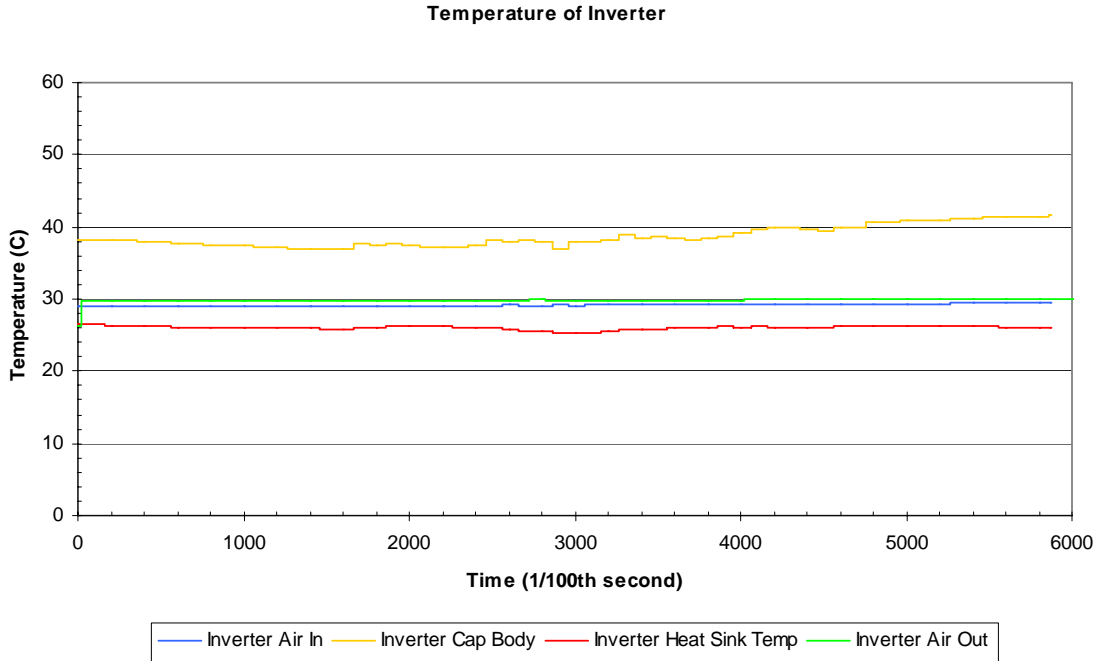


Figure 3.3-14
Monitoring inverter temperatures

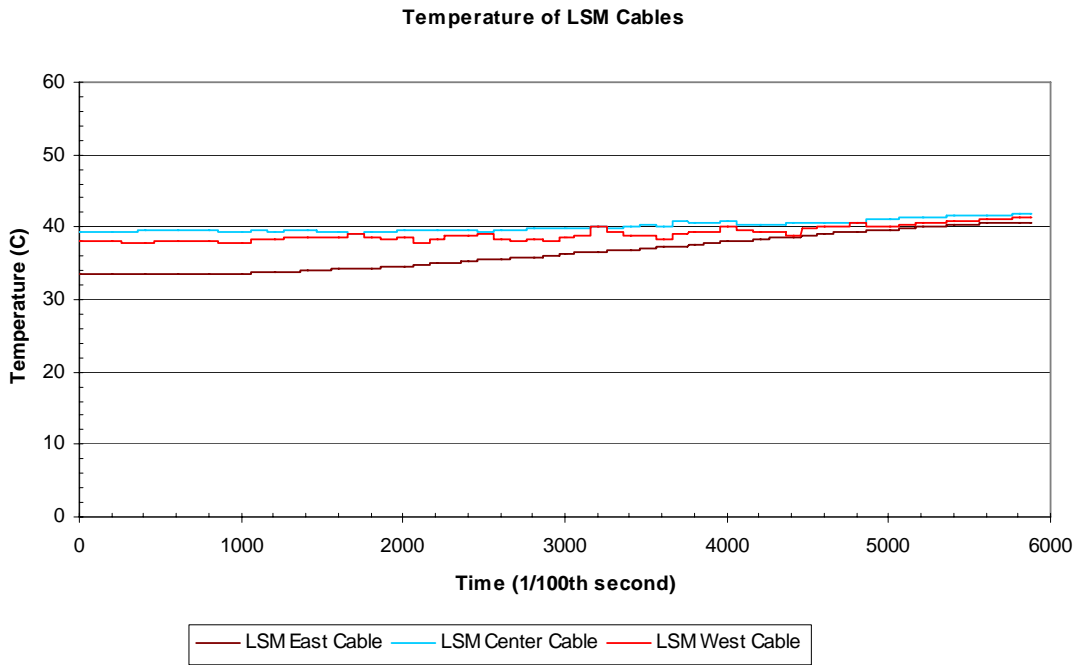


Figure 3.3-15
Monitoring LSM cable temperatures

A photograph of the data acquisition system computer is shown in Figure 3.3-16.



Figure 3.3-16
Data acquisition computer station

In the following Phase 2 testing section, examples of the data acquisition displays are provided for actual test runs of the General Atomics Urban Maglev test vehicle during the months of October and November 2004.

3.3.2.2 ***Phase 2 Testing***

The objective of Phase 2 testing was to evaluate the range of stable operating conditions for four different vehicle test weights. Stable operation is achieved when the levitation gap does not grow with time and thrust can be modulated without exciting resonances in the system. The four different test weights selected were: 6,500 kg, 8,000 kg, 9,000 kg, and 10,500 kg. The test configuration parameters include jerk limit, cruise speed and lift current “ I_d ”. Simulations have been run for the selected vehicle weights. A jerk limit of 0.1 g/sec (1.0 m/sec^3) was used for all the runs to reduce overshooting of the levitation gap.

Inverter and LSM Motor Control System. The first step in the Phase 2 testing was to operate the inverter and LSM motor control system at speeds sufficient to levitate the test vehicle. This allows implementing key operating functions of the control system software, monitoring the performance of these features, and debugging and adjusting the software as required to provide stable operation.

The key operating functions of the control system include (1) the speed regulator which develops the “ I_q ” command, (2) the feed forward which is used to compensate the current command for

changes in magnetic drag as a function of clearance between the magnets and the Litz track, and (3) the vertical force balance to verify that the “Id” command current generates the appropriate (either downward or upward) lift force to maintain the desired vehicle ride height.

Speed Regulator. A speed regulator develops the “Iq” command. The speed regulator varies the thrust to maintain a desired velocity profile. The magnetic drag is highly nonlinear at low speeds, which would cause large variations in vehicle acceleration if the speed regulator did not properly develop the “Iq” command for the desired velocity/acceleration profile. In the following Figure 3.3-17, the velocity command, actual velocity and the current “Iq” command are compared. The vehicle weight at this point had been increased from the initial 6500 kg to 8000 kg.

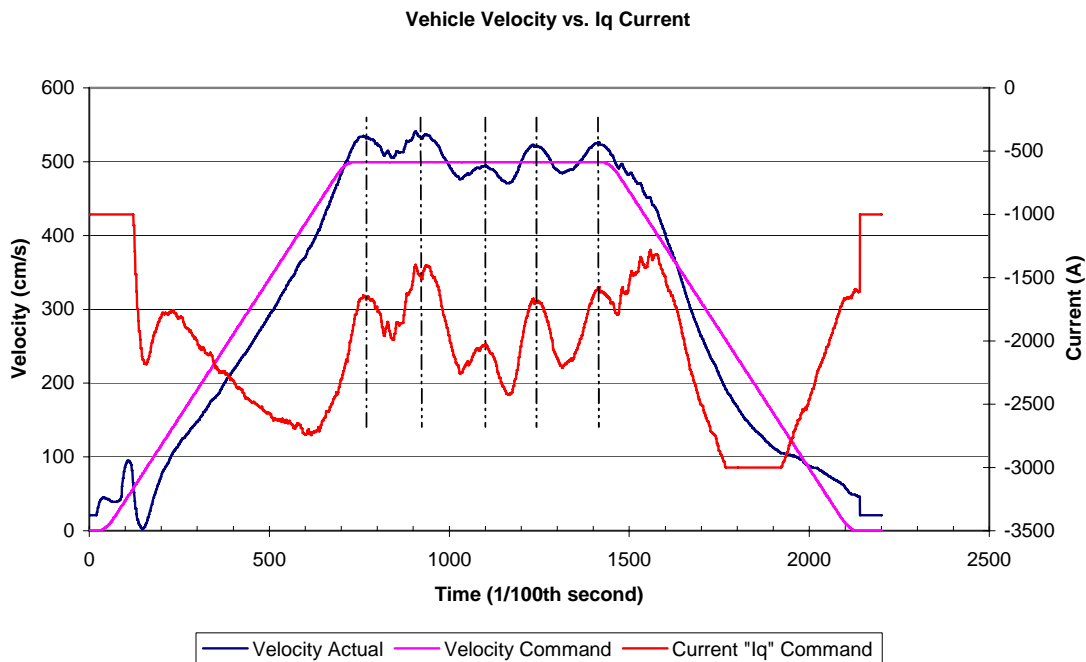


Figure 3.3-17
Actual vehicle velocity vs. “Iq” current command

In this case the speed regulator is active, but the “Id” control loop is disabled, allowing the “Id” value to float (see Figure 3.3-18).

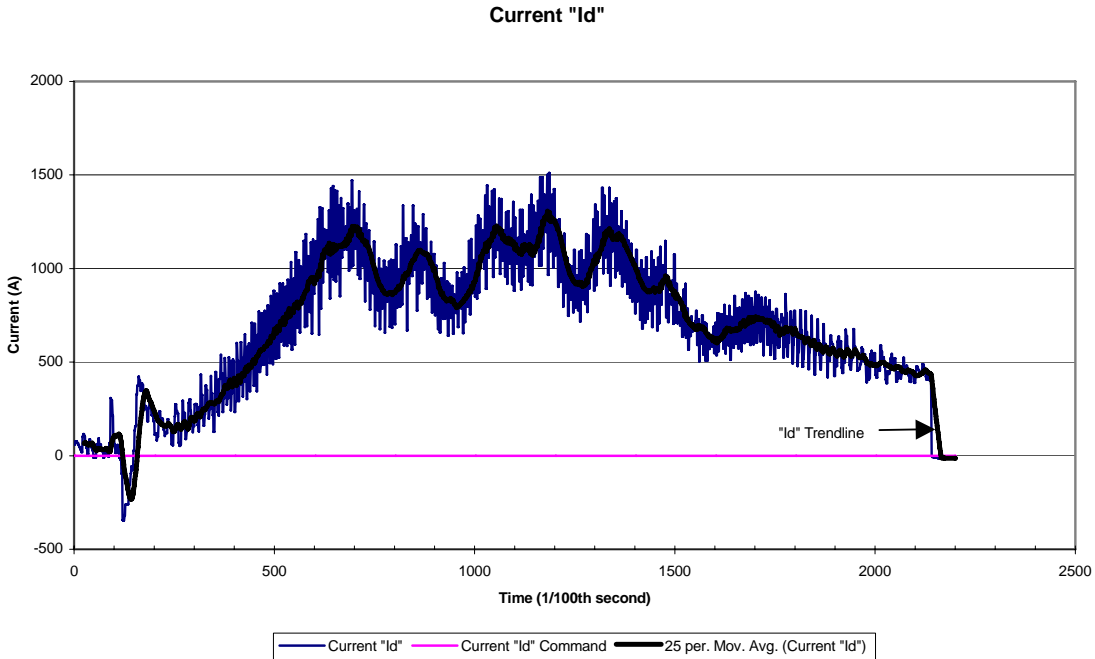


Figure 3.3-18
Actual vehicle "Id" current value

In Figure 3.3-19 the "Id" current trendline is compared to the "Iq" current command and vehicle velocity. In this comparison the period of the current oscillations is similar, except that the amplitude is opposite.

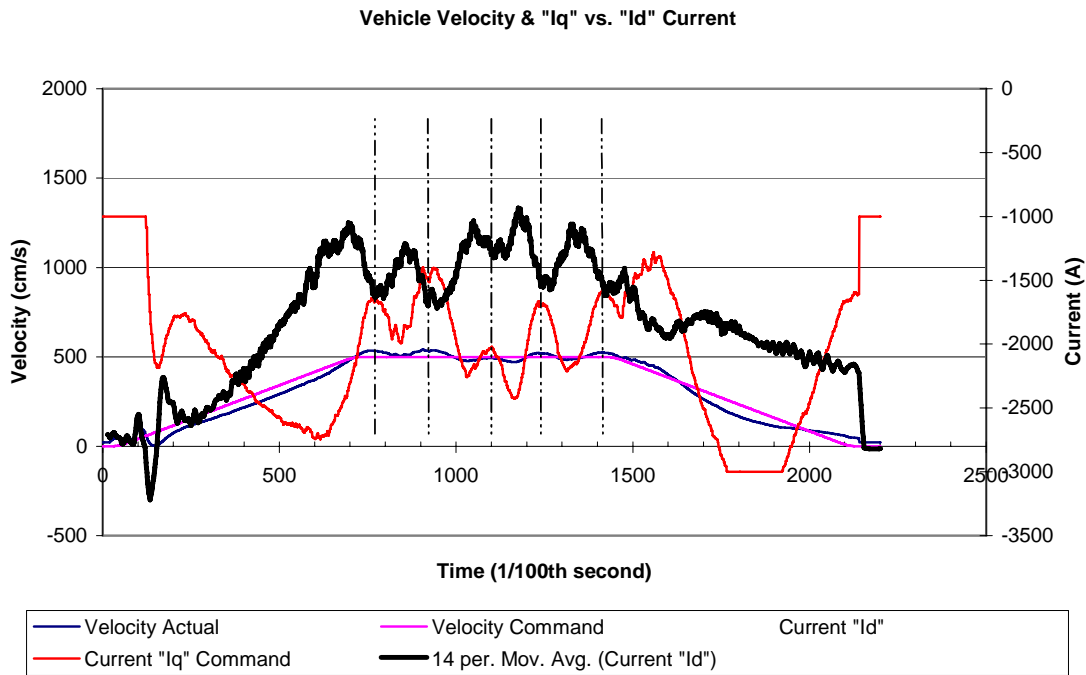


Figure 3.3-19
"Id" and "Iq" current value comparisons with velocity

In the next set of figures, the results of another test run of the maglev test vehicle are presented. In this case additional weight has been added to the vehicle to bring the total weight up to 8500 kg.

In Figure 3.3-20 the resulting vehicle velocity, and “Iq” and “Id” currents are shown (as in Figure 3.3-19). The velocity of the vehicle is again commanded to a maximum of 5 m/sec and the “Id” value is allowed to float.

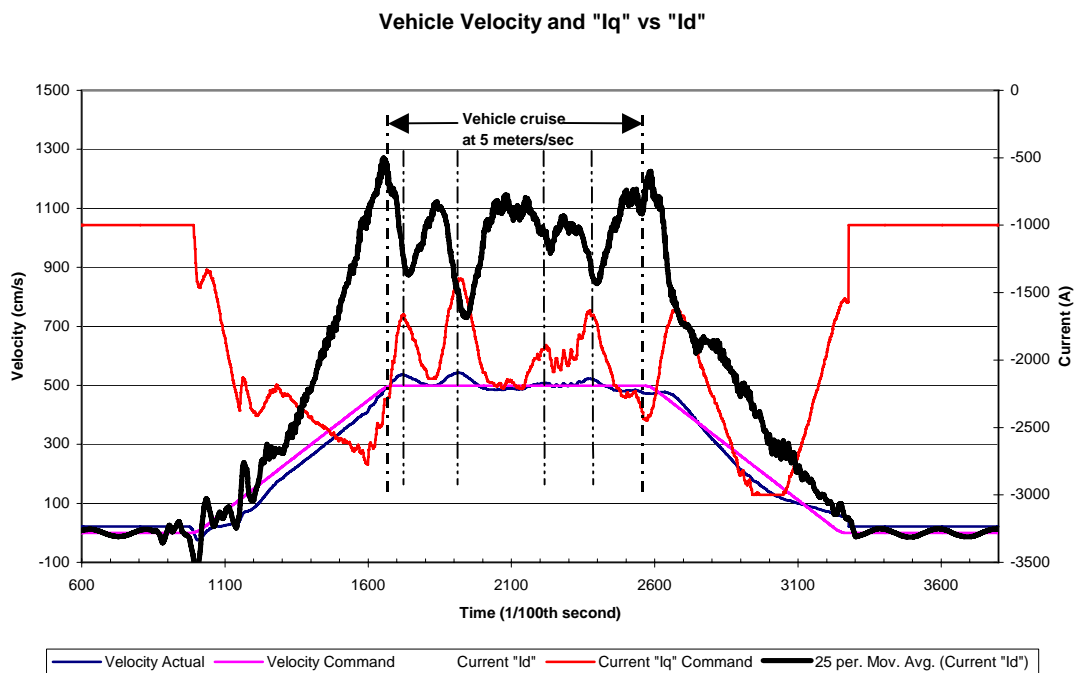


Figure 3.3-20
“Id” and “Iq” current value comparisons with velocity

In the next four figures (Figure 3.3-21 through 3.3-24) we increased the vehicle velocity to 6 m/sec and displayed the data from the gap sensors. Also, overlaid with the gap data is the vehicle velocity, using a second “Y” axis. Currently the gap sensors measure the gap changes between the magnet arrays and the Litz track rungs. Due to the gaps between the Litz rungs and the reflective nature of the stainless steel, the gap sensor data is quite noisy. Therefore, we use a running average of 100 points to display the gap sensor data. In the future, we plan to add a white tape to the Litz track so that the optical sensors have a more reliable surface from which to measure the gap.

From these gap sensors we can see under-damped chassis oscillations, which is not surprising in view of the fact that we are not controlling the ride height of the vehicle at this time by controlling the “Id” current (vertical balance force control).

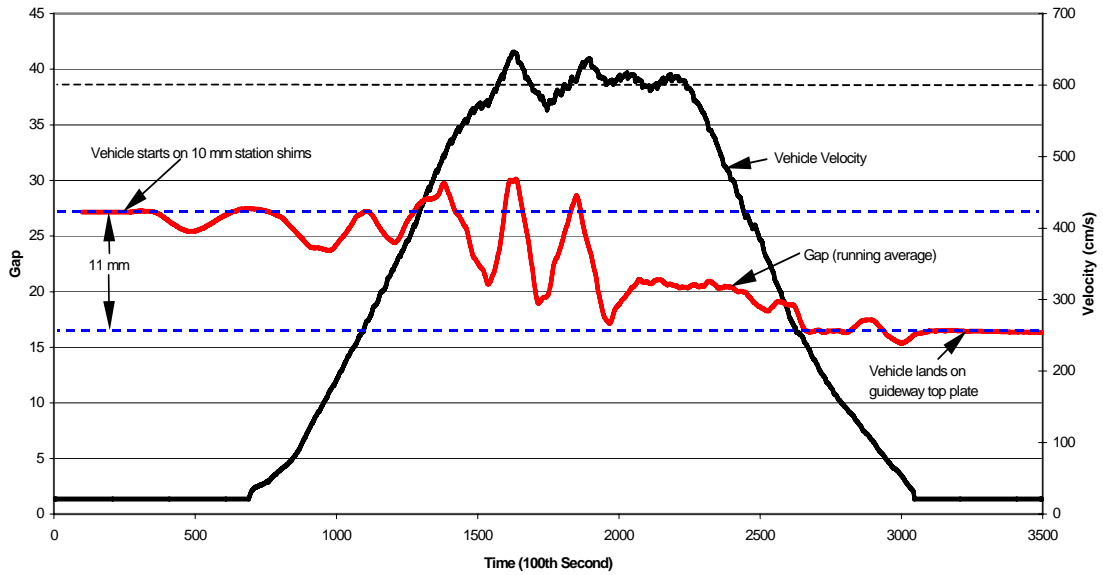


Figure 3.3-21
Gap sensor data for NW corner of vehicle

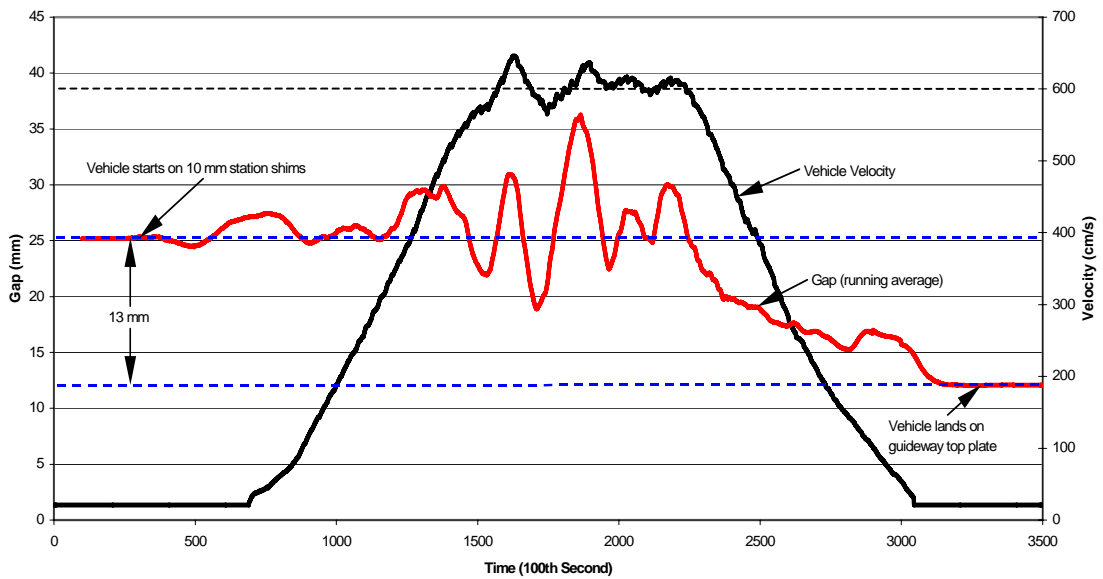


Figure 3.3-22
Gap sensor data for NE corner of vehicle

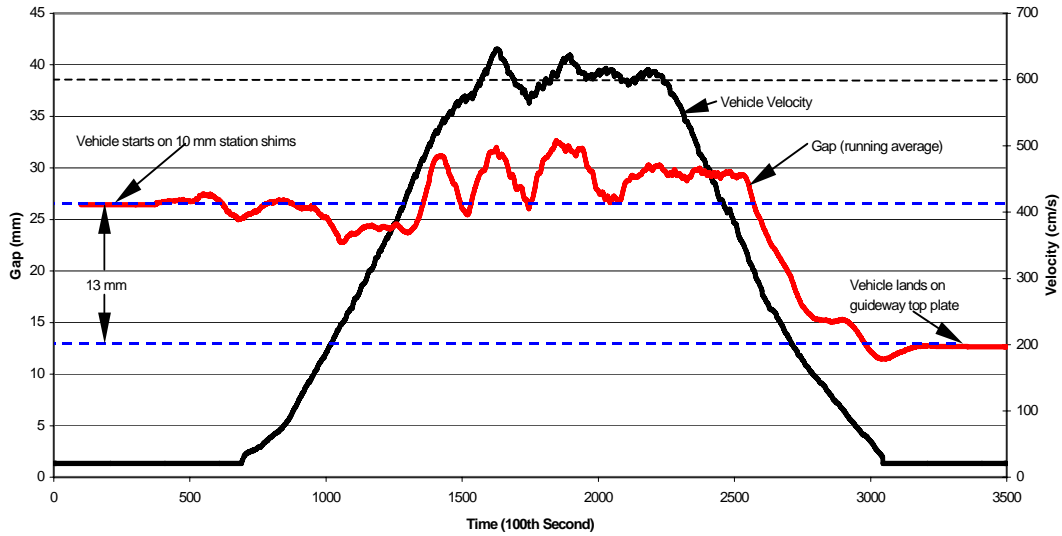


Figure 3.3-23
Gap sensor data for SE corner of vehicle

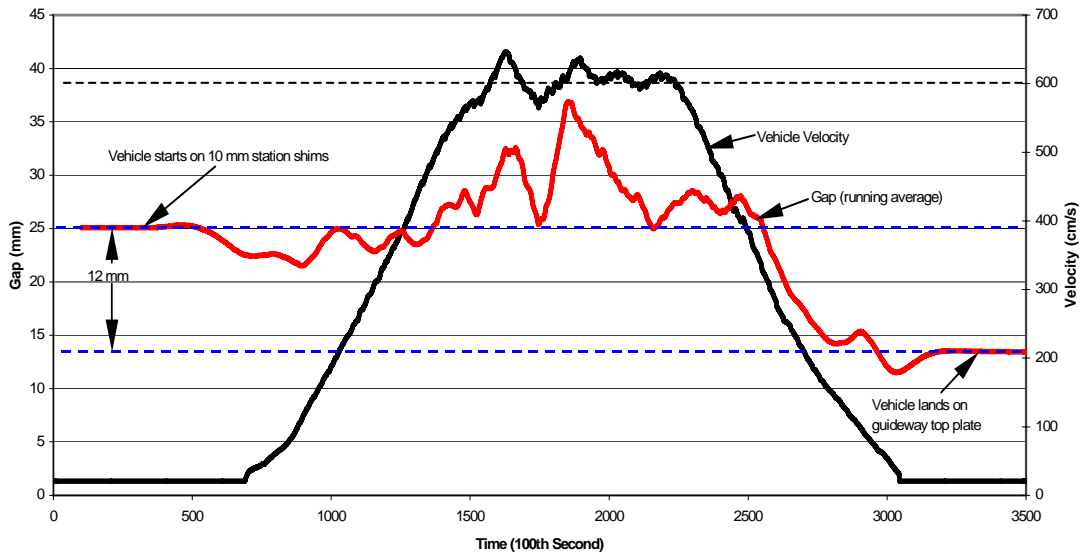


Figure 3.3-24
Gap sensor data for SW corner of vehicle

The LSM thrust is affected by these gap changes. The “feed forward” feature described in Section 3.3.1.1 is designed to adjust the “Iq” current thrust command to compensate for these changes. However, without knowing the actual average gap of the vehicle with the Litz track, it is not possible to send the proper adjustment. Decreasing magnet drag with increasing speed, results in the vehicle overshooting the selected cruise velocity; the velocity controller tries to slow the vehicle. As the velocity switches from acceleration to de-acceleration the vehicle

itches forward, decreasing the gap resulting in increased Litz track magnetic drag, and increased LSM's thrust efficiency. These two factors make it difficult for the velocity controller to prevent the vehicle from once again overshooting the selected cruise velocity, causing the velocity controller to command the vehicle to slow its velocity. This constant cyclic adjusting of vehicle velocity sets up a vertical oscillation in the vehicle ride height, which can be seen in the above examples.

Current Regulator. In order to begin the process of controlling this vehicle thrust oscillations, it was clear that we needed to control the vehicle ride height. The first step in this process was to add the current regulator to the control software program. This allows us to set an "Id" command, which provides vertical force changes to either add to the total lift or subtract from the total lift (see Section 3.3.1.2). However, at this point we are only setting the "Id" to a specific value, not allowing it to float as in the earlier examples. In order for us to use this current regulator to set the vehicle ride height to a nominal value, we must input the gap sensor data into the controller and adjust the "Id" command correspondingly.

In Figure 3.3-25, we have set the "Id" command to zero. An "Id" value of zero results in a phase angle of zero degrees. As is explained in Section 3.3.1.2, this results in an active lift component of the LSM of zero. The figure displays the actual "Id" current as the vehicle travels from the south end to the north end of the test track.

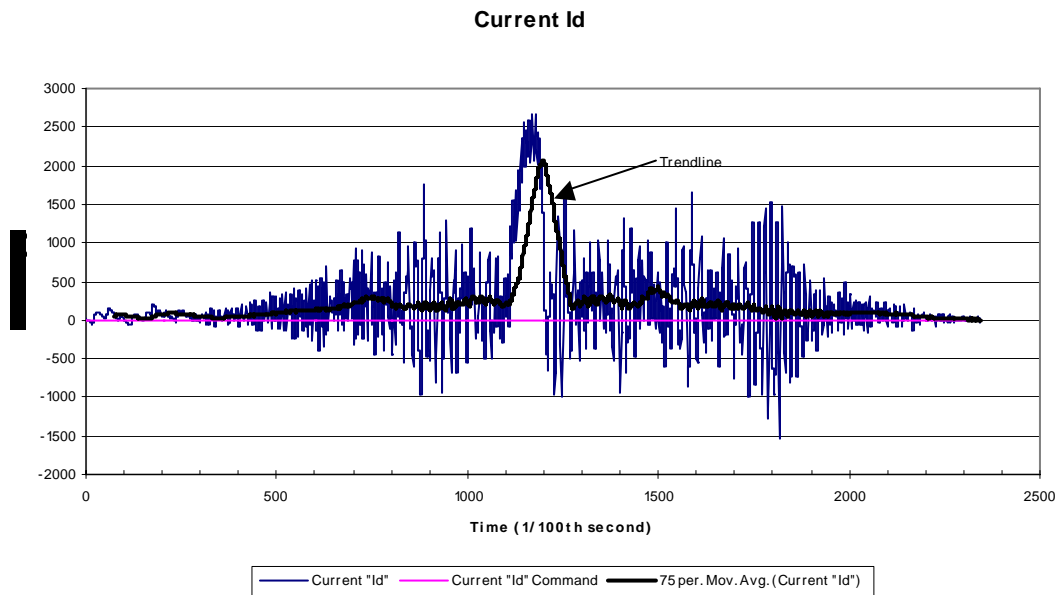


Figure 3.3-25
"Id" current command set to zero

In Figure 3.3-26, we have set the “Id” command to a positive 500 A. A positive 500 A “Id” current results in a positive phase angle, which generates an active LSM force pushing the vehicle down or reducing the total vehicle levitation force.

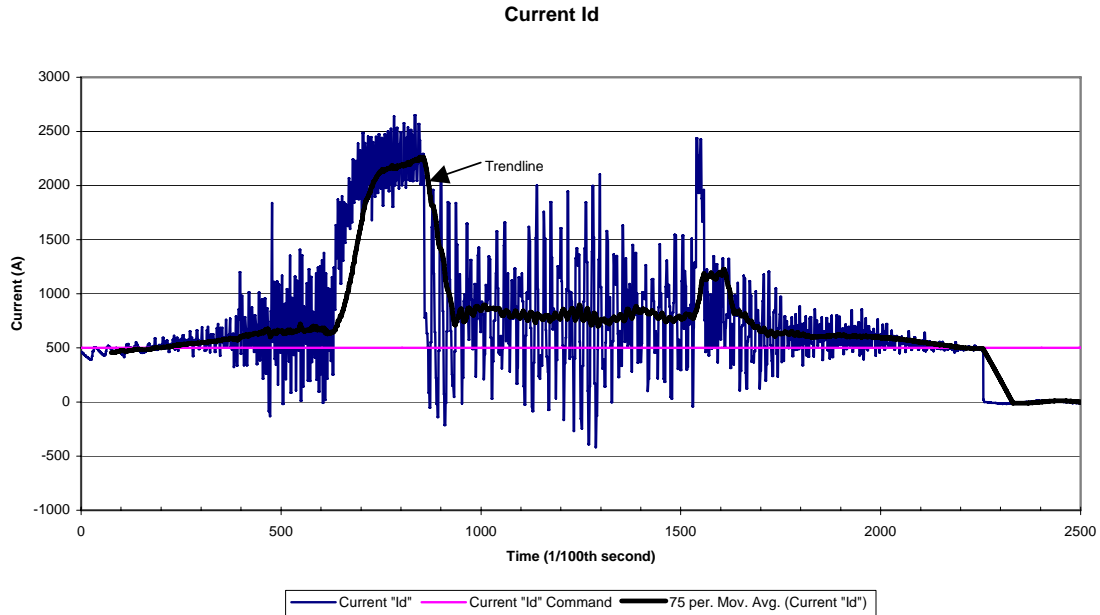


Figure 3.3-26
“Id” current command set to +500 A

While the current regulator is attempting to maintain the selected “Id” current, the same oscillations occur in the velocity controller as the vehicle magnet gap again varies affecting the LSM motor thrust efficiency and magnetic drag (see Figure 3.3-27).

In both the examples in Figures 3.3-25 and 3.3-26, the limits of the systems to control “Id” current fall out of range allowing the current to drift until the vehicle stabilizes enough for the controller to come back into adjustment range. In order to properly control and maintain a constant vehicle ride height, it will be necessary to monitor the average magnetic gap and adjust “Id” current to maintain a near constant magnetic gap. This will make the job of controlling the vehicle velocity to a selected value much easier and stable.

Adding the gap measurement and control feature to the current regulator will be a very high priority, as new funding becomes available and testing resumes.

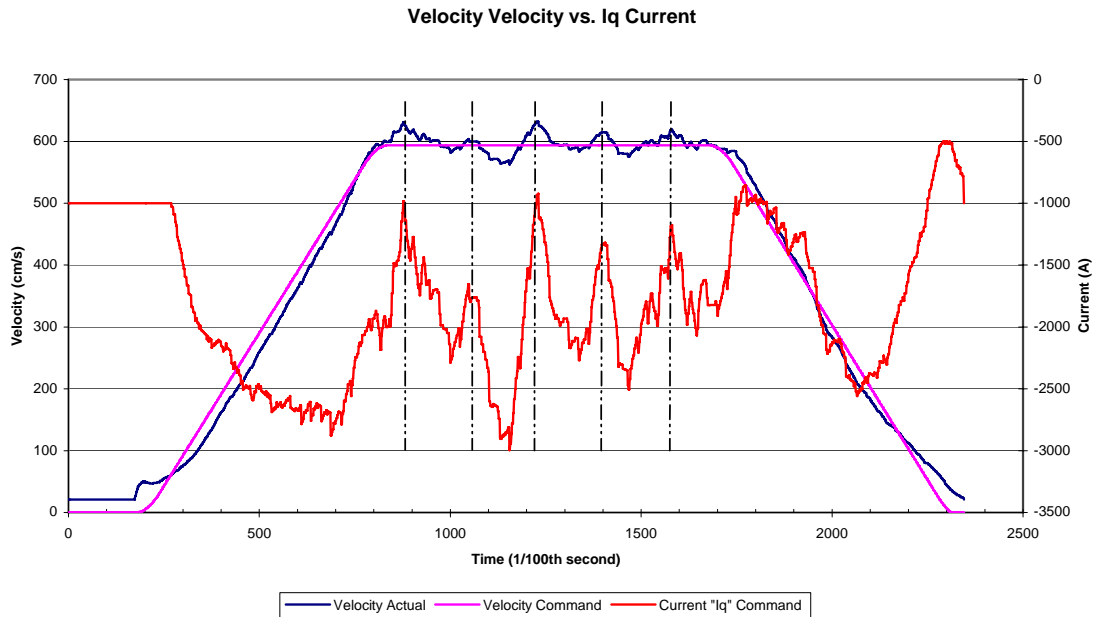


Figure 3.3-27
Actual vehicle velocity vs. “Iq” current command

Conclusions. During this task the final elements of the test track were installed, the system integration completed, and many of the elements of the urban maglev test plan, including portions of Phase 1 and Phase 2 testing were completed. In addition, the control and instrumentation system software and hardware were integrated, debugged and tested. Additional testing is required to complete the test matrix cited in the test plan, which covers a range of weights and speeds up to 10 m/s. As discussed the control software still needs to be refined, to ensure better control of the “Id” current component, which we believe can have significant effects on ride quality.

3.4 Laminated Track Development

The baseline design of the levitation track is configured as a “ladder track,” with the “rungs” made up of litz-wire cables encapsulated in square-cross-section stainless-steel tubes. Although the encapsulated litz-wire cable track circuit configuration certainly works from a mechanical and electrical standpoint, we have been evaluating an alternative configuration which has the potential for easier manufacturing, lower cost, and improved performance. This section describes the theoretical and experimental work performed during Supplemental #3 on the “laminated ladder-track” concept. During Supplemental #1 and #2, a sub-scale test rig was constructed at Lawrence Livermore National Laboratory to test the laminated track concept, and compare with theoretical predictions. Previously, two types of magnet configurations were tested: a single-sided magnet array with 5 magnets on top, and a “5x3 magnet array” with

5 magnets on the top and 3 magnets on the bottom magnet structure. During this phase of the effort, we developed:

- A "fields-based" analysis technique to accurately analyze the forces and the losses in a laminated track. The detailed formulation of the approach and comparison with experiments is published in a Maglev 2004 conference paper, provided in Appendix C.
- Measurement of the lift and drag forces of a "5x4" magnet array, which has the potential to be more efficient as far as eddy current losses are concerned.

The laminated track is made up of thin conductor sheets, bonded together and reinforced above and below with thin sheets of fiber composite, for example, G-10 fiberglass or carbon-fiber-filled epoxy. To create the ladder-track type of circuits, the conductor sheets are slotted in the transverse direction, with the slots being terminated at the edges of the sheet, so as to allow for current flow in the longitudinal direction (as in the shorting bus bars of the litz-wire cable ladder track). This configuration is shown schematically in Figure 3.4-1.

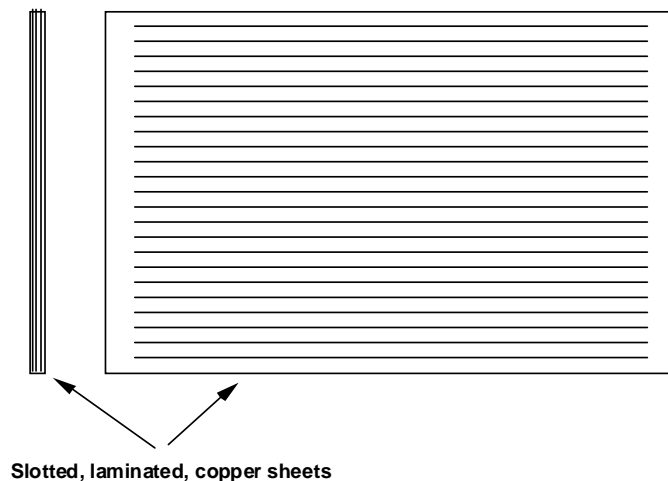


Figure 3.4-1
Schematic drawing of laminated track configuration

3.4.1 Laminated Track Test Rig.

The Laminated Track Test Rig was designed and built to provide an experimental check on the laminated-track computer code calculations and to help build a data base for designing a laminated track system. The use of this rig enabled making accurate measurements (as a function of velocity) of the lift, drag, and stiffness coefficients of a laminated track interacting with both single and double Halbach array configurations. In the test rig, a section of laminated track is pulled (on precision guide rails) through a Halbach array assembly and mount which is instrumented to measure the lift and the drag forces. The critical dimensions of the test rig, i.e., wavelength of the Halbach arrays, and the thickness of the laminated track, are scaled down by a factor of four from a full-size system. As a result, the data that are taken can be extrapolated to a full-size system by using known scaling laws. By moving the track instead of the Halbach

arrays, and by using pressure sensors with near-zero displacement under load, all inertial and displacement-sensitive corrections to the forces are eliminated, simplifying data reduction and improving the experimental accuracy.

Figure 3.4-2 is a photograph of the test rig, showing the assembly that holds the Halbach array and the vertical force sensor, together with the carrier for the laminated track elements, propelled through the Halbach arrays by a gravity-driven pulley-and-weight system (not shown).

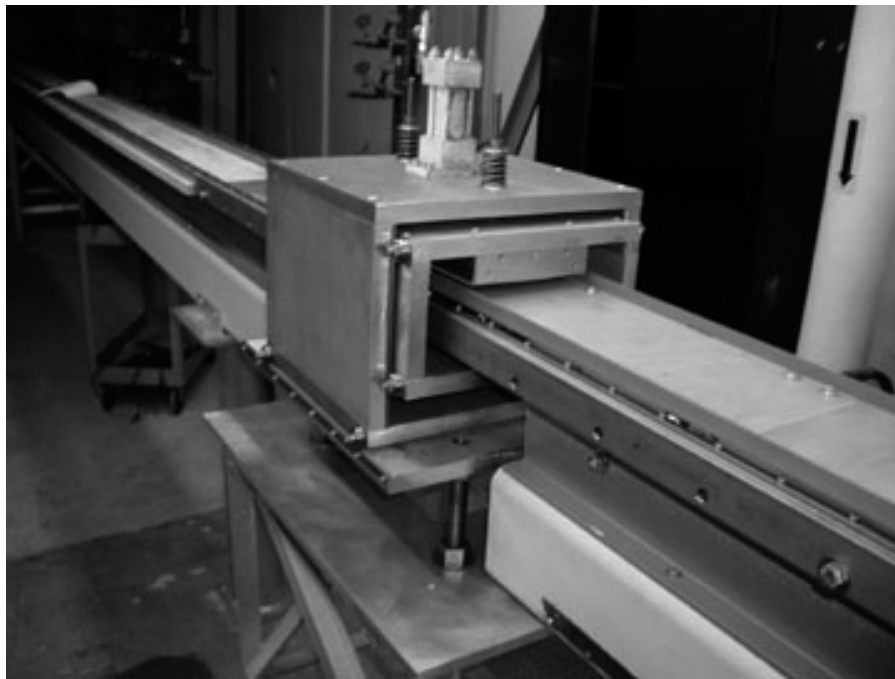


Figure 3.4-2
Photograph of test rig, showing assembly within which Halbach arrays are mounted, vertical force sensor, and movable carrier for the laminated track

The track itself is made up of a stack of 0.5 mm thick copper sheets. The sheets are 20 cm wide and the slots in the sheet are 15 cm wide, leaving “shorting” strips at each end that are 2.5 cm in width. The slots, made by chemical etching, using printed circuit techniques, are 0.5 mm wide, and the strip conductors between them are 2.5 mm wide. The laminate stack is 15 sheets thick. Longitudinally, the track is constructed of three such stacks, each approximately 75 cm long. The stacks are butted together at their ends, but no provision was made for longitudinal electrical conduction continuity of the track at the butt joints.

The stacks are mounted on a carrier “cart” equipped with v-grooved rollers that are captured between precision-ground guide rails, ensuring accurate vertical and horizontal positioning of the cart. Since the peak forces exerted by the Halbach arrays on the track are large (100 kg or more), the rollers were spaced at many locations along the cart and additional support against vertical displacements was provided by rubber-tired rollers, located so as to engage the cart as it passed through the Halbach-array mounting structure. Even with these precautions local

deflections of a fraction of a millimeter occurred in some situations, leading to measurement errors that were, however, deemed to be acceptably small upon analysis of the data and the computer-code results.

As previously noted, the choice to move the track under stationary Halbach arrays rather than vice-versa was based on the consideration that the force measurements could be made without any influence from inertial effects, since “zero-displacement” force sensors could be used. Based on previous experience, our choice was to use spring-loaded hydraulic pistons equipped with solid-state pressure sensors for the force measurements. To measure the velocity of the track as it moved through the Halbach array assembly we employed a tachometer generator attached to a rubber-edged wheel that engaged the edge of the cart as it moved by. Both systems worked well in the experiments.

The track is propelled through the Halbach arrays by a flexible stainless-steel cable that was tensioned by a gravity-driven pulley-and-weight system. The design of the drive system was based on a simple analytical formula for such systems. In order to achieve adequate acceleration, i.e., to accelerate the cart (weight about 50 kg), to velocities of order 10 m/s in the available distance of 4 m, accelerations of order 1.0 g are required. As the analysis showed, accelerations this high can only be obtained in a gravity-driven system by using a multi-cable system, in our case a four-pulley, four-cable system. The driver weight consisted of a stack of lead bricks loaded onto a carrier attached to the end of the steel cable.

3.4.2 Test Results

During Supplemental #2, we tested a single-sided and a “5x3” magnet array. Those results are discussed in the Supplemental #2 Completion Report (GA-C24496). The “5x3” magnet array is what is currently being used on the test track. The “5x4” array tested here is of interest because of its higher lift-to-drag ratio (i.e., more efficient), and its stiffer suspension characteristics (less motion of the primary magnetic system). For the tests below the test rig at LLNL was reconfigured in the 5x4 configuration and the appropriate parameters were entered into the levitation code to allow comparisons with the theoretical models. Owing to the additional “stiffness” of a double-sided configuration, the experimental data obtained are much more sensitive to small errors in the gap, and this sensitivity was observed in the scatter in the data. Nevertheless the results obtained showed agreement within the estimated experimental error with the code predictions. Figures 3.4-3 and 3.4-4 show measured values of lift and drag forces for the 5x4 magnet array configuration, and compared with theoretical predictions. Upper and lower curves represent displacements of ± 1 mm from the actual measured gap (this quantifies the effect on the measurements of gap variations from track geometrical distortions arising from levitation forces and other sources). These variations are accentuated for sub-scale testing.

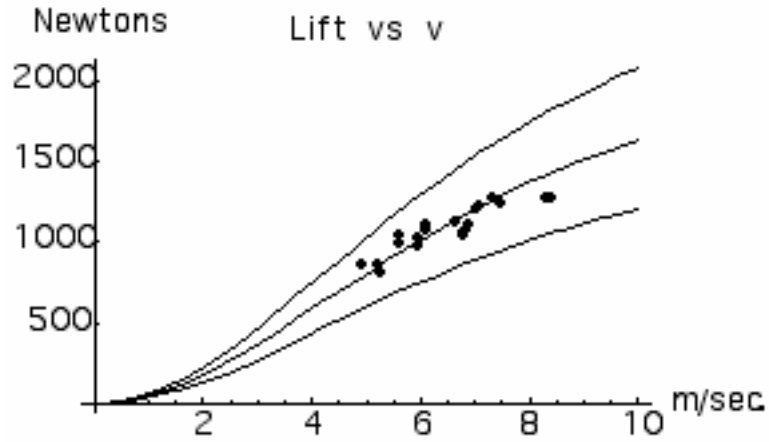


Figure 3.4-3
Lift force versus speed for the “5x4” magnet array,
compared with theoretical predictions

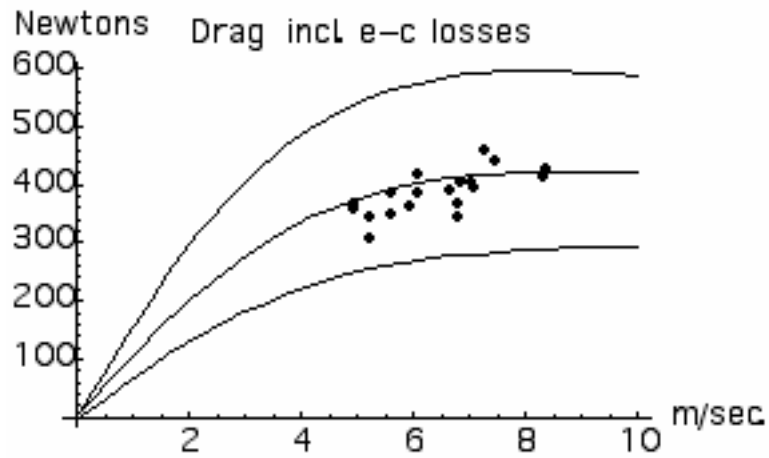
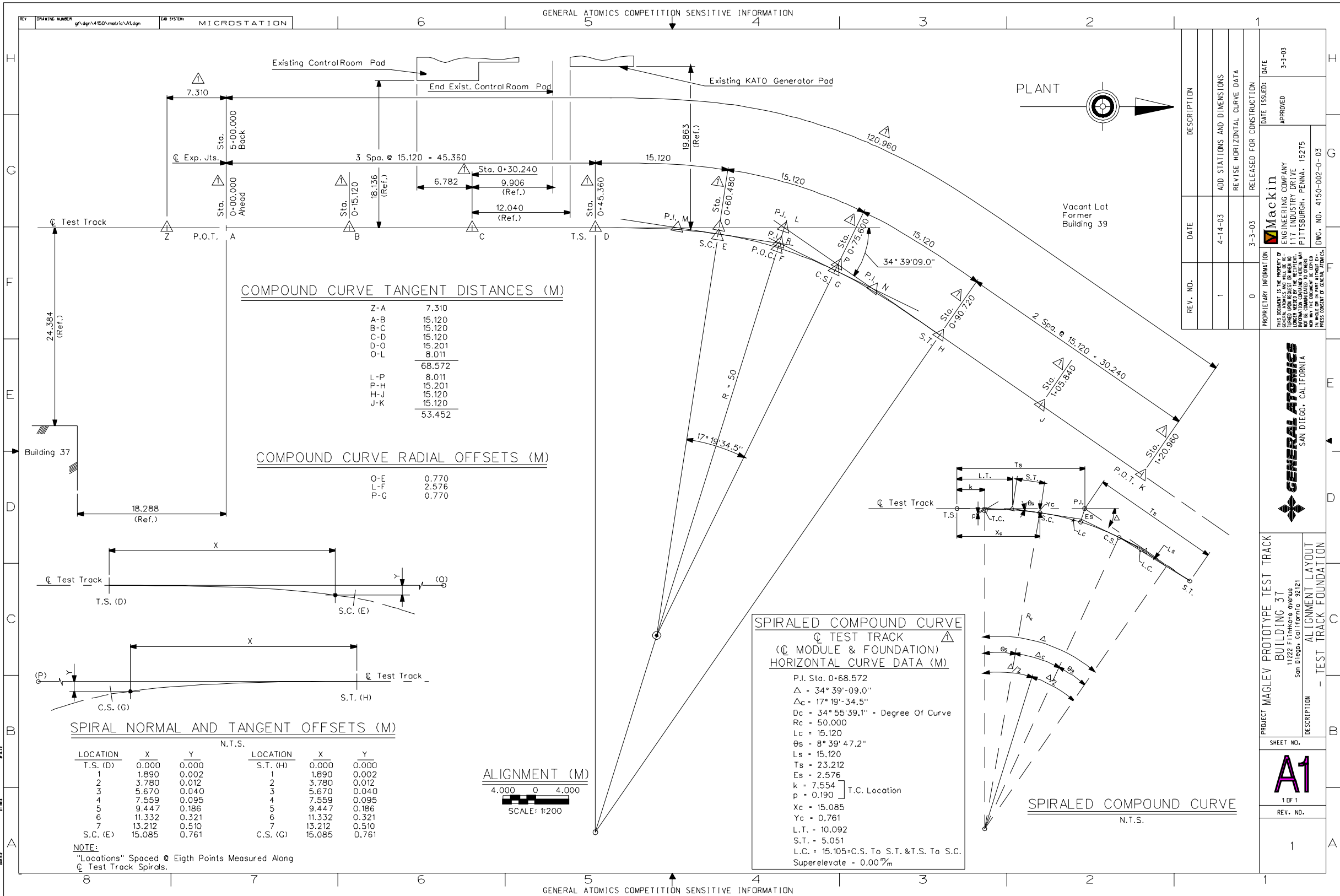


Figure 3.4-4
Magnetic drag force versus speed for the “5x4” magnet array,
compared with theoretical predictions

This page intentionally left blank



COMPOUND CURVE TANGENT DISTANCES (M)

Z-A	7.310
A-B	15.120
B-C	15.120
C-D	15.120
D-O	15.201
O-L	8.011
L-P	8.011
P-H	15.201
H-J	15.120
J-K	15.120
Total	68.572
L-F	2.576
P-G	0.770
Total	53.452

COMPOUND CURVE RADIAL OFFSETS (M)

O-E	0.770
L-F	2.576
P-G	0.770

SPIRALED COMPOUND CURVE
 (Q TEST TRACK)
 (Q MODULE & FOUNDATION)
 HORIZONTAL CURVE DATA (M)

P.I. Sta. 0+68.572
 $\Delta = 34^\circ 39' 09.0''$
 $\Delta_c = 17^\circ 19' 34.5''$
 $D_c = 34^\circ 55' 39.1'' = \text{Degree Of Curve}$
 $R_c = 50.000$
 $L_c = 15.120$
 $\theta_s = 8^\circ 39' 47.2''$
 $L_s = 15.120$
 $T_s = 23.212$
 $E_s = 2.576$
 $k = 7.554$ T.C. Location
 $p = 0.190$
 $X_c = 15.085$
 $Y_c = 0.761$
 $L.T. = 10.092$
 $S.T. = 5.051$
 $L.C. = 15.105 = C.S. \text{ To } S.T. \text{ \& } T.S. \text{ To } S.C.$
 Superelevate = 0.00%

SPIRAL NORMAL AND TANGENT OFFSETS (M)

N.T.S.		
LOCATION	X	Y
T.S. (D)	0.000	0.000
1	1.890	0.002
2	3.780	0.012
3	5.670	0.040
4	7.559	0.095
5	9.447	0.186
6	11.332	0.321
7	13.212	0.510
S.C. (E)	15.085	0.761



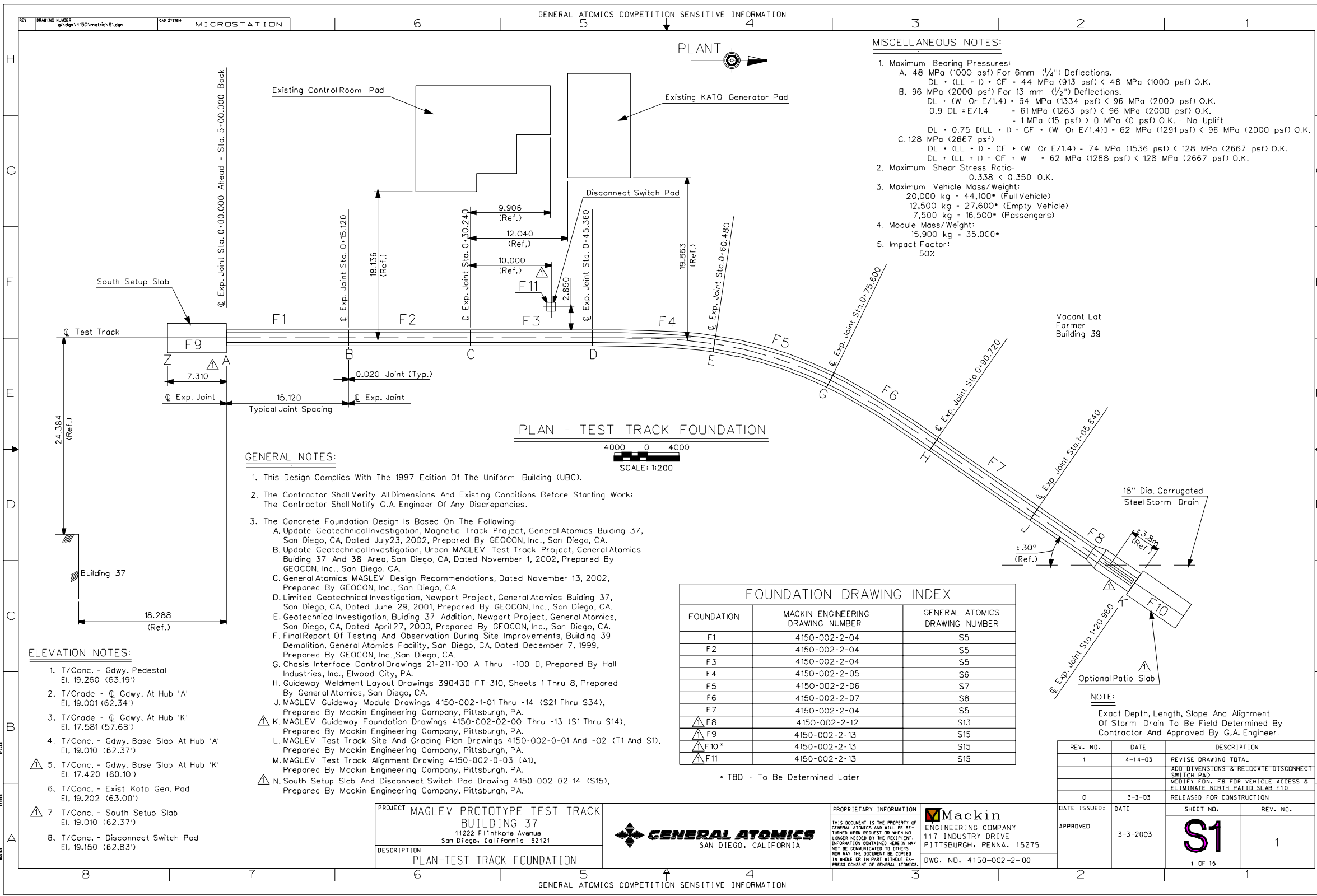
REV. NO.	DATE	DESCRIPTION
1	4-14-03	ADD STATIONS AND DIMENSIONS
0	3-3-03	RELEASED FOR CONSTRUCTION

DATE ISSUED: 3-3-03
 APPROVED: [Signature]
 PROJECT: MAGLEV PROTOTYPE TEST TRACK
 BUILDING 37
 11222 Finkbine Avenue
 San Diego, California 92121
 DESCRIPTION: ALIGNMENT LAYOUT
 TEST TRACK FOUNDATION



PROJECT: MAGLEV PROTOTYPE TEST TRACK
 BUILDING 37
 11222 Finkbine Avenue
 San Diego, California 92121
 DESCRIPTION: ALIGNMENT LAYOUT
 TEST TRACK FOUNDATION

SHEET NO. **A1**
 1 OF 1
 REV. NO. 1



- MISCELLANEOUS NOTES:**
- Maximum Bearing Pressures:
 - A. 48 MPa (1000 psf) For 6mm (1/4") Deflections.
DL + (LL + I) + CF + 44 MPa (913 psf) < 48 MPa (1000 psf) O.K.
 - B. 96 MPa (2000 psf) For 13 mm (1/2") Deflections.
DL + (W Or E/1.4) + 64 MPa (1334 psf) < 96 MPa (2000 psf) O.K.
0.9 DL + E/1.4 + 61 MPa (1263 psf) < 96 MPa (2000 psf) O.K.
+ 1 MPa (15 psf) > 0 MPa (0 psf) O.K. - No Uplift
 - C. 128 MPa (2667 psf)
DL + (LL + I) + CF + (W Or E/1.4) + 74 MPa (1536 psf) < 128 MPa (2667 psf) O.K.
DL + (LL + I) + CF + W + 62 MPa (1288 psf) < 128 MPa (2667 psf) O.K.
 - Maximum Shear Stress Ratio: 0.338 < 0.350 O.K.
 - Maximum Vehicle Mass/Weight:
 - 20,000 kg = 44,100* (Full Vehicle)
 - 12,500 kg = 27,600* (Empty Vehicle)
 - 7,500 kg = 16,500* (Passengers)
 - Module Mass/Weight: 15,900 kg = 35,000*
 - Impact Factor: 50%

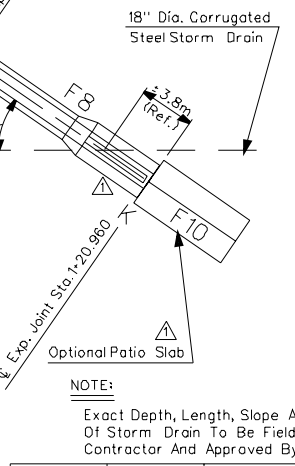
- GENERAL NOTES:**
- This Design Complies With The 1997 Edition Of The Uniform Building (UBC).
 - The Contractor Shall Verify All Dimensions And Existing Conditions Before Starting Work: The Contractor Shall Notify G.A. Engineer Of Any Discrepancies.
 - The Concrete Foundation Design Is Based On The Following:
 - A. Update Geotechnical Investigation, Magnetic Track Project, General Atomics Building 37, San Diego, CA, Dated July 23, 2002, Prepared By GEOCON, Inc., San Diego, CA.
 - B. Update Geotechnical Investigation, Urban MAGLEV Test Track Project, General Atomics Building 37 And 38 Area, San Diego, CA, Dated November 1, 2002, Prepared By GEOCON, Inc., San Diego, CA.
 - C. General Atomics MAGLEV Design Recommendations, Dated November 13, 2002, Prepared By GEOCON, Inc., San Diego, CA.
 - D. Limited Geotechnical Investigation, Newport Project, General Atomics Building 37, San Diego, CA, Dated June 29, 2001, Prepared By GEOCON, Inc., San Diego, CA.
 - E. Geotechnical Investigation, Buidng 37 Addition, Newport Project, General Atomics, San Diego, CA, Dated April 27, 2000, Prepared By GEOCON, Inc., San Diego, CA.
 - F. Final Report Of Testing And Observation During Site Improvements, Building 39 Demolition, General Atomics Facility, San Diego, CA, Dated December 7, 1999, Prepared By GEOCON, Inc., San Diego, CA.
 - G. Chassis Interface Control Drawings 21-211-100 A Thru -100 D, Prepared By Hall Industries, Inc., Elwood City, PA.
 - H. Guideway Weldment Layout Drawings 390430-FT-310, Sheets 1 Thru 8, Prepared By General Atomics, San Diego, CA.
 - J. MAGLEV Guideway Module Drawings 4150-002-1-01 Thru -14 (S21 Thru S34), Prepared By Mackin Engineering Company, Pittsburgh, PA.
 - K. MAGLEV Guideway Foundation Drawings 4150-002-02-00 Thru -13 (S1 Thru S14), Prepared By Mackin Engineering Company, Pittsburgh, PA.
 - L. MAGLEV Test Track Site And Grading Plan Drawings 4150-002-0-01 And -02 (T1 And S1), Prepared By Mackin Engineering Company, Pittsburgh, PA.
 - M. MAGLEV Test Track Alignment Drawing 4150-002-0-03 (A1), Prepared By Mackin Engineering Company, Pittsburgh, PA.
 - N. South Setup Slab And Disconnect Switch Pad Drawing 4150-002-02-14 (S15), Prepared By Mackin Engineering Company, Pittsburgh, PA.

- ELEVATION NOTES:**
- T/Conc. - Gdwy. Pedestal
El. 19.260 (63.19')
 - T/Grade - @ Gdwy. At Hub 'A'
El. 19.001 (62.34')
 - T/Grade - @ Gdwy. At Hub 'K'
El. 17.581 (57.68')
 - T/Conc. - Gdwy. Base Slab At Hub 'A'
El. 19.010 (62.37')
 - T/Conc. - Gdwy. Base Slab At Hub 'K'
El. 17.420 (60.10')
 - T/Conc. - Exist. Kato Gen. Pad
El. 19.202 (63.00')
 - T/Conc. - South Setup Slab
El. 19.010 (62.37')
 - T/Conc. - Disconnect Switch Pad
El. 19.150 (62.83')

FOUNDATION DRAWING INDEX

FOUNDATION	MACKIN ENGINEERING DRAWING NUMBER	GENERAL ATOMICS DRAWING NUMBER
F1	4150-002-2-04	S5
F2	4150-002-2-04	S5
F3	4150-002-2-04	S5
F4	4150-002-2-05	S6
F5	4150-002-2-06	S7
F6	4150-002-2-07	S8
F7	4150-002-2-04	S5
F8	4150-002-2-12	S13
F9	4150-002-2-13	S15
F10*	4150-002-2-13	S15
F11	4150-002-2-13	S15

* TBD - To Be Determined Later



NOTE:
Exact Depth, Length, Slope And Alignment Of Storm Drain To Be Field Determined By Contractor And Approved By G.A. Engineer.

REV. NO.	DATE	DESCRIPTION
1	4-14-03	REVISE DRAWING TOTAL ADD DIMENSIONS & RELOCATE DISCONNECT SWITCH PAD
0	3-3-03	MODIFY FDN. F8 FOR VEHICLE ACCESS & ELIMINATE NORTH PATIO SLAB F10 RELEASED FOR CONSTRUCTION

DATE ISSUED:	DATE	SHEET NO.	REV. NO.
APPROVED	3-3-2003	S1	1

1 OF 15

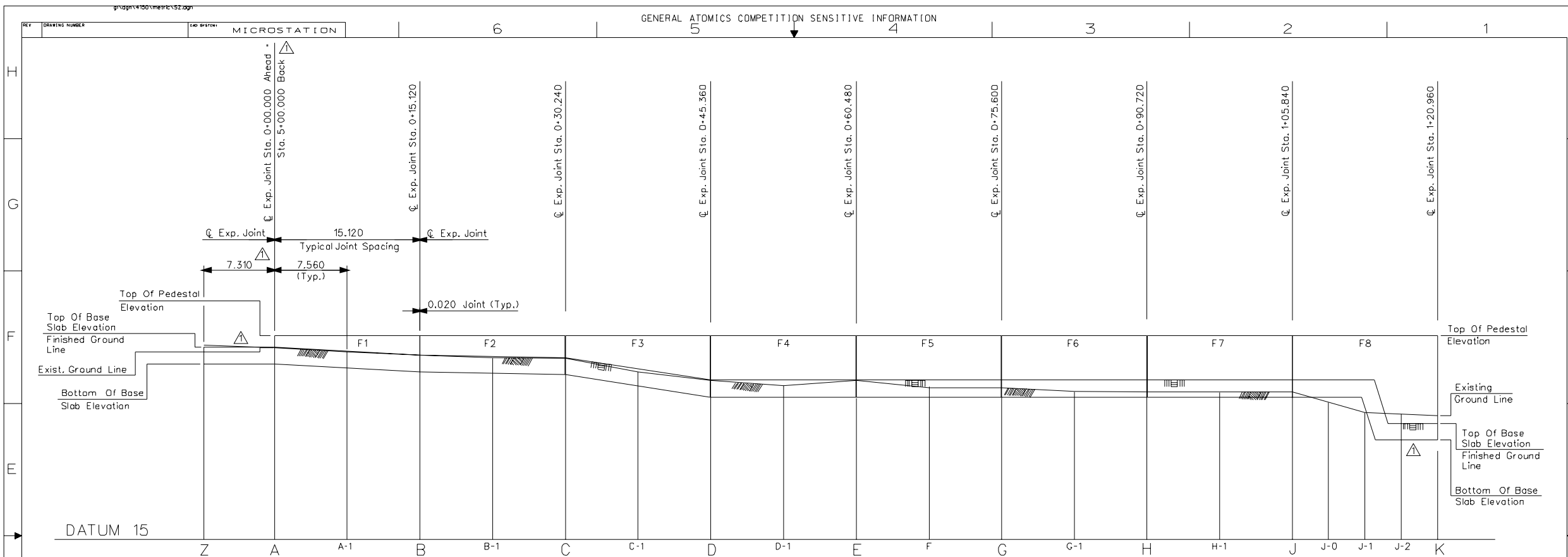
PROJECT **MAGLEV PROTOTYPE TEST TRACK BUILDING 37**
11222 FlintKote Avenue
San Diego, California 92121

DESCRIPTION
PLAN-TEST TRACK FOUNDATION



PROPRIETARY INFORMATION
THIS DOCUMENT IS THE PROPERTY OF GENERAL ATOMICS AND WILL BE RETURNED UPON REQUEST OR WHEN NO LONGER NEEDED BY THE RECIPIENT. INFORMATION CONTAINED HEREIN MAY NOT BE COMMUNICATED TO OTHERS AND MAY BE COPIED IN WHOLE OR IN PART WITHOUT EXPRESS CONSENT OF GENERAL ATOMICS.

Mackin ENGINEERING COMPANY
117 INDUSTRY DRIVE
PITTSBURGH, PENNA. 15275
DWG. NO. 4150-002-2-00



ELEVATION - TEST TRACK FOUNDATION



TEST TRACK ELEVATIONS

FOUNDATION	LOCATION	TOP OF PEDESTAL	TOP OF BASE SLAB	BOTTOM OF BASE SLAB	EAST FACE EXISTING GROUND	CENTERLINE EXISTING GROUND	WEST FACE EXISTING GROUND
F9	Z	19.010	18.660	18.967	19.050	19.133	
	A	19.010	18.660	18.929	19.001	19.062	
F1	A	19.260	19.010	18.660	18.961	19.035	
	A-1				18.880	18.952	
F2	B		18.850	18.500	18.832	18.864	
	B-1		18.850	18.500	18.832	18.864	
F3	C				18.777	18.797	
	C-1				18.790	18.696	
	D				18.790	18.696	
F4	D-1				18.502	18.484	
	E		18.320	17.970	18.302	18.312	
F5	F		18.320	17.970	18.302	18.306	
	G		18.320	17.970	18.208	18.212	
F6	G-1				18.212	18.216	
	H		18.320	17.970	18.268	18.312	
F7	H-1		18.320	17.970	18.268	18.346	
	J				18.190	18.140	
F8	J-0		18.320	17.970	18.144	18.150	
	J-1		18.320	17.970	18.144	18.150	
	J-2		18.320	17.970	18.086	18.092	
	K		18.320	17.970	18.049	18.069	
			18.320	17.970	18.049	18.069	

* - Interpolated Value

PROJECT MAGLEV PROTOTYPE TEST TRACK BUILDING 37
11222 Flintkote Avenue
San Diego, California 92121



PROPRIETARY INFORMATION
THIS DOCUMENT IS THE PROPERTY OF GENERAL ATOMICS AND WILL BE RETURNED UPON REQUEST OR WHEN NO LONGER NEEDED BY THE RECIPIENT. INFORMATION CONTAINED HEREIN MAY NOT BE COMMUNICATED TO OTHERS NOR MAY THE DOCUMENT BE COPIED IN WHOLE OR IN PART WITHOUT EXPRESS CONSENT OF GENERAL ATOMICS.

Mackin ENGINEERING COMPANY
117 INDUSTRY DRIVE
PITTSBURGH, PENNA. 15275
DWG. NO. 4150-002-2-01

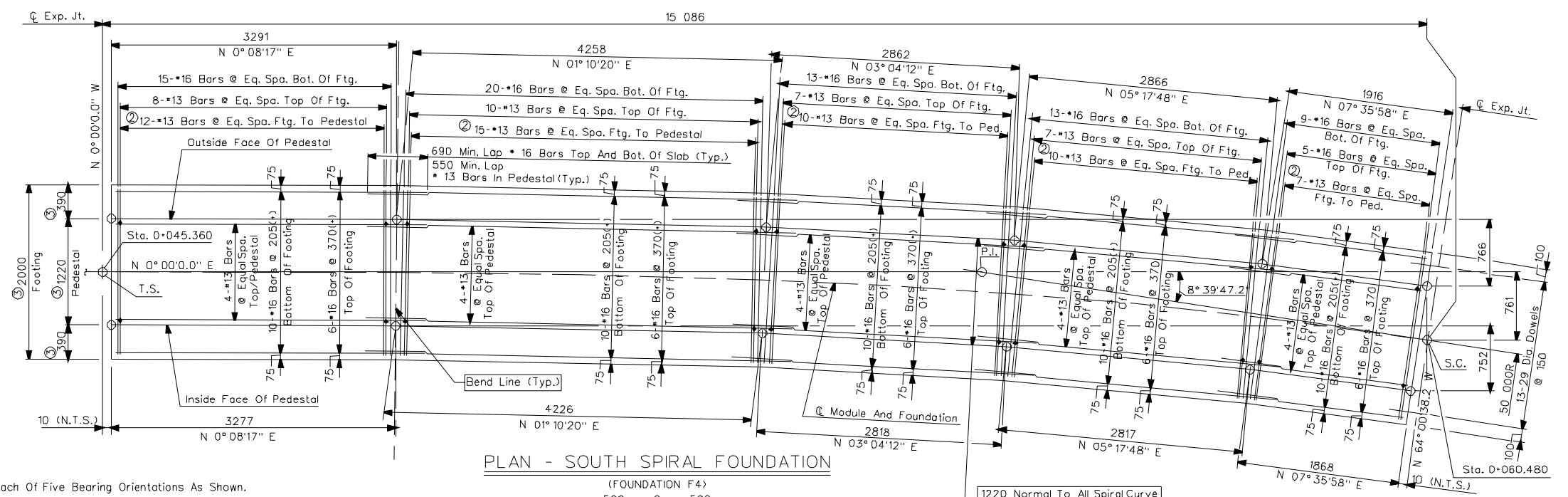
REV. NO.	DATE	DESCRIPTION
1	4-14-03	REVISE DRAWING TOTAL
		REVISE STATION & ADD DIMENSION
		MODIFY FDN. FB FOR VEHICLE ACCESS & ADD SOUTH SETUP SLAB
0	3-3-03	RELEASED FOR CONSTRUCTION

DATE ISSUED: 3-3-2003

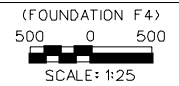
APPROVED

SHEET NO. **S2** REV. NO. 1

2 OF 15

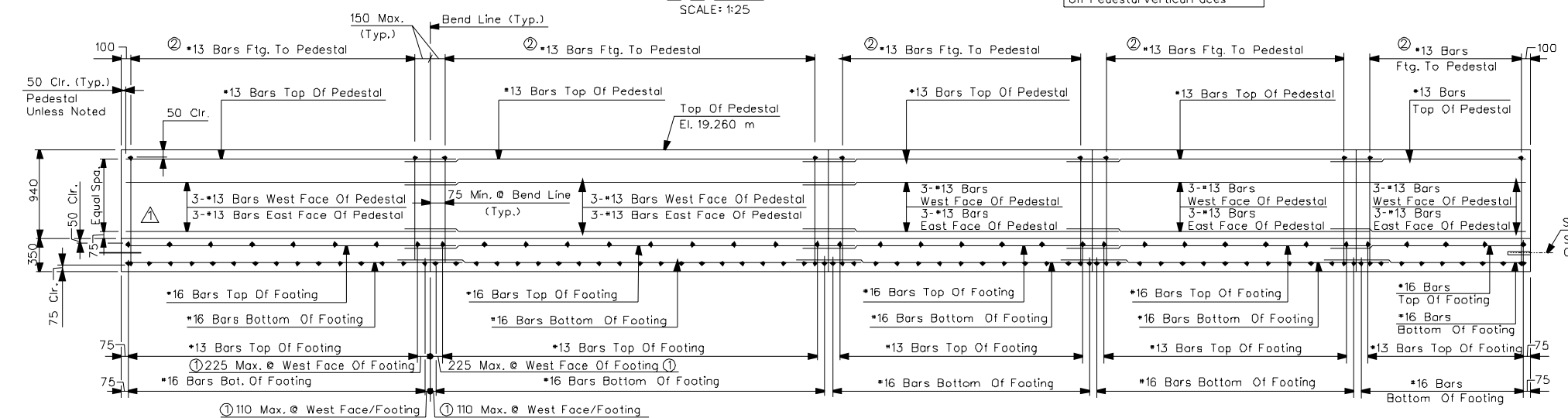


PLAN - SOUTH SPIRAL FOUNDATION

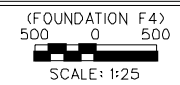


1220 Normal To All Spiral Curve Simulations With Parallel Chords On Pedestal Vertical Faces

③ Typ. @ Each Of Five Bearing Orientations As Shown.



ELEVATION - SOUTH SPIRAL FOUNDATION



NOTES:
 • Refer To Sheet A1 For Listing Of Horizontal Geometry Data For "Module And Foundation" As A Spiraled Compound Curve.

① Typ. About Each Bend Line Of Foundation F4
 ② See Sht. 5 "TYPICAL SECTION" And "OPTIONAL SECTION"

KEY:
 Eq. Spa. - Equal Spacing
 Exp. Jt. - Expansion Joint
 Bot. - Bottom
 Ftg. - Footing
 Ped. - Pedestal

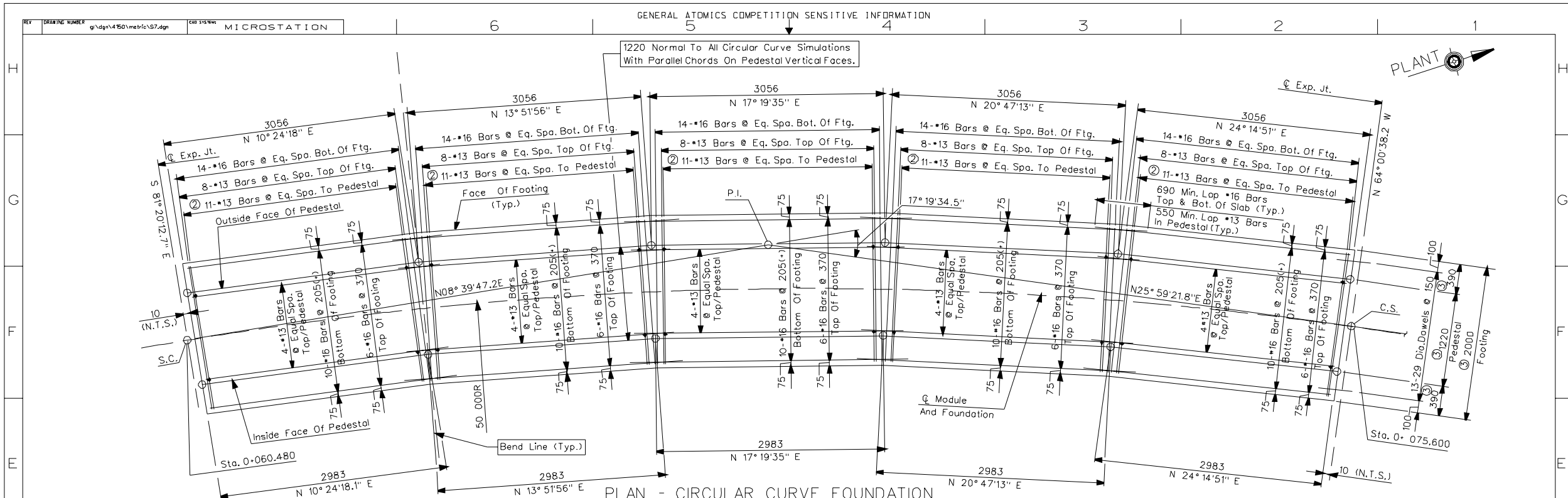
PROJECT MAGLEV PROTOTYPE TEST TRACK BUILDING 37
 11222 Flintkote Avenue
 San Diego, California 92121
 DESCRIPTION SOUTH SPIRAL FOUNDATION - TEST TRACK FOUNDATION



PROPRIETARY INFORMATION
 THIS DOCUMENT IS THE PROPERTY OF GENERAL ATOMICS AND WILL BE RETURNED UPON REQUEST OR WHEN NO LONGER NEEDED BY THE RECIPIENT. INFORMATION CONTAINED HEREIN MAY NOT BE COMMUNICATED TO OTHERS NOR MAY THE DOCUMENT BE COPIED IN WHOLE OR IN PART WITHOUT EXPRESS CONSENT OF GENERAL ATOMICS.
Mackin
 ENGINEERING COMPANY
 117 INDUSTRY DRIVE
 PITTSBURGH, PENNA. 15275
 DWG. NO. 4150-002-1-05

REV. NO.	DATE	DESCRIPTION
1	4-14-03	REVISE DRAWING TOTAL
0	3-03-03	RELEASED FOR CONSTRUCTION

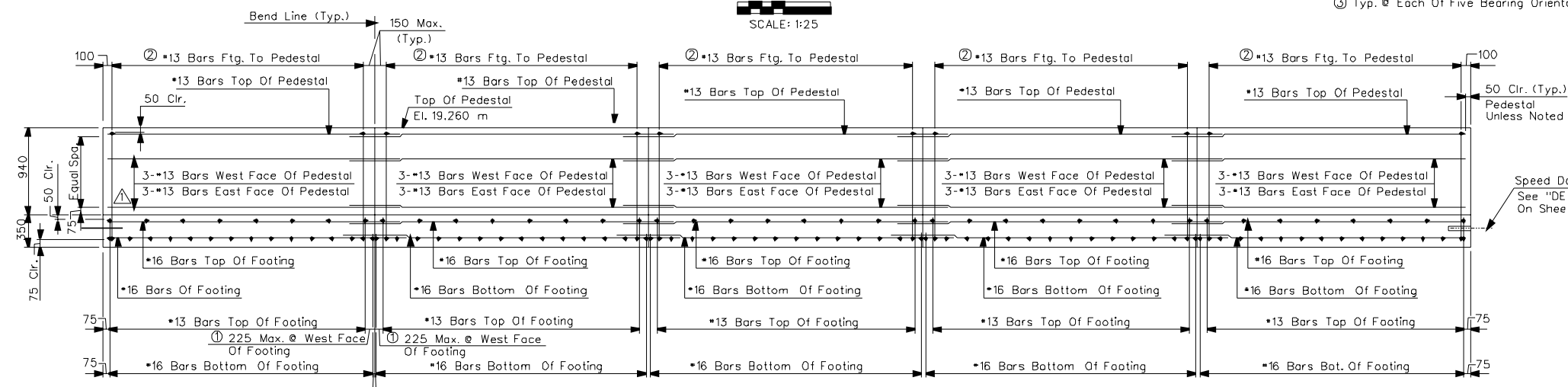
DATE ISSUED:	DATE	SHEET NO.	REV. NO.
APPROVED	3-03-2003	S6 6 OF 15	1



PLAN - CIRCULAR CURVE FOUNDATION

(FOUNDATION F5)
500 0 500
SCALE: 1:25

③ Typ. @ Each Of Five Bearing Orientations As Shown.



ELEVATION - CIRCULAR CURVE FOUNDATION

(FOUNDATION F5)
500 0 500
SCALE: 1:25

NOTES:
• Refer To Sheet A1 For Listing Of Horizontal Geometry Data For "Module And Foundation" As A Spiraled Compound Curve.

KEY:
Eq. Spa. - Equal Spacing
Exp. Jt. - Expansion Joint
Bot. - Bottom
Ftg. - Footing
Ped. - Pedestal

① Typ. @ Each Bend Line
② See Sht. 5 "TYPICAL SECTION" And "OPTIONAL SECTION"

PROJECT MAGLEV PROTOTYPE TEST TRACK
BUILDING 37
11222 Flintkote Avenue
San Diego, California 92121
DESCRIPTION CIRCULAR CURVE FOUNDATION
-TEST TRACK FOUNDATION

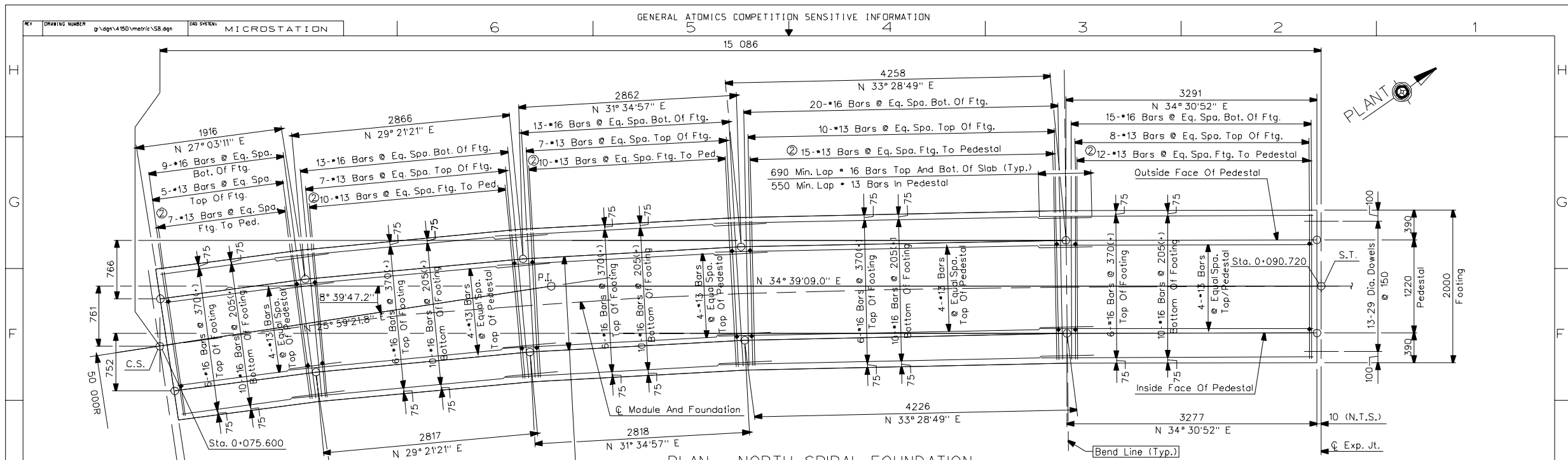


PROPRIETARY INFORMATION
THIS DOCUMENT IS THE PROPERTY OF GENERAL ATOMICS AND WILL BE RETURNED UPON REQUEST OR WHEN NO LONGER NEEDED BY THE RECIPIENT. INFORMATION CONTAINED HEREIN MAY NOT BE COMMUNICATED TO OTHERS NOR MAY THE DOCUMENT BE COPIED IN WHOLE OR IN PART WITHOUT EXPRESS CONSENT OF GENERAL ATOMICS.

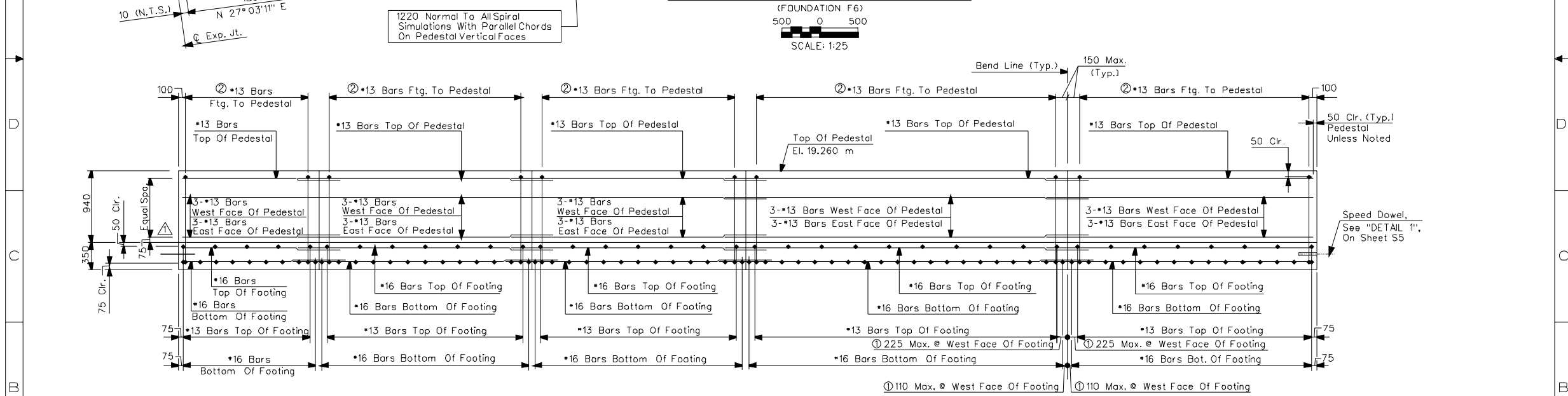
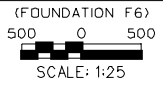
Mackin
ENGINEERING COMPANY
117 INDUSTRY DRIVE
PITTSBURGH, PENNA. 15275
DWG. NO. 4150-002-1-06

REV. NO.	DATE	DESCRIPTION
1	4-14-03	REVISE DRAWING TOTAL
0	3-03-03	RELEASED FOR CONSTRUCTION

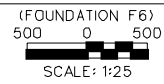
DATE ISSUED:	DATE	SHEET NO.	REV. NO.
APPROVED	3-03-2003	S7	1



PLAN - NORTH SPIRAL FOUNDATION



ELEVATION - NORTH SPIRAL FOUNDATION



KEY:
 Eq. Spa. = Equal Spacing
 Exp. Jt. = Expansion Joint
 Bot. = Bottom
 Ftg. = Footing
 Ped. = Pedestal

① Typ. @ Each Bend Line
 ② See Sht. 5 "TYPICAL SECTION" And "OPTIONAL SECTION"

NOTES:
 • Refer To Sheet A1 For Listing Of Horizontal Geometry Data For "© Module And Foundation" As A Spiraled Compound Curve.

REV. NO.	DATE	DESCRIPTION
1	4-14-03	REVISE DRAWING TOTAL
0	3-03-03	ADD DOWEL BARS TO SOUTH END OF SLAB RELEASED FOR CONSTRUCTION

DATE ISSUED:	DATE	SHEET NO.	REV. NO.
APPROVED	3-03-2003	S8 8 OF 15	1

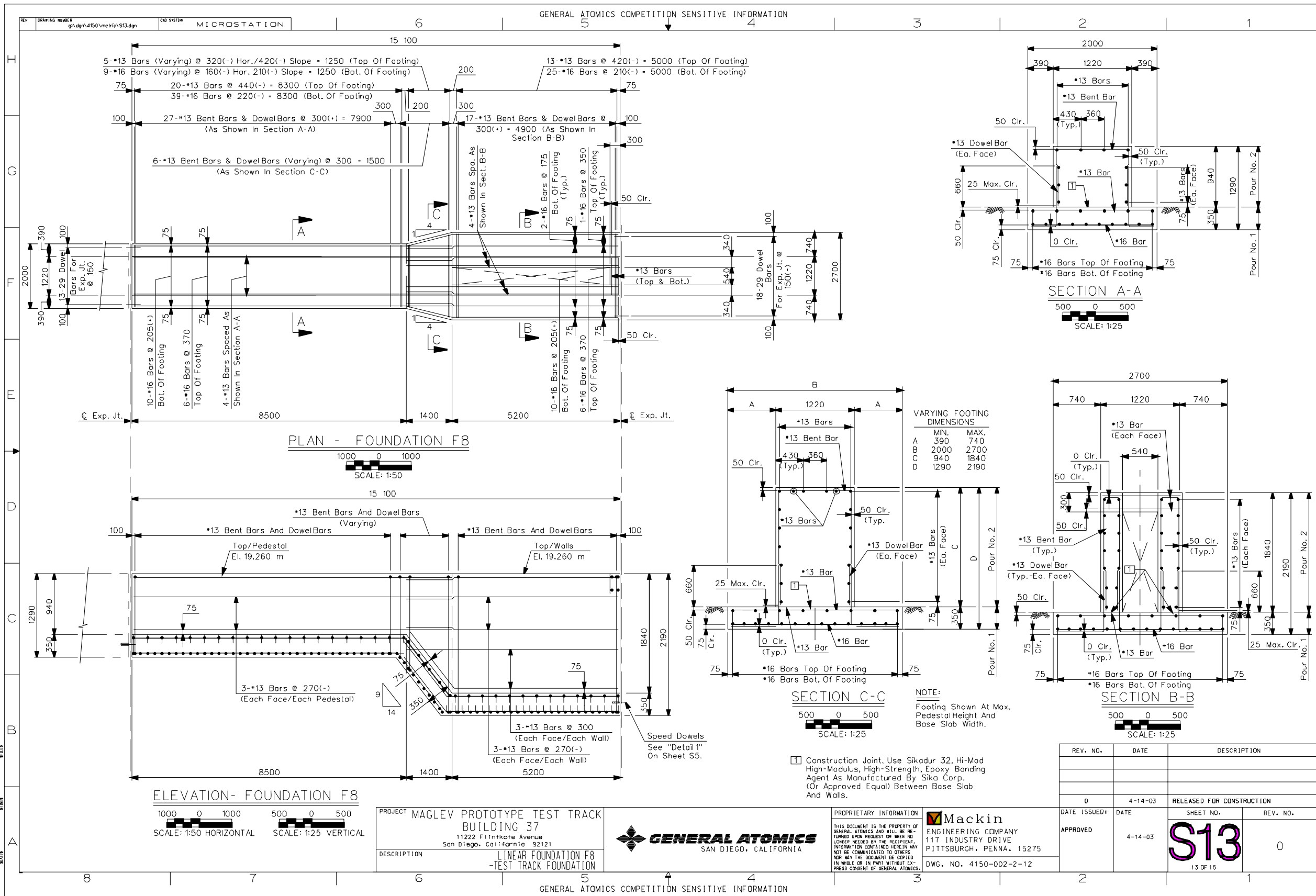
PROJECT: MAGLEV PROTOTYPE TEST TRACK BUILDING 37
 11222 Flintkate Avenue
 San Diego, California 92121

DESCRIPTION: NORTH SPIRAL FOUNDATION - TEST TRACK FOUNDATION



PROPRIETARY INFORMATION
 THIS DOCUMENT IS THE PROPERTY OF GENERAL ATOMICS AND WILL BE RETURNED UPON REQUEST OR WHEN NO LONGER NEEDED BY THE RECIPIENT. INFORMATION CONTAINED HEREIN MAY NOT BE COMMUNICATED TO OTHERS NOR MAY THE DOCUMENT BE COPIED IN WHOLE OR IN PART WITHOUT EXPRESS CONSENT OF GENERAL ATOMICS.

Mackin ENGINEERING COMPANY
 117 INDUSTRY DRIVE
 PITTSBURGH, PENNA. 15275
 DWG. NO. 4150-002-1-07



PLAN - FOUNDATION F8

SCALE: 1:50

ELEVATION- FOUNDATION F8

SCALE: 1:50 HORIZONTAL
SCALE: 1:25 VERTICAL

VARYING FOOTING DIMENSIONS

	MIN.	MAX.
A	390	740
B	2000	2700
C	940	1840
D	1290	2190

SECTION C-C

SCALE: 1:25

SECTION B-B

SCALE: 1:25

NOTE:
Footing Shown At Max. Pedestal Height And Base Slab Width.

Construction Joint. Use Sikadur 32, Hi-Mad High-Modulus, High-Strength, Epoxy Bonding Agent As Manufactured By Sika Corp. (Or Approved Equal) Between Base Slab And Walls.

PROJECT	MAGLEV PROTOTYPE TEST TRACK BUILDING 37
DESCRIPTION	LINEAR FOUNDATION F8 - TEST TRACK FOUNDATION

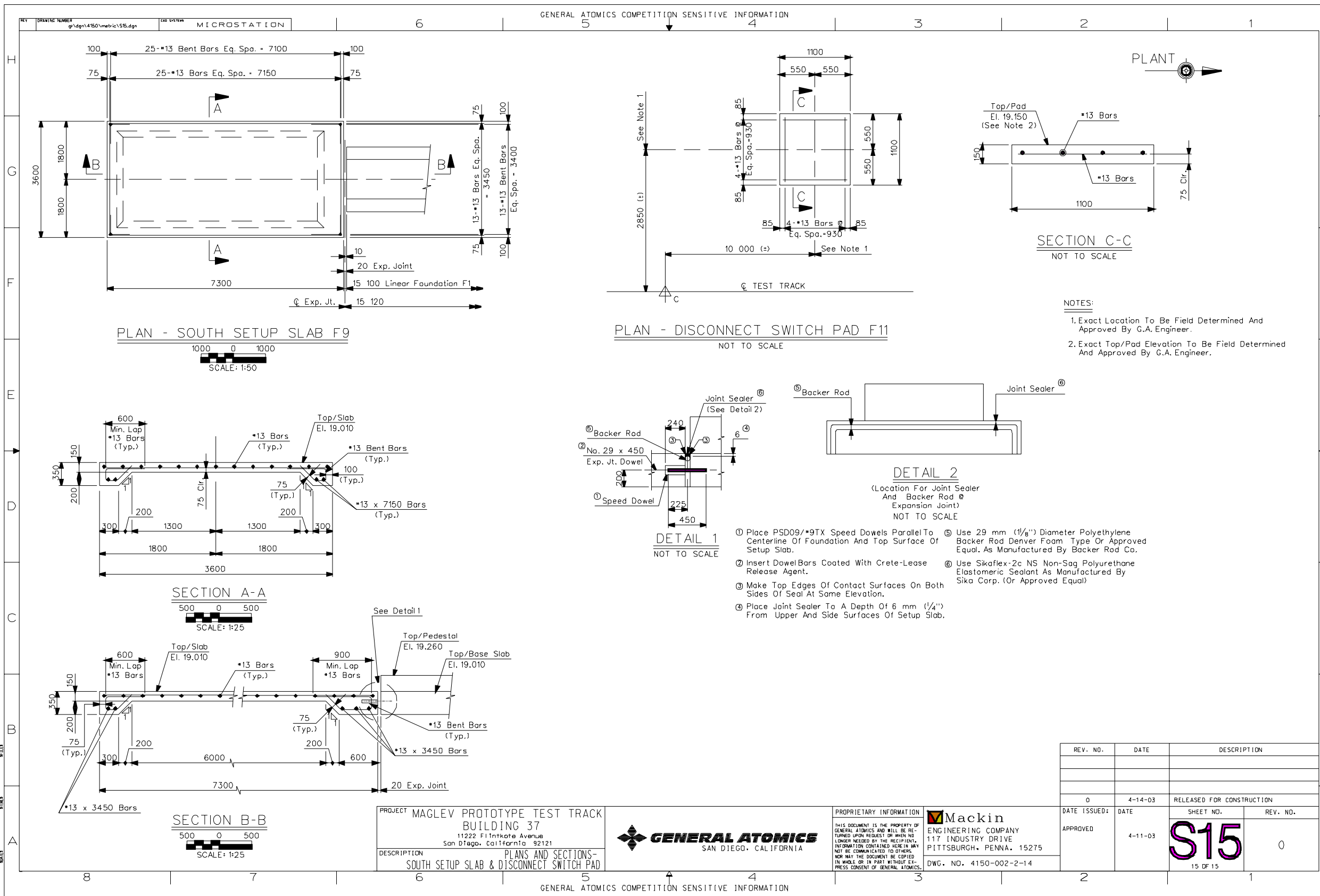


PROPRIETARY INFORMATION
THIS DOCUMENT IS THE PROPERTY OF GENERAL ATOMICS AND WILL BE RETURNED UPON REQUEST OR WHEN NO LONGER NEEDED BY THE RECIPIENT. INFORMATION CONTAINED HEREIN MAY NOT BE COMMUNICATED TO OTHERS NOR MAY THE DOCUMENT BE COPIED IN WHOLE OR IN PART WITHOUT EXPRESS CONSENT OF GENERAL ATOMICS.

Mackin ENGINEERING COMPANY
117 INDUSTRY DRIVE
PITTSBURGH, PENNA. 15275
DWG. NO. 4150-002-2-12

REV. NO.	DATE	DESCRIPTION
0	4-14-03	RELEASED FOR CONSTRUCTION

DATE ISSUED:	DATE	SHEET NO.	REV. NO.
APPROVED	4-14-03	S13	0



This page intentionally left blank

4. Conclusions

With the funding provided by this Supplemental #3, the construction of the General Atomics Urban Maglev test track has been completed. It is 120 meters in length, with a 50-meter radius curve. The facility includes a test chassis, electrical equipment to provide power to the track, all control and data acquisition equipment, and a control/electrical room for test operations. The following conclusions summarize the project status and findings to date.

- Detailed test and safety plans have been completed to provide a formal and safe framework for all testing operations.
- All static check-out testing of the power, propulsion, magnetics, track tolerances, and power equipment has been completed.
- Preliminary testing indicates more lift than the nominal 20–25 mm (which is desirable). However, this additional lift results in the vehicle inner wheels hitting the top-plate, contributing to dynamic oscillations, which need to be reduced.
- The measured lift-off speeds were below the goal value of 5 m/s for chassis weights up to 8,500 kg (which is desirable).
- The LSM propulsion system provides more than the maximum goal acceleration value of 1.6 m/s^2 , with accelerations of 2.5 m/s^2 .
- A few issues with respect to mechanical clearances and the control system were found, which need to be addressed. Specifically, the in-board wheels hit the top-plate, and the control system is not able to maintain the desired current and “motor angle.” The combination of insufficient mechanical clearances and control system not maintaining the desired motor angle, result in chassis oscillations, including a “pitching motion”.
- The original wiggly wire concept for speed and location detection did not work reliably due to electrical noise interference from the LSM windings. To solve the noise problem, a laser system was used for speed and location detection. While this system works well most of the time, it is not an all-weather solution. Therefore, development of a non-optical, eddy-current based sensor is planned, which based on laboratory tests, appears to be quite suitable.
- The laminated track testing performed on the sub-scale test facility at LLNL, shows good agreement with theoretical calculations performed using calculation tools developed on this program. The laminated track shows good performance potential with respect to manufacturing cost and electrical characteristics.

Based on these conclusions, a number of “*lessons learned*” are summarized below along with future technology development plans.

- *The mechanical clearances are too tight.* Adjustments are planned to the chassis to increase mechanical clearances of the wheels and magnets to eliminate interference between the wheel support structure on the chassis and the top plate on the guideway module.
- *The control system does not adequately control the I_d current (which controls the vertical lift force component of the LSM). It also overshoots the steady-state speed more than desired.* Better control of the operating motor angle and the speed profile software is planned by making modifications to the control system software.
- *All-weather operation of the speed and position detection system is needed.* A non-optical speed and position detection system on the chassis will be tested. A candidate which has been tested in a laboratory environment is a non-optical, “eddy current” sensor.
- *The pitching motion of the chassis needs to be reduced.* Addressing the first two items above should help provide greater control. In addition, it is planned to add a second chassis which will modify the mass moment of inertia, which will significantly reduce pitching motion.
- *The current track component design is labor-intensive to fabricate.* The large steel weldments undergo significant weld distortions during fabrication, and the litz track has significant number of parts, resulting in high manufacturing costs. Future plans include engineering and testing a “hybrid girder” (which eliminates the large steel structures), and a laminated track (which greatly reduces the number of parts as well as improves performance by reducing magnet drag).

5. References

1. Gurol S., Baldi R., and Post R.F., “Overview of the General Atomics Low Speed Urban Maglev Technology Development Program”, 17th International Conference on Magnetically Levitated Systems and Linear Drives, Lausanne, Switzerland, September 4-8, 2002.
2. R. F. Post, D. D. Ryutov, “The Inductrack: A Simpler Approach to Magnetic Levitation,” I.E.E.E, Transactions on Applied Superconductivity, **10**, 901 (2000)
3. U.S. Department of Transportation (Federal Transit Administration). Low Speed Maglev Technology Development Program – Final Report, FTA-CA-26-7025-02.1, March 2002.
4. David.W. Doll, Robert D. Blevins, and Dilip Bhadra, “Ride Dynamics of an Urban Maglev,” Maglev 2002, Lausanne, Switzerland, September 4-8, 2002.
5. In-Kun Kim, Robert Kratz, and David W. Doll, “Technology Development for U.S. Urban Maglev,” Maglev 2002, Lausanne, Switzerland, September 4-8, 2002.
6. K. Kehrer, W. McKenna, and W. Shumaker, “Maglev Design for Permanent Magnet Levitation Electrodynamic Suspension (EDS) System,” Maglev 2002, Lausanne, Switzerland, September 4-8, 2002.

This page intentionally left blank

Appendix A

Final Test Plan

This page intentionally left blank

**General Atomics Low Speed Maglev
Technology Development Program**

Final Test Plan

**Sponsored by:
Department of Transportation
Federal Transit Administration
Office of Research Demonstration & Innovation
TRI-2, Room 6431B
400 7th Street, SW
Washington, D.C. 20590**

Submitted by:

**General Atomics
PO Box 85608
San Diego, CA 92186-5608**

30 June 2004

Approved by:

**R. Baldi
H. Gurol
I. Kim**

DISTRIBUTION STATEMENT

Distribution authorized to U.S. Government agencies only to protect information not owned by the U.S. Government and protected by a contractor's "limited rights" statement, or received with the understanding that it not be routinely transmitted outside the U.S. Government. Other requests for this document shall be referred to or FTA/TRI-2.0 and/or the Recipient Administrator.

This page intentionally left blank

ACKNOWLEDGEMENT

The Department of Transportation, Federal Transit Administration, and Office of Research Demonstration & Innovation sponsored this work as part of Cooperative Agreement CA-26-7025.

The following companies participated in the preparation of this document:

- Booz-Allen Hamilton
- Carnegie Mellon University
- General Atomics
- Hall Industries
- Lawrence Livermore National Laboratory
- Mackin Engineering Company
- P J Dick
- Pennsylvania Department of Transportation (PennDOT)
- Union Switch & Signal
- Western Pennsylvania Maglev Development Corporation

This page intentionally left blank

TABLE OF CONTENTS

1.0	BACKGROUND	1
3.0	TEST SYSTEM DESCRIPTION	3
4.0	COMPONENT AND SUBSYSTEM TESTING.....	17
5.0	TEST PARAMETERS	17
5.1	Weight of Test Vehicle	17
5.2	Test Speed Profile.....	18
5.3	Station Shims	19
5.4	LSM Current I_d	19
6.0	ANALYSES AND SIMULATIONS FOR TEST OPERATIONS	19
7.0	TEST PHASES.....	22
7.1	Phase 1 Testing	22
7.2	Phase 2 Testing	24
7.3	Phase 3 Testing	26
8.0	CONCLUSION	27
APPENDIX A COMPONENT TESTS COMPLETED AS PART OF SUPPLEMENTAL #1 AND SUPPLEMENTAL #2		29
APPENDIX B CHECKLISTS FOR MAGLEV TEST SYSTEM OPERATION		39

LIST OF FIGURES

Figure 1	Test vehicle on the test track.....	2
Figure 2	Test track and control room.....	10
Figure 3	Test vehicle chassis –cross section.....	11
Figure 4	Test vehicle (with water tanks to simulate passenger loading).....	11
Figure 5	DC rectifier (left) and inverter (right)	12
Figure 6	Data acquisition system architecture.....	13
Figure 7	Laser sensor (left) and optical tape (right)	16
Figure 8	Doppler radar unit for ATP speed	16
Figure 9	ATP speed profiles	17
Figure 10	Typical speed profiles for the dynamic test.....	18
Figure 11	Force equilibrium as a function of velocity and levitation gap.....	20
Figure 12	Vehicle motion and forces.....	21
Figure 13	Electrical demands	21

LIST OF TABLES

Table 1 Comparison of Key System Requirements with Corresponding Test Track Parameters5

Table 2 List of Vehicle Borne Sensors.....13

Table 3 Wayside Sensors.....15

Table 4 Test Vehicle Weight Summary18

Table 5 Test Matrix for Phase 122

Table 6 Test Matrix for Phase 225

Table 7 Test Matrix for Phase 326

LIST OF ACRONYMS

DAQ	Data Acquisition
EDS	Electro-Dynamic System
EMALS	Electromagnetic Aircraft Launch System
IGBT	Insulated Gated Bi-polar Transistors
LSM	Linear Synchronous Motor
PWMC	Pulse Width Modulation Card
VVVF	Variable Voltage Variable Frequency

This page intentionally left blank

1.0 BACKGROUND

The main purpose of the Maglev System Test Program is to demonstrate levitation, propulsion, and guidance. Our approach uses permanent magnets in a Halbach array arrangement for levitation and a Linear Synchronous Motor (LSM) reacting with additional Halbach arrays for guidance, propulsion and braking. Successful testing will validate our design and analysis leading to demonstration and commercial system deployment.

Specific goals of the test program include:

Test Parameter	Desired Result
Levitation	Stable levitation, magnetic gap 25 mm
Propulsion	Speed control $\pm 10\%$ of planned speed profile
Lift-off Speed	$\pm 10\%$ of predicted lift-off speed
Guidance	Maintain stable levitation while negotiating 50 meter turn radius
Max Acceleration	0.16g (1.6 m/s ²)
Max Jerk	0.25g/s (2.5 m/s ³)

The testing has been planned to be in two distinct phases defined by the two separate supplemental funding increments:

- Supplemental Funding #2: Construction and operation of a 15 m straight guideway module and a test vehicle (single chassis).
- Supplemental Funding #3: Construction of 7 additional guideway modules and operation of test vehicle developed during Supplemental #2. The total length of the test track, including all eight guideway modules, is 120 m. It includes 5 straight sections, one curved section, and two transition modules. Once the test track is completed, it will have sufficient length to enable the test vehicle to be levitated while negotiating a 50 m radius curve. This will verify operational performance.

The supplemental #2 tasks have been completed and supplemental #3 is currently in progress.

2.0 INTRODUCTION

A series of system level dynamic tests will verify full-scale levitation, propulsion and guidance as well as characterize the vehicle dynamics.

The major components of the test track that have already been completed include:

- Guideway Foundation (At Grade)
- Eight Guideway Modules (120m long)
- One Test Vehicle Chassis (4 m long, 6.5 tones)
- One Variable Voltage Variable Frequency (VVVF) propulsion Inverter (~2.5 MW)

- Inverter Control – Hardware and Software
- Data Acquisition System
- Position and Speed Detection System
- Automatic Train Protection System

During the Supplemental #2 phase, component tests on the vehicle chassis, inverter and the 1st guideway module were completed. As part of Supplement #3, the remaining guideway modules, position and speed detection system and data acquisition system are currently being manufactured and tested. These components will be tested independently as they are assembled and as a system before the start of the dynamic testing.

The test vehicle on the test track is pictured in Figure 1. It consists of a single full-scale chassis. Functionally, the chassis is essentially identical to the chassis of a full vehicle. It also has many unique features including:

- Extensive instrumentation
- Adjustable features (such as magnet gaps for both levitation and propulsion)
- Safety wheels to help guide the vehicle
- Water tank to simulate passenger loading conditions



Figure 1. Test vehicle on the test track

For reference, a full vehicle will include two chassis units connected by an articulation unit. As such, the test vehicle is one-half the magnetic length of a full vehicle, but is otherwise full size.

During a normal test operation, the vehicle starts at one end of the 120 m long test track and accelerates to a predetermined cruise speed, then decelerates back to zero speed at the other end

of the track. Dynamic performance parameters such as speed, levitation gap, lateral motions and power input to the inverter will be measured and recorded.

The dynamic testing will be conducted in three phases. The initial phase is a system checkout phase and is designated Phase 1. Phase 1 testing will validate the performance of the components by slowly rolling the (empty) test vehicle on its wheels at low speed along the 120-m track. This series of testing will assure system readiness for the next phases. Phase 2 testing will begin verification of levitation, propulsion and guidance of the maglev system. During this phase, a total of four different representative vehicle weights will be evaluated to validate our theoretical predictions. Phase 3 testing will further investigate the dynamic performance of the system for a selected fixed vehicle weight.

In preparation for phase 2 and 3 dynamic tests, analyses and simulations have been conducted to predict the test results. As part of this activity, a 3D dynamic model of the system was developed and the range of test operations have been simulated to predict the dynamic behavior.

The test results will be compared with the analyses and simulations in Phase 3. A measure of success is how well the test results validate the analytical model predicting the test performance and give confidence in the design.

3.0 TEST SYSTEM DESCRIPTION

A comparison of key system requirements with corresponding test track parameters is provided in Table 1. The key system requirements summarized in Table 1 were taken from the General Atomics Low Speed Maglev Technology Development Program Requirements Document (General Atomics Report Number 39043S-OO-001C, dated 15 November 2001). Included in Table 1 are the key test track parameters that correspond to each key requirement. Each of the requirements to be verified on the test track is highlighted. During this test program, a best effort, based on available funding, will be performed to verify each of these highlighted requirements. Any requirements which were left unverified during this current test program would be covered in a future funded test program.

Test Track — The overall test track and the Maglev control building layout is shown in Figure 2. The control of the test vehicle and data acquisition and monitoring will be conducted from the control room, which also houses the power equipment. The 120-m long test track consists of eight 15-m guideway modules. There are 5 straight modules, two transition modules and one 50-m radius curved module with 1.5 degrees of super elevation. The guideway modules are equipped with LSM windings for propulsion and Litz track for levitation. The first guideway module was installed during the supplemental #2 phase and remaining seven modules will be installed during the supplemental #3 phase.

This page intentionally left blank

Table 1. Comparison of Key System Requirements with Corresponding Test Track Parameters

Key Parameters* (Taken from General Atomics Low Speed Maglev Technology Development Program – Requirements Document Report No. 39043S-OO-001-C, dated 15 Nov. 2001)	System Requirements*	Alignment Requirements*	System Concept Definition Requirements*	Summary of Key System Requirements (Typical Deployment System)	Corresponding Test Track Parameters	Verification Planned (During Supp. #3 & Beyond)
	Reference Page No.					
AC Electric Field, Occupational Allowable	14			Permissible exposure limits, see reference requirements document	Same requirement	Verify
AC Electric Field, Public Allowable	13			Permissible exposure limits, see reference requirements document	Same requirement	Verify
AC Electric Field, Whole Working Day, Occupational Allowable	14			Permissible exposure limits, see reference requirements document	Same requirement	Verify
AC Magnetic Field Sub-Radio Frequency Occupational Allowable	14			Permissible exposure limits, see reference requirements document	Same requirement	Verify
AC Time-Varying Magnetic Field, Public Allowable	13			Permissible exposure limits, see reference requirements document	Same requirement	Verify
Acceleration, Max. Longitudinal (Performance)	7			Standing 0.16g (1.6 m/s ²) and Seated 0.25g (2.5 m/s ²)	0.16g (1.6 m/s ²)	Verify
Acceleration, Maximum Longitudinal (Ride Comfort)	9			Standing 0.16g (1.6 m/s ²) and Seated 0.25g (2.5 m/s ²)	0.16g (1.6 m/s ²)	Verify
Acceleration, Maximum Lateral	9			0.25g	Same requirement	Verify
Acceleration, Maximum Vertical	9			0.3 g	Same requirement	Verify
Acceleration, Vector Combinations	9			Standing: Lat/Long 0.3 g, Lat/Vertical 0.3g, Total: 0.36g Seated: Lat/Long 0.6 g, Lat/Vertical: 0.4g, Total: 0.6g	Same requirement	Verify
Accessibility Standards	6			Americans for Disabilities Act	Not applicable for current test vehicle	
Accessibility Standards			65	Americans with Disabilities Act (ADA) access provisions	Not applicable for current test vehicle	
Aesthetics Philosophy	15			Non-Intrusive Design and construction	Not applicable for current test track	
Ambient Temperature and Humidity	12			-32°C (-26°F) to 50°C (122°F). 95% non-condensing relative humidity at 30 °C (86 °F)	Ambient only	
Ambient Temperature and Humidity		55		Same as system requirement	Ambient only	
Amenities - Heating Ventilation and Air Conditioning (HVAC) and Lighting	10			15 m ³ of ventilation fresh conditioned air per hour per passenger. Temp. Range: 18 to 23°C	Not applicable for current test vehicle	
Automatic Train Control (ATC)			64	System Operation Requirement	Not applicable for current test vehicle	
Automatic Train Operation (ATO)			64	System Operation Requirement based on predetermined speed pattern	Not applicable for current test vehicle	
Automatic Train Protection (ATP)			64	System Operation Requirement to prevent collision and over speed	The test track will be equipped with an ATP system	Verify
Auxiliary Power Subsystem			57	Hotel power estimated at 20kW	Test vehicle is powered by an on board battery bank	
Availability Goal	15			> 99.99% - 20 hours/day, 365 days per year	Not applicable	
Braking Subsystems			56	Regenerative electric brake, Hydraulic brake, Fail-safe emergency mechanical brake	Electric braking supplied by LSM and mechanical brake	Verify
Braking, Deceleration	8			Standing 0.16 g (1.6 m/s ²), Seated 0.25 g (2.5 m/s ²)	0.16 g	Verify
Braking, Emergency	8			0.36 g (3.5 m/s ²)	0.36 g	Verify
Braking, Independent and Redundant	8			Dynamic brake, Mechanical brake, Emergency brake	Dynamic brake, Mechanical brake	Verify
Bridges, Number and Span Length of		54		TBD	Not applicable for current test vehicle	
Communication, Passenger Subsystem			57	Audio and Visual Communications shall meet ASCE 21-96 Chapter 6 standards	Not applicable for current test vehicle	
Construction Materials			59	High strength concrete box beam, concrete piers, footing and caissons	Not applicable for current test track	

Restriction – Use, duplication, or disclosure is subject to the restrictions as stated in Agreement CA-26-7025 between the FTA and the Recipients.

Key Parameters* (Taken from General Atomics Low Speed Maglev Technology Development Program – Requirements Document Report No. 39043S-OO-001-C, dated 15 Nov. 2001)	System Requirements*	Alignment Requirements*	System Concept Definition Requirements*	Summary of Key System Requirements (Typical Deployment System)	Corresponding Test Track Parameters	Verification Planned (During Supp. #3 & Beyond)
	Reference Page No.					
Cost, Capital Goal of Guideway	16			<\$13.67 Million/km (<\$22 Million/mile)	Not applicable for current test track	
Cost, Capital Goal of Stations	16			<\$2 Million/station	Not applicable for current test track	
Cost, Capital Goal of System	16			<\$50 Million / km (<\$80 Million / mile)	Not applicable for current test track	
Cost, Capital Goal of Vehicles	16			<\$1.5 Million / vehicle	Not applicable for current test vehicle	
Cost, Operation Goal	16			<\$9 vehicle-km (<\$15 vehicle-mile)	Not applicable for current test vehicle	
Crest Curvature capability, Minimum (Vertical Radius)	11			1000 meters	Vertical radius currently not designed into test track	
Cross Section			59	1200/1650 Box Beam with a 250 x 2,300 mm Deck and 100 x 1,200 Haunches. 1200/1800 Box Beam with a 250 x 2,300 mm Deck and 100 x 1,200 mm Haunch.	Current test track designed without elevated guideway	
Design Loads			59	Preliminary design based on 18,000 kg (40,000 lbs) for each vehicle including passengers	Same Requirement	Verify
Elevation Change, Maximum		54		38 meters	Current test track is designed without change in vertical height	
Emergency Egress			60	TBD	Not applicable for current test vehicle	
Extendible and Flexible System	6			Modular Design	Test track can be extended	
Fare Collection		65		Automatic	Not applicable for current test track	
Fault Protection			62	100% Back-up and interlocked to prevent paralleling	Same Requirement	Verify
Fire Safety, Combustibility and Toxicity Standards			57	Meet NFPA 70 and NFPA 130 standards	Not applicable for test vehicle	
Gap, Levitation			58	2.5 cm	Same Requirement	Verify
Grade and Length, Maximum		54		7% Grade, 545 meter length	Current test track designed with 0% grade	
Grade, Maximum capability	7			10% for a minimum of 460 meters	Same Requirement	
Grade, Operating capability	7			7% at line speed with no degradation of performance	Same Requirement	
Guidance			56	Permanent Magnet Halbach Array and LSM	Same Requirement	Verify
Guideway	10			The guideway should be grade separated for exclusive use	Not applicable for current test track	
Guideway Design			58	Design Guideway to AASHTO LRFD Bridge Design specification, 2 nd edition, along with 1999 and 2000 interim specifications	Same Requirement	
Guideway power			63	4-car train required 2.3 MW peak, 1.5 MW average	Not applicable for current test vehicle	
Guideway Switches			59	Min. of 4 switches to accommodate switching at either end of the alignment and an off-line	Not applicable for current test track	
Guideway Tolerances, Construction and Installation			60	See Requirements Specification	Same Requirement	Verify
Guideway, Nominal Height			60	9,200 mm	Current test track designed without elevated guideway	
Handicapped Access			58	Comply with Americans with Disabilities Act (ADA)	Not applicable for current test vehicle	
Heating, Ventilation and Air Conditioning (HVAC)			57	15 m ³ of ventilated fresh conditioned air per hour per passenger. Temp. Range 18 to 23 ^o C	Not applicable for current test vehicle	
Horizontal Curvature, Minimum Crest and Sag Radius		54		Crest and Sag Radius 1000 meters	Same Requirement, but not required for current test track	
Ice	12			≤ 6 mm (0.25 inch)	Not applicable for current test track	

Key Parameters* (Taken from General Atomics Low Speed Maglev Technology Development Program – Requirements Document Report No. 39043S-OO-001-C, dated 15 Nov. 2001)	System Requirements*	Alignment Requirements*	System Concept Definition Requirements*	Summary of Key System Requirements (Typical Deployment System)	Corresponding Test Track Parameters	Verification Planned (During Supp. #3 & Beyond)
	Reference Page No.					
Input Power Reliability (Redundancy)			62	Provide two-utility source system over separate lines from separate generation points	Not applicable for current test track	
Inter-modal Stations, Location and Number of			65	Provide connections to inter-modal facilities	Not applicable for current test track	
Jerk, Lateral	9			0.25 g/s	Same Requirement	Verify
Jerk, Longitudinal	8			0.25 g/s	Same Requirement	Verify
Jerk, Longitudinal	9			0.25 g/s	Same Requirement	Verify
Jerk, Vertical	9			0.3 g/s	Same Requirement	Verify
Levitation			56	Permanent Magnet Halbach Array and Ladder track design concept	Same Requirement	Verify
Levitation Plate Adjustability			60	±2 mm Vertically and Laterally	Same Requirement	
Life, System (Civil Works)	16			>75 years	Not applicable for current test track	
Life, System (Vehicle & Electrical/Electronic Systems)	16			30 Years	Not applicable for current test vehicle	
Lightning	13			Compliance with IEEE Std. 1100	Not applicable for current test vehicle	
Lightning (Primary Alignment)		55		Compliance with IEEE Std. 1100	Not applicable for current test vehicle	
Lightning Protection			62	Compliance with IEEE Std. 1100	Not applicable for current test vehicle	
Lightning Protection Requirements			58	Compliance with IEEE Std. 1100	Not applicable for current test vehicle	
Load Interruption Protection			63	Full Load Interruption	Same Requirement	
Magnetic Fields, Passenger Compartment Allowable			57	Static Field: ≤ 5 Gauss, AC Field (60 Hz): ≤ 1 Gauss	Same Requirement	Verify
Maintainability Target	14			MTTR (First Level) < 30 min, MTTR (Second Level < 2 hours	Not applicable for current test vehicle	
Maintenance Facility Requirements			66	System Operational Requirement Minimum of one Maintenance and Storage Facility	Not applicable for current test vehicle	
Noise Level - Inside passenger compartment	10			≤ 67 dBA (Goal)	Not applicable for current test vehicle	
Noise Level - Outside 15.2 meters from guideway centerline	10			≤ 67 dBA (Goal) 70 dBA (Goal)	Same Requirement	Verify
Operation, Fully Automatic	7			Fully automatic Train Control (ATC) per ASCE 21-96-Part1, Chapter 5 (except as noted) for Driver-less operation	Prototype train control system will be tested	Verify
Overload Protection			62	Limited Protection of power conditioning equipment	Same Requirement	
Passenger Capacity Loading Requirements			57	AW3 (Crush Load) 100 passengers per vehicle	Simulated on current test vehicle	Verify
Passenger Communications System (PCS)			64	System Operation Requirement	Not applicable for current test vehicle	
Passenger Minimum Waiting Time	6			Trip delay threshold of three minutes	Not applicable for current test vehicle	
Piers, Footings and Caissons			59	Cast-in-Place or segmented piers with a T-shaped or L-shaped hammerhead, Cast-in-place footings, Drilled Caissons	Current test track designed without elevated guideway	
Power Conditioner Redundancy			62	100% Redundancy	Not applicable for current test track	
Power, Housekeeping			63	20 kW/Vehicle	Test vehicle is powered by an on board battery bank	
Propulsion			56	Active guideway LSM	Same Requirement	
Propulsion System Layout, Design & Installation			61	LSM selected due mainly to the large gap and large gap variation of the EDS	Same Requirement	Verify
Propulsion, LSM Block-length, Inverter and Switching Stations			61	Block-Length 490 m, 70 Inverters, Switches per zone = 8 for a total of 560 switches	Currently the test track is designed with one inverter and no block switches, however, the capability exists to add inverters and block switches	

Key Parameters* (Taken from General Atomics Low Speed Maglev Technology Development Program – Requirements Document Report No. 39043S-OO-001-C, dated 15 Nov. 2001)	System Requirements*	Alignment Requirements*	System Concept Definition Requirements*	Summary of Key System Requirements (Typical Deployment System)	Corresponding Test Track Parameters	Verification Planned (During Supp. #3 & Beyond)
	Reference Page No.					
Rain	13			≤ 75 mm (3 inches) / hr	Same Requirement	
Rain (Primary Alignment)		55		≤ 75 mm (3 inches) / hr	Same Requirement	
Reliability, Vehicle Goal			67	MTTF = TBD	Not applicable for current test vehicle	
Ride Quality Standard	8			Design goal is 1-hour reduced comfort, based on ISO 2631/1 1985, figures A1 & A2.	Same Requirement	
Route Characteristics		17		See Requirements Document	Not applicable for current test track	
Route Length		54		13.5 km	Currently the test track is 120 meters long	
Safety Goal	14			<0.1 Incidents/million passenger miles, <0.1 Injuries/100 million passenger miles, Zero fatalities	Safety Plan and Hazardous Work Authorization Plan. (Classes will be conducted to ensure safe operation during testing)	Verify
Safety Risk Assessment	14			Safety risk assessment shall per performed in accordance with Notice of Proposed Rule Making (NPRM) draft – 8/30/2000	Not applicable for current test vehicle	
Sag Curvature capability, Minimum (Vertical Radius)	11			1000 m	Vertical radius currently not designed into test track	
Salt Atmosphere	13			System components and finishes to withstand salt fog atmosphere up to 49 hours	Not applicable for current test vehicle	
Salt Atmosphere (Primary Alignment)		55		Local standards	Not applicable for current test vehicle	
Seating Requirement, Minimum			57	TBD seats	Not applicable for current test vehicle	
Security, Station	15			Create a Station Security Plan	Not applicable for current test vehicle	
Security, Station (Primary Alignment)		66		Same as System Requirement	Not applicable for current test vehicle	
Security, Vehicle	15			Create a Vehicle Security Plan	Not applicable for current test vehicle	
Security, Vehicle (Primary Alignment)		66		Same as System Requirement	Not applicable for current test vehicle	
Seismic	12			System shall be designed to survive seismic level of selected site without permanent damage.	Same Requirement	
Seismic (Primary Alignment)		55		Acceleration coefficient of primary alignment is 4	California Standards Apply	
Seismic Requirements			61	Acceleration coefficient = 4	California Standards Apply	
Snow	12			≤ 300 mm (12 inches) / hr	Same Requirement, but not likely in San Diego	
Snow (Primary Alignment)		55		≤ 300 mm (12 inches) / hr	Same Requirement, but not likely in San Diego	
Speed, Average	7			50 km/h (31 mph)	Test Track is currently designed for a maximum speed of 10 meters/sec (22 mph)	Verify
Speed, Maximum Operational	7			160 km/h (100 mph)	Same Requirement	
Static Magnetic Field, Occupational Allowable	13			Permissible exposure 1 G (workers with cardiac pacemakers) 10 G at 60 Hz, 600 G.f (to 300 Hz), 2 G (300 Hz – 30 kHz)	Same Requirement	Verify
Static (DC) Magnetic Field, Public Allowable	13			Permissible exposure: 5 Gauss (G) (medical electronic wearers)	Same Requirement	Verify
Station Layout		54		See Requirements Document	Not applicable to current test track	
Station Platforms Requirements			65	System Operational Requirement	Not applicable to current test track	
Stations	11			System Operational Requirements for 4 car train	Not applicable to current test vehicle	
Stations, Aesthetics and General Layout			65	Elevated stations designed in accordance to local codes and criteria	Not applicable to current test track	
Stations, Berthing Space Requirement			65	Size and number of stations berths based on throughput	Not applicable to current test track	
Stations, Number of		54		15 (See Route Characteristics paragraph 2.1 of Requirements Document)	Not applicable to current test track	
Super Elevation, Maximum			60	6 Degrees maximum (10.5% slope) with spiraling	Currently the test track is designed for a 1.5 ⁰ cant with spiraling	Verify

Key Parameters* (Taken from General Atomics Low Speed Maglev Technology Development Program – Requirements Document Report No. 39043S-OO-001-C, dated 15 Nov. 2001)	System Requirements*	Alignment Requirements*	System Concept Definition Requirements*	Summary of Key System Requirements (Typical Deployment System)	Corresponding Test Track Parameters	Verification Planned (During Supp. #3 & Beyond)
	Reference Page No.					
Super Elevation, Maximum		54		6° cant angle	1.5° cant angle, however, 6° cant angle is possible with a longer track	Verify
Surveillance Communication System (SCS)			64	System Operational Requirement	Not applicable to current test track	
Suspension, Secondary			56	Air Spring, Dampers and axial support struts	Same Requirement	Verify
Switching	11			Switching at line speed	Not applicable to current test track	
System Architecture			63	ATCS architecture. The Train control system consists of devices located on each train (vehicle), at each station (Wayside), and at the central control (Central) room.	Same Requirement	Verify
System Efficiency			61	≥ 95% (Power losses in the power conditioning equipment and distribution line should be less than 5%)	Same Requirement	
Technology	6			Use magnetic fields for suspension, propulsion, guidance and braking	Same Requirement	Verify
Throughput	6			12,000 passengers / hour / direction	Not applicable to current test track	
Total Traffic Control (TTC)			64	System operation requirement. Total fleet will be controlled and monitored by a TTC computer at the Central Control Room (CCR).	Not applicable to current test track	
Tracks, Number of			59	Dual track guideway	Single track guideway	
Transient Voltage Surge Protection (TVSP)			63	Fully protected	Same Requirement	
Transportation, Connection to Other Modes of		54		Provide connections to inter-modal facilities and other transportation facilities	Not applicable to current test vehicle	
Turn Radius, Minimum capability	11			18.3 m (60 ft)	50 m (164 ft)	
Usage (Hours of Operation)	6			20 hours / day, 365 days per year	Not applicable to current test vehicle	
Utility Interface Compatibility			61	Harmonic distortion < 3% into utility grid	Same Requirement	Verify
Vehicle Recovery	6			The vehicle system will be designed to allow push recovery	Not applicable to current test vehicle	
Weather Operation	6			All weather operation	Same Requirement	
Weight Goal, Vehicle			58	1.0 Tonnes / meter	Same Requirement	
Wind	12			Operational threshold up to 50 km/h (~30 mph), Ride comfort threshold up to 80 km/h (~50 mph), Structural threshold up to 160 km/h (~100 mph)	Same Requirement	
Wind (Primary Alignment)		55		Same as system requirement document	Same Requirement	

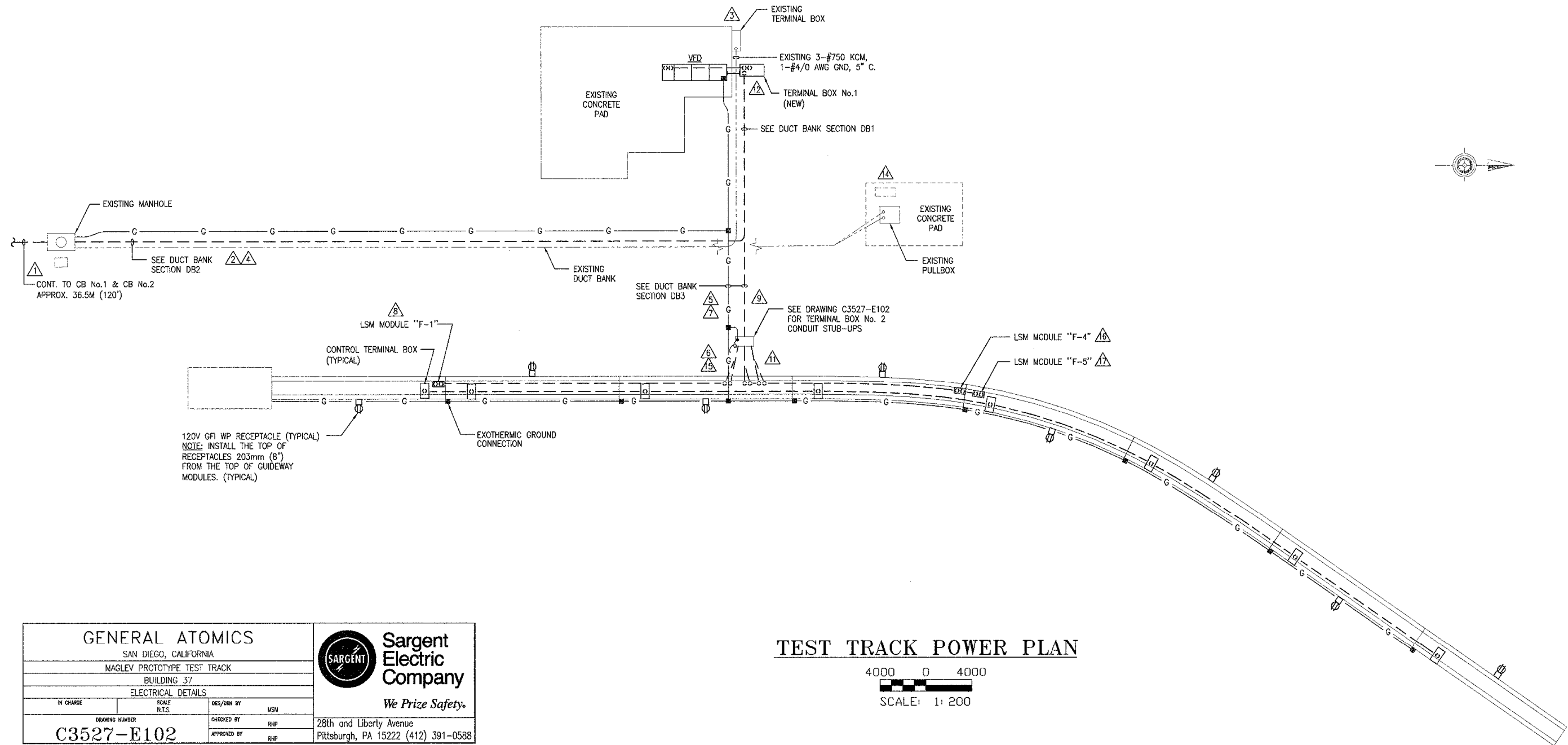


Figure 2. Test track and control room

Test Vehicle — The test vehicle for the dynamic test consists of one full-scale chassis, which represents one half the magnetic length of a full-size urban Maglev vehicle. It weighs approximately 6.5 tonnes when empty. The fully loaded vehicle (with water tanks simulating passenger loading) weighs 11.0 tonnes. The 4 m long test vehicle chassis is equipped with three layers of Halbach array magnets as shown in Figure 3. The top layer of magnets interfaces with the LSM coils and provide propulsion, passive lift, and guidance. The layers of magnets above and below the Litz track provide levitation. An illustration of the complete vehicle assembly (with water tanks in installed to simulated passenger loading) is shown in Figure 4. The chassis has a total of eight landing wheels to provide support when not levitated and four inboard safety wheels to limit upward and lateral motions.

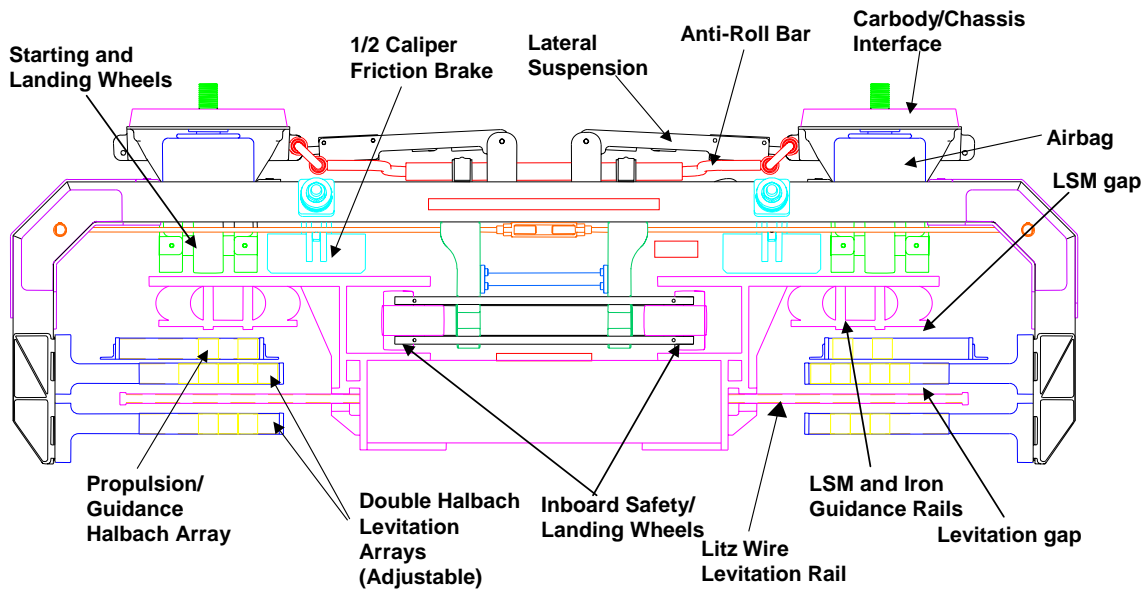


Figure 3. Test vehicle chassis –cross section

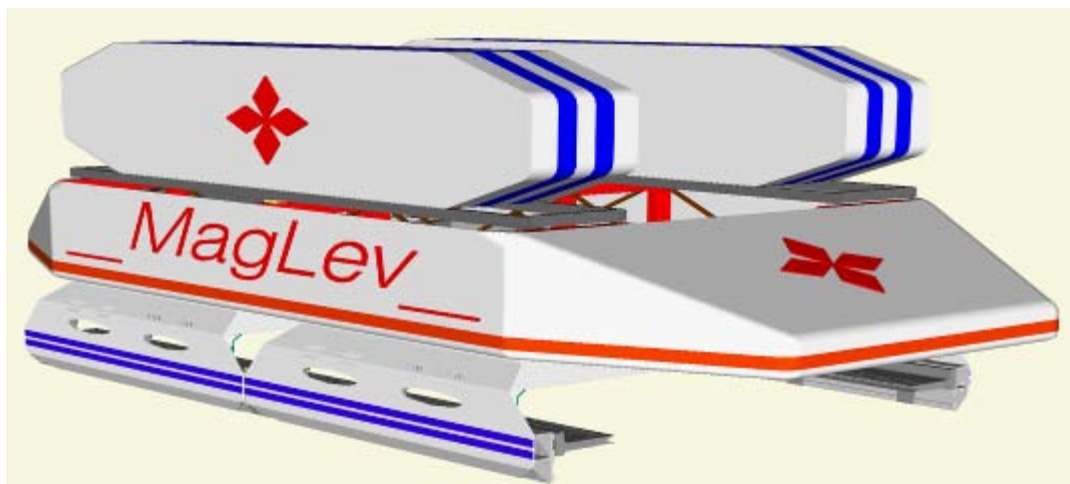


Figure 4. Test vehicle (with water tanks to simulate passenger loading)

Variable Voltage Variable Frequency (VVVF) Inverter and Control – The propulsion system inverter was specifically built for the test track by General Atomics. It is based on advanced power electronics using Insulated Gated Bi-Polar Transistor (IGBT) technology. Figure 5 shows the DC rectifier and inverter as installed in the power equipment room of the Maglev test track control building. This inverter was originally designed for Electromagnetic Aircraft Launch System (EMALS) but was modified for the Maglev application. It is configured to deliver 3-phase power using a single pulsed width modulation card (PWMC) with an output power capability of 2.5 MW rms. The control system for the inverter has the capability to control the phase angle of the output current. Inverter hardware is protected for both over-current and over-voltage. The protection current and voltage limits are 5800 A and 1475 V, respectively.



Figure 5. DC rectifier (left) and inverter (right)

The inverter control is designed to provide the necessary current and frequency to the LSM winding in a controlled fashion to produce commanded thrust that propels the vehicle at the desired speed. Both control hardware and software are involved.

Data Acquisition System – A schematic diagram of the data acquisition system is shown in Figure 6 and the list of sensors (assigned to date) is shown in Tables 2 and 3. As shown, instrumentation is provided both on the vehicle and wayside.

The data acquisition system on the vehicle can collect and store up to 64 sensor signals. At present, a total of 51 sensors on the vehicle have been assigned. Ten (10) of these signals will be wirelessly transmitted for real time monitoring and will be displayed in the control room. The signals to be displayed include:

- 4 Levitation gaps
- 2 Lateral Gaps
- 1 Vehicle Speed
- 1 Vehicle Position
- 1 Vehicle Weight
- 1 Battery Voltage

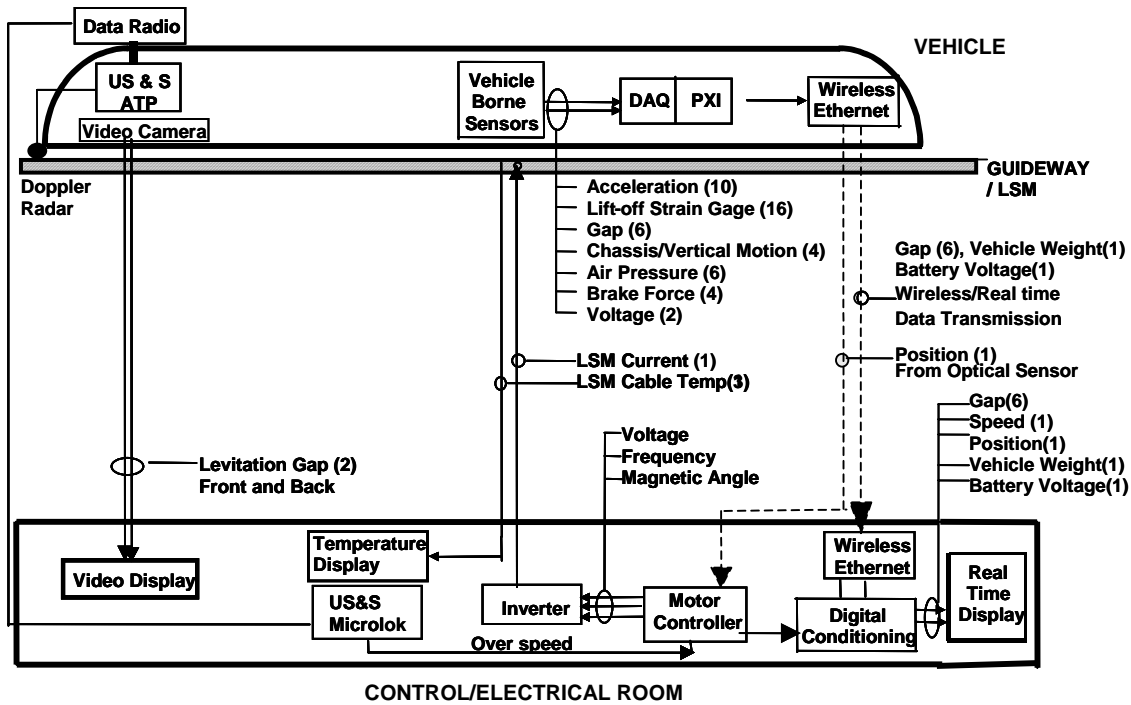


Figure 6. Data acquisition system architecture

The remaining signal data will be stored on the computer onboard the test vehicle for subsequent downloading and processing.

In addition, wayside data will be displayed in the control room. These signals include:

- Rectifier Voltage
- Inverter Voltage and Current
- Calculated position and speed
- LSM temperature

The data acquisition system will be completed and checkout tested before the start of the testing.

A list of sensors that are on the vehicle is shown in Table 2. As shown, at present there are a total of 51 sensors.

Table 2. List of Vehicle Borne Sensors

ID	Channel #	Sensor Type	Sensor Location	Sensor Mfg	Mfg Part #
1	1	Strain gauge	Wheel # 1 key	Omega	SG-3/1000-DY11
2	2	Strain gauge	Wheel # 1 90	Omega	SG-3/1000-DY11
3	3	Strain gauge	Wheel # 2 key	Omega	SG-3/1000-DY11
4	4	Strain gauge	Wheel # 2 90	Omega	SG-3/1000-DY11
5	5	Strain gauge	Wheel # 3 key	Omega	SG-3/1000-DY11
6	6	Strain gauge	Wheel # 3 90	Omega	SG-3/1000-DY11
7	7	Strain gauge	Wheel # 4 key	Omega	SG-3/1000-DY11

Restriction – Use, duplication, or disclosure is subject to the restrictions as stated in Agreement CA-26-7025 between the FTA and the Recipients.

ID	Channel #	Sensor Type	Sensor Location	Sensor Mfg	Mfg Part #
8	8	Strain gauge	Wheel # 4 90	Omega	SG-3/1000-DY11
9	9	Strain gauge	Wheel # 5 key	Omega	SG-3/1000-DY11
10	10	Strain gauge	Wheel # 5 90	Omega	SG-3/1000-DY11
11	11	Strain gauge	Wheel # 6 key	Omega	SG-3/1000-DY11
12	12	Strain gauge	Wheel # 6 90	Omega	SG-3/1000-DY11
13	13	Strain gauge	Wheel # 7 key	Omega	SG-3/1000-DY11
14	14	Strain gauge	Wheel # 7 90	Omega	SG-3/1000-DY11
15	15	Strain gauge	Wheel # 8 key	Omega	SG-3/1000-DY11
16	16	Strain gauge	Wheel # 8 90	Omega	SG-3/1000-DY11
17	17	Lateral gap	*Primary (NW)	Micro-Epsilon	optoNCDT 1400
18	18	Lateral gap	*Primary (SW)	Micro-Epsilon	optoNCDT 1400
19	19	Vertical gap	*Primary (NW)	Micro-Epsilon	optoNCDT 1400
20	20	Vertical gap	*Primary (NE)	Micro-Epsilon	optoNCDT 1400
21	21	Vertical gap	*Primary (SE)	Micro-Epsilon	optoNCDT 1400
22	22	Vertical gap	*Primary (SW)	Micro-Epsilon	optoNCDT 1400
23	23	Lateral motion	Secondary	Omega	LVDT LD 610
24	24	Lateral motion	Secondary	Omega	LVDT LD 610
25	25	Vertical motion	Secondary	Sensor Solutions	A12-870AP2-RACB1
26	26	Vertical motion	Secondary	Sensor Solutions	A12-870AP2-RACB1
27	27	Acceleration	Primary (dual use)	GS sensors	GSA 208-005
28	28	Acceleration	Primary (dual use)	GS sensors	GSA 208-005
29	29	Acceleration	Primary (dual use)	GS sensors	GSA 208-002
30	30	Acceleration	Primary (dual use)	GS sensors	GSA 208-002
31	31	Acceleration	Primary (dual use)	GS sensors	GSA 208-002
32	32	Acceleration	Secondary (dual use)	GS sensors	GSA 208-005
33	33	Acceleration	Secondary (dual use)	GS sensors	GSA 208-005
34	34	Acceleration	Secondary (dual use)	GS sensors	GSA 208-002
35	35	Acceleration	Secondary (dual use)	GS sensors	GSA 208-002
36	36	Acceleration	Secondary (dual use)	GS sensors	GSA 208-002
37	37	Cylinder pressure	Cylinders	Honeywell Invensys	SPT 4V PG5W02
38	38	Cylinder pressure	Cylinders	Honeywell Invensys	SPT 4V PG5W02
39	39	Airbag pressure	Cylinders	Honeywell Invensys	SPT 4V PG5W02
40	40	Airbag pressure	Cylinders	Honeywell Invensys	SPT 4V PG5W02
41	41	Airbag pressure	Cylinders	Honeywell Invensys	SPT 4V PG5W02
42	42	Airbag pressure	Cylinders	Honeywell Invensys	SPT 4V PG5W02
43	43	Brake force	Brakes	OmegaDyne	LC8300
44	44	Brake force	Brakes	OmegaDyne	LC8300
45	45	Brake force	Brakes	OmegaDyne	LC8300
46	46	Brake force	Brakes	OmegaDyne	LC8300
47	47	Battery voltage	Battery bank	n/a	resistor divider
48	48	12V supply voltage	Power Supply	n/a	resistor divider
49	49	120 VAC	AC inverter		
50	50	Vertical motion	Secondary	Sensor Solutions	A12-870AP2-RACB1
51	51	Vertical motion	Secondary	Sensor Solutions	A12-870AP2-RACB1

Restriction – Use, duplication, or disclosure is subject to the restrictions as stated in Agreement CA-26-7025 between the FTA and the Recipients.

A list of sensors that are wayside is shown in Table 3. As shown, at present there are a total of 15 sensors.

Table 3. Wayside Sensors

ID	Channel #	Sensor Type	Sensor Location	Sensor Mfg	Mfg Part #
101	101	dc +V	Inverter		
102	102	dc -V	Inverter		
103	103	Phase A V	Inverter		
104	104	Phase B V	Inverter		
105	105	Phase C V	Inverter		
106	106	Phase A I	Inverter		
107	107	Phase B I	Inverter		
108	108	Phase C I	Inverter		
109	109	Vehicle Position	Motor controller (calculated)		firmware
110	110	Vehicle Speed	Motor controller (calculated)		firmware
111	111	Heat Sink Temperature	Inverter	Omega	
112	112	Stack in Air Temperature	Inverter	Omega	
113	113	Stack out Air Temperature	Inverter	Omega	
203	203	LSM winding Temperature 1	GM #4	Omega	?
204	204	LSM winding Temperature 2	GM #4	Omega	
205	205	LSM winding Temperature 3	GM #4	Omega	
206	206	Proximity (Trip Switch)	GM #2	TBD	
207	207	Proximity (Trip Switch)	GM #2	TBD	
208	208	Proximity (Trip Switch)	GM #7	TBD	
209	209	Proximity (Trip Switch)	GM #7	TBD	

Position and Speed Detection System — The position detection system employs a laser reflective sensor mounted on the vehicle and optical tape on the Litz track. The optical tape is made of 18-mm wide alternating white and black stripes with resets at every motor wave length (432 mm). The position information collected from the laser sensor is transmitted to the control room for inverter control and position display. A 450 MHz radio link between the vehicle and control room allows for the wireless transmission of the data. The laser sensor and optical tape are shown in Figure 7.



Figure 7. Laser sensor (left) and optical tape (right)

Initial position and direction of travel will be provided by a Differential Global Positioning Satellite (DGPS) system. The vital vehicle speed for the car borne ATP (independent of the initial position/speed detection system) is provided by a Doppler radar unit (DRS1000). The radar unit will be mounted on the vehicle and uses the Litz track as the target (Figure 8).

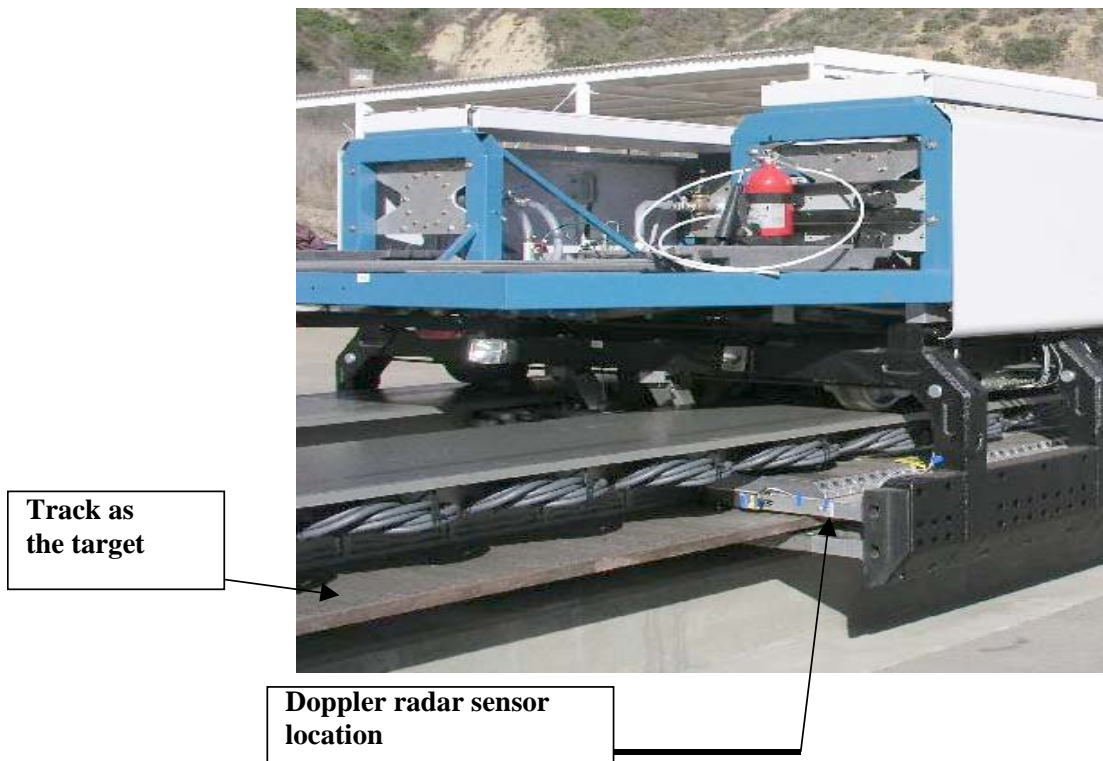


Figure 8. Doppler radar unit for ATP speed

The car borne ATP has a maximum civil speed profile in its memory (Figure 9). If at any time the vehicle speed exceeds the envelop of the maximum speed profile, a command is sent to apply

the emergency brakes and a command is sent to the Microlok system to power-down the inverter.

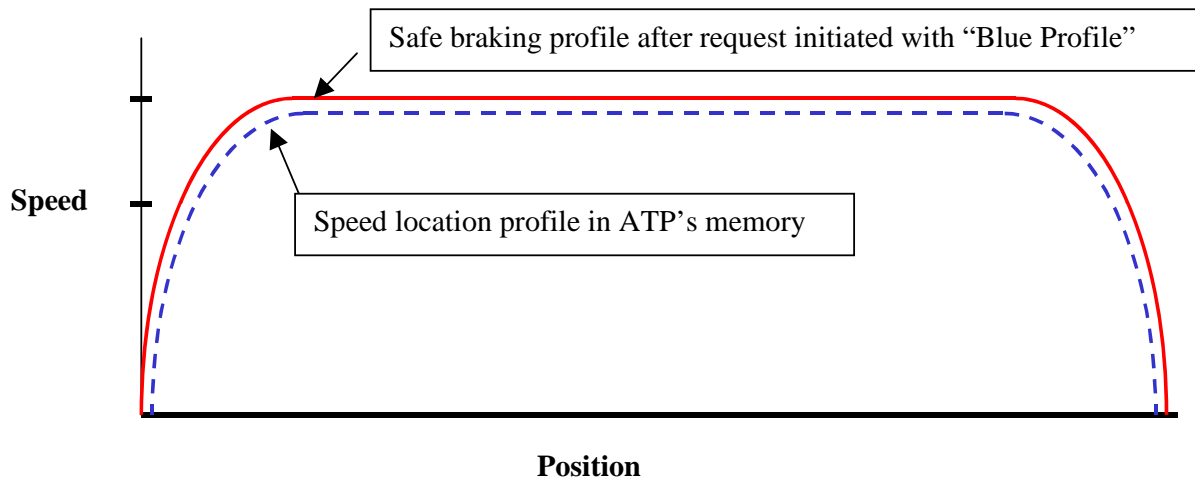


Figure 9. ATP speed profiles

4.0 COMPONENT AND SUBSYSTEM TESTING

The following component tests were conducted as part of Supplemental #1 and #2 activity and the results are summarized in Appendix A.

1. LSM Static Bench Test
1. Track and Vehicle Measurements
2. LSM Static Test on the Test Track
3. Position Detection Test
4. LSM Static Lift Force Measurement
5. Data Acquisition System test

Checkout testing has continued as part of Supplemental #3 activity using the test vehicle chassis on the 1st guideway module.

5.0 TEST PARAMETERS

5.1 WEIGHT OF TEST VEHICLE

The vehicle mass and center of gravity are two of the most important parameters controlling the vehicle dynamics. The test vehicle was designed to allow adjustment of both of these parameters to simulate operational conditions ranging from an empty to fully loaded vehicle.

Table 4 provides a weight breakdown of the major components.

Table 4. Test Vehicle Weight Summary

Item	Weight
Primary (unsuspended)	4,220 kg
Secondary (suspended)	1,850 kg
Water tank (suspended)	1,100 kg
Water	0–3,500 kg (1,750 kg per side)
Instrumentation, etc.	200 kg
Additional steel weight	0–1,000 kg as necessary
Total	Range from 6,500–10,500 kg

Based on the above weight summary, the range of achievable test vehicle weights is between 6,500 and 10,500 kg. The Phase 1 test configurations will use a 6500 kg vehicle weight. For Phase 2 test configurations, the vehicle weight will be varied between 6500 kg and 10500 kg. For Phase 3 test configurations, the vehicle weight will be fixed at a selected value that is currently projected to be 9000 kg. This value may be adjusted pending the test results obtained in Phase 2. An objective of the dynamic test is to determine the range of vehicle weights that can be levitated and propelled with the levitation and propulsion magnet arrays.

5.2 TEST SPEED PROFILE

The inverter power to the LSM winding will be pre-programmed to drive the vehicle following a speed profile assigned for each test run. Typical speed profiles (speed vs. position) are shown in Figure 10. A peak cruise speed of up to 10 m/s is possible at the 50-m radius curve section of the test track. A test run starts with the vehicle at one end of the track after all the pre-test checks are completed. The stationary vehicle with known weight accelerates to a cruise speed and decelerates to a stop at the other end of the track.

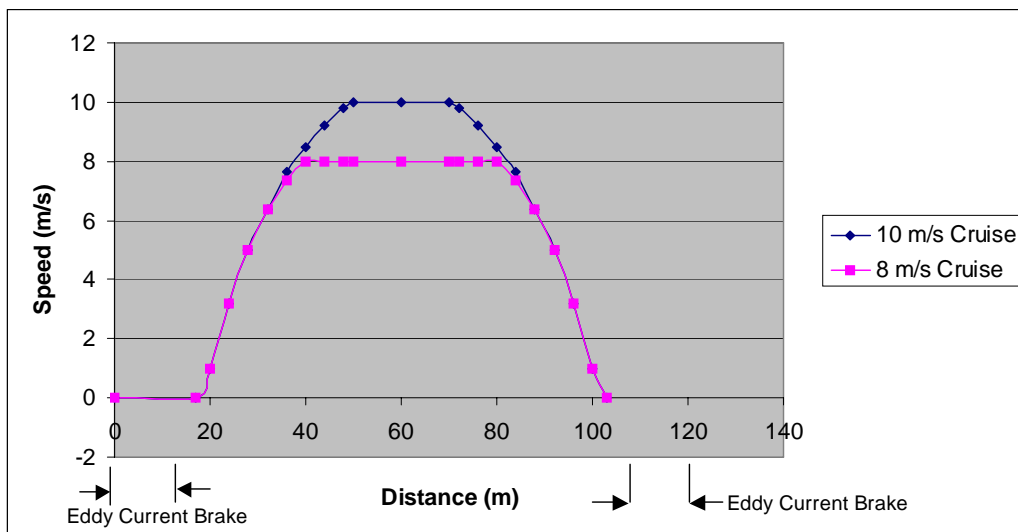


Figure 10. Typical speed profiles for the dynamic test

During the initial stage of the test, various shorter test runs will be made to establish the stopping distances from various cruise speeds. Both electromagnetic and eddy current brakes will be used to ensure safe stopping distances.

5.3 STATION SHIMS

Station shims will be used to reduce peak power requirements. Basically, the station shims are located beneath the wheels of the test vehicle chassis and raises the vehicle to reduce the gap to the LSM. This improves the efficiency of the LSM and reduces the peak power requirement. With this arrangement, the vehicle starts near its intended levitated height and the shim is designed to taper away at the point along the test track where the vehicle will have sufficient speed to levitate. For Phase 1, no station shims will be used. For phases 2 and 3, station shims of 5 mm and 10 mm thickness will be prepared for testing. Initially, the 5 mm shims will be initially be used with the option to change to the 10 mm should further power reductions prove necessary. The first 15 m of the guideway, at each end of the test track will be equipped with the shims. It is recognized that changing the initial gap will slightly affect the lift-off speed. The predicted lift-off speeds associated with 5-mm shim have been estimated and are given in Section 7 (Tables 6 and 7).

5.4 LSM CURRENT I_d

One of the control knobs for the active LSM lift force is the motor lift current, I_d . The LSM thrust peaks at the I_d current of 0 A, where the lift is zero. The positive I_d current generates an active LSM force component pushing downward while a negative I_d current will generate upward force. During Phase 2 testing, the I_d current will be varied between -1000 A and 2000 A.

This feature has the potential benefit for commercial deployment, in that the I_d current can be set before the vehicle leaves the station to compensate for variations in total vehicle weight based on passenger loading. The precise relationship between the vehicle weight and I_d current will be validated during testing.

6.0 ANALYSES AND SIMULATIONS FOR TEST OPERATIONS

An extensive analysis has been conducted to predict the test results, and simulations have been conducted to determine the dynamic performance of the system. The test parameters selected and the predictions of the test results are derived from the analyses and simulation studies. For the Electro-Dynamic System (EDS) Maglev system to maintain stable operation, the forces from various magnets must be in stable equilibrium. Based on the vehicle weight and magnet arrangement, it is possible to identify quasi-static equilibrium conditions for various vehicle speeds. Figure 11 shows an example of the quasi-static stability region for zero I_d current. This figure provides guidance for selecting the fixed weight for the vehicle for Phase 3 tests and predicting the corresponding lift-off speed. Based on this analysis, stable levitation is predicted for test vehicle weights between 9,000 and 12,000 kg. Furthermore, for a 9000-kg test vehicle, lift-off speed is predicted to be 5.2 m/s with 5mm station shim and 4.0 m/s when no shims are used.

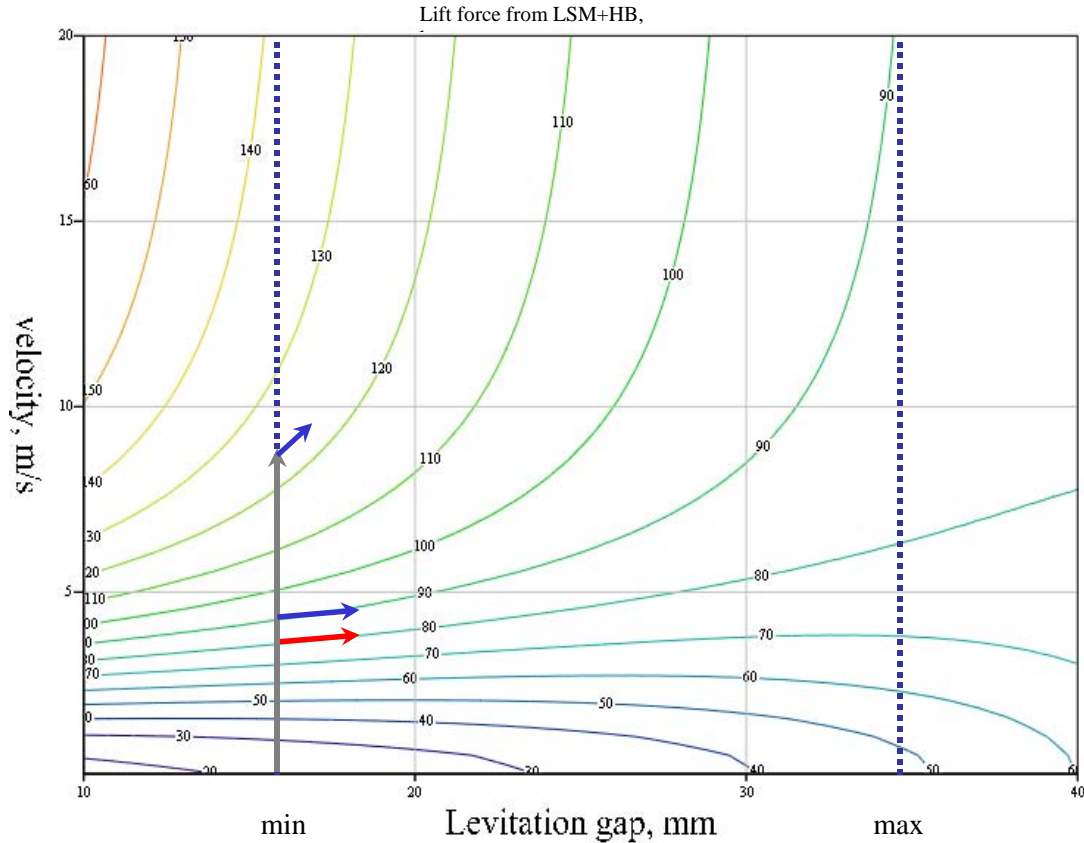


Figure 11. Force equilibrium as a function of velocity and levitation gap

The dynamic motion of the vehicle is non-linear and involves second order differential equations in all six-degrees of freedom. This dynamic motion has been simulated using Simulink. The model includes the vehicle, LSM, inverter and control system. The model recreates the conditions of real operation including the control steps to produce the vehicle motion and power demands associated with this motion. The sample simulation results for a 9000 kg vehicle starting with no shim and 0 degree phase angle are shown in Figures 12 and 13. The simulation indicates that stable levitation is possible but a very high current of 3000A is required at the lift off speed, which corresponds to the point at which peak magnetic drag occurs.

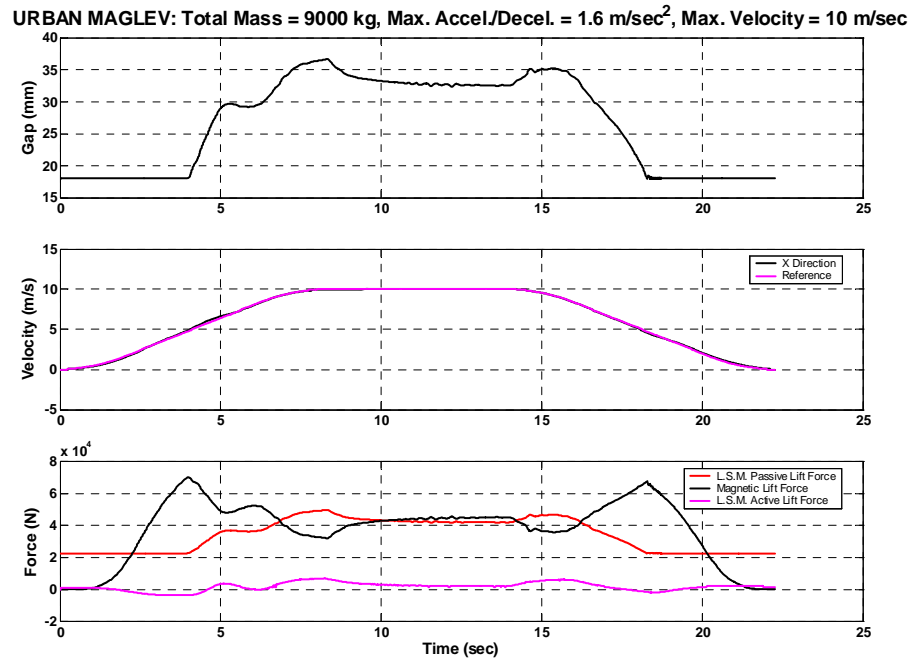


Figure 12. Vehicle motion and forces

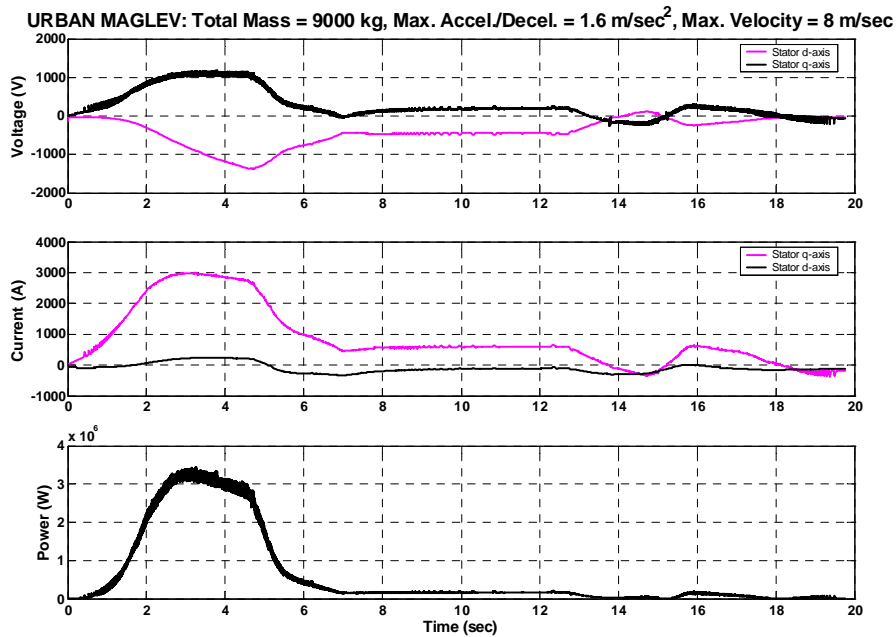


Figure 13. Electrical demands

7.0 TEST PHASES

The main purpose of Maglev system dynamic testing is to verify levitation, propulsion, and guidance performance of the Urban Maglev System. In addition, we plan to evaluate the range of capability by incrementally varying the test and control parameters such as vehicle weight, speed, I_d current, etc. The results of this testing will be compared with our analyses and simulation models to validate our ability to predict design performance.

The tests will be conducted in three phases. Phase 1 is a checkout phase to ensure that key components are ready for dynamic testing in Phases 2 and 3. The performance of the components will be checked by moving an empty test vehicle from one end of the track to the other end, without levitation, at a low speed (~1 m/s). The Phase 2 testing is designed to validate control algorithms that will establish stable operating conditions under levitation for each of the four vehicle weights in the testable range. In Phase 3, dynamic performance of the vehicle over a range of operating parameters will be checked out with a selected fixed test vehicle.

7.1 PHASE 1 TESTING

The test matrix of Phase 1 is shown in Table 5. For Phase 1, seven test configurations are identified. The vehicle will move on LSM power with feedback control. Since the selected speed for these test configurations is too low for levitation to occur, the vehicle will remain on the wheels throughout Phase 1. As shown in Table 5, a primary purpose has been assigned for each configuration. We will attempt to achieve three successful runs for each test configuration. No station shims are used for phase 1 tests.

Table 5. Test Matrix for Phase 1

Test Configuration #	Vehicle Weight (kg)	Cruise Speed (m/s)	Accel/ Decel (m/s ²)	Id Current (A)	Lift-off Speed (m/s)	Cruise Gap (mm)	Peak* Vq (V)	Peak* Iq (A)	Peak* Power (MVA)	Primary Purpose
1-1	6500	1	0.5	0	N/A	17	500	1000	0.5	Position detection
1-2	6500	1	0.5	0	N/A	17	500	1000	0.5	Inverter control
1-3	6500	1	0.5	0	N/A	17	500	1000	0.5	DAQ performance
1-4	6500	1	0.5	0	N/A	17	500	1000	0.5	Levitation gap variation
1-5	6500	1	0.5	0	N/A	17	500	1000	0.5	LSM cable Temp
1-6	6500	1	0.5	0	N/A	17	500	1000	0.5	Inverter temp
1-7	6500	1	0.5	0	N/A	17	500	1000	0.5	Brake performance
1-8	6500	1	0.5	0	N/A	17	500	1000	0.5	ATP performance

*Estimated Motor Parameters

Test Configuration #1-1 Position Detection System Verification — The position information is required for motor control feedback. The position information, counting of 18-mm stripes, originates on the vehicle. This information is transmitted wirelessly to the motor controller located in the control room, and instantaneous vehicle speed is calculated. The primary purpose of this test is to verify:

- No missing pulses or resetting failure
- No position detection failure over the gap between guideway modules
- Successful delivery of position information to the motor controller
- Position accuracy of <20 mm within a wavelength of 432 mm
- Availability of position and speed information to the real-time monitor

Test Configuration #1-2 Motor Control Performance — The primary purpose of this test is to verify:

- The vehicle follows a predetermined speed profile
- The vehicle position accuracy is <20mm within a wavelength
- I_d current is controlled to near zero

Test Configuration #1-3 Performance of Data Acquisition System — The data signals from the vehicle will be collected and stored in the data acquisition computer (PXI). The primary purpose of this test is to verify:

- System generation and storage of signals
- All sensors can be calibrated and conditioned
- Signals transmitted wirelessly to interface computer and display
- Stored data can be retrieved from PXI after the testing

Test Configuration #1-4 Magnetic Gap Variation — The vehicle has four gap sensors, one located at each corner of the vehicle. The physical gaps for the entire track will be monitored during this test. The gap sensors measure the physical gap, which is the vertical distance between levitation magnets and Litz track. The physical gap is 17 mm with no shims. However, manufacturing and installation tolerances may result in variations in actual gap height along the track length. Departure from the design value will be measured. These measured gap variation will be very informative in analyzing the ability of the long “magnet skis” to filter out these irregularities. The primary purpose of this test is to verify:

- Gap measurements displayed on the computer monitor conform to actual physically measured gaps values

Test Configuration #1-5 Inverter Temperature Rise. — Ohmic heating from IGBT switching is transferred to the heat sink plates and then to the airflow in the exhaust stack. These temperatures are monitored to protect IGBTs. The primary purpose of this test is to verify:

- Inlet and exhaust air temperature change through the cooling stack
- Heat sink temperatures

Test Configuration #1-6 LSM Cable Temperatures — To protect the cable insulation, the insulation material temperature will be monitored and limited to 105°C. However, accurate measurement of the maximum temperature in the insulation is not simple. For the current phase, a maximum temperature of 90°C will be used. When the cable temperature reaches this limit, the test will stop until the cable cools to 40°C. For the reliability of the temperature measurement, three thermocouples will be embedded at different locations on the cable.

Test Configuration #1-7 Emergency Braking Performance — For emergency stop test runs, the inverter power will be disconnected and the mechanical brake will be engaged simultaneously. An emergency button in the control room will activate this command. The primary purpose of this test is to verify:

- Emergency command is reliably performed
- Brake engages safely and maintains contact over the irregularities in the top plate such as the joint between two guideway modules

The test results will be carefully evaluated to assure that all the components are working and their performance is satisfactory. When all the test configurations of Phase 1 are completed, the test system will be ready for the Phase 2 and Phase 3 dynamic testing.

Test Configuration #1-8 Automatic Train Protection Performance — The ability of the automatic train protection (ATP) system will be evaluated by intentionally running the vehicle, in a safe manner, above a (reduced limit) programmed braking profile. The primary purpose of this test is to verify:

- Braking and inverter shut down commands perform reliably.

7.2 PHASE 2 TESTING

The test matrix for Phase 2 is shown in Table 6. Phase 2 is intended to validate the algorithms used to control the LSM/track/vehicle interactions. The objective of this testing is to evaluate the range of stable operating conditions for each of four different configurations of testing weight for the vehicle. Stable operation is defined as when the levitation gap does not grow with time and thrust can be modulated without exciting resonance in the system. The four different test configurations for the vehicle were selected: 6500 kg, 8000 kg, 9000 kg, and 10500 kg. The test configuration parameters include jerk limit, cruise speed and lift current I_d . Simulations have been run for the selected vehicle weights. A jerk limit of 0.1 g/s (1.0 m/s³) will be used for all the runs to reduce overshooting of the levitation gap. A key objective for this phase of testing is to verify that the I_d command current generates the appropriate (either downward or upward) lift force. A 5-mm-thick station shim will be installed on the first GM module at each end of the test track. However, 10-mm shims may be necessary if the peak currents, with 5-mm shims, are beyond the limit of the present inverter.

Table 6. Test Matrix for Phase 2

Test Conf. #	Vehicle Weight (kg)	Cruise Speed (m/s)	Accel/Decel (m/s ²)	Id Current (A)	Lift-off Speed (m/s)	Cruise Gap (mm)	Peak* Vq (V)	Peak* Iq (A)	Peak* Power (MVA)	Remarks
2-1	6500	2	1.6	0	N/A	22/17	1000	1500	1.8	Short runs, no lift
2-2	6500	3	1.6	0	N/A	22/17	1100	1700	2.4	Short runs, no lift
2-3	6500	8	1.6	0	4	29	1100	1800	2.5	Short runs, short lift
2-4	6500	8	1.6	1000	5	29	1150	1900	2.6	Full runs
2-5	6500	8	1.6	2000	6	28	1200	2000	2.8	Full runs
2-6	8000	8	1.6	0	6.5	30	1100	2100	2.5	Short runs, short lift
2-7	8000	8	1.6	500	6.3	29	1150	2200	2.8	Short runs, short lift
2-8	8000	8	1.6	1000	6	28	1100	2500	2.6	Full runs
2-9	9000	10	1.6	0	6	29	1200	2300	2.6	Full runs,
2-10	9000	10	1.6	250	6.3	28	1100	2350	2.5	Short runs, short lift
2-11	9000	10	1.6	500	6.5	28	1000	2400	2.4	Short runs, short lift
2-12	10500	10	1.6	0	8.5	26	1200	2700	3	Short runs, short lift
2-13	10500	10	1.6	-600	8	27	1100	2600	2.8	Full runs

*Estimated motor parameters based on 5 mm station shims

The range of weight for the Phase 2 test vehicle is between 6,500 and 10,500 kg. The 6,500 kg vehicle is the lightest, without the water tanks on the vehicle. This weight translates to a full-size (2 chassis) vehicle of 13,000 kg. For the test configurations with the 6,500 kg weight vehicle, three I_d current values of 0A, 1000A, and 2000A will be evaluated. Since test configurations

#2-1 and #2-2 will not generate enough force to achieve lift off, the vehicle will remain on its wheels. However, the strain gages on the wheels may show how much lift force is being generated during the test. The simulations indicate that a large I_d current, in the vicinity of 2000A, is required to achieve stable levitation (Test configuration #2-5).

Test configuration #2-3 will generate sufficient force for lift off, but levitation may not be stable, based on the simulation analysis. As such, a few short runs will be made before a full track run will be attempted. It is intended that any unstable test runs from test configuration #2-3 and #2-4 be used to identify the general behavior of the vehicle. Test configurations 2-3, 2-4, and 2-5 will allow determination of an optimum I_d current for the most stable operation. The test parameters will be varied to some extent to find a set of the most stable operational conditions for the vehicle weight.

A test procedure similar to that planned for the 6500 kg vehicle will be used for the 8000 kg vehicle tests (test configurations 2-6, 2-7, and 2-8). The water tanks, which weigh 1100 kg, will be mounted and filled with 400 kg of water to achieve a combined total weight of 8000 kg. Our simulation models indicate that the most stable operation may be found at an I_d current in the vicinity of +1000A (test configuration #2-8). However, two preliminary runs (test configuration

#2-6 and #2-7) will be made to investigate the lift generated before the test configuration #2-8 is conducted.

Test configurations will be made for the vehicle weights of 9,000 and 10,500 kg. Additional water will be added to the water tanks to achieve the required vehicle weights. Again, the I_d current will be varied for each vehicle weight until the most stable condition is found.

7.3 PHASE 3 TESTING

The test matrix is shown in Table 7. The objective of Phase 3 testing is to quantify the system performance in areas including ride quality, curve negotiation, and 6 DOF dynamics during acceleration and deceleration, etc. For all test configurations of the Phase 3 testing, we plan to hold the weight of the vehicle and the station shim height constant. Presently, the preferred fixed weight of the test vehicle and the station shim height are 9000 kg and 5 mm, respectively (as shown in Table 7). However, these values may change based on the results of Phase 2 testing.

Table 7. Test Matrix for Phase 3

Test Config. #	Vehicle Weight (kg)	Cruise Speed (m/s)	Accel/Decel (m/s ²)	Id Current (A)	Lift-off Speed (m/s)	Cruise Gap (mm)	Peak Vq (V)	Peak Iq (A)	Peak Power (MVA)	Remarks
3-1	9000	7	1.6	0	6.5	27	1000	2400	2.4	5-mm shim
3-2	9000	8	1.6	0	6.5	28	1000	2400	2.4	Monitor effect of cruise speed
3-3	9000	9	1.6	0	6.5	28.5	1000	2400	2.4	On ride quality
3-4	9000	10	1.6	0	6.5	29	1000	2400	2.4	
3-5	9000	7	1.6	0	6.5	27	1000	2400	2.4	5mm shim
3-6	9000	8	1.6	0	6.5	28	1000	2400	2.4	Monitor effect of cruise speed
3-7	9000	9	1.6	0	6.5	28.5	1000	2400	2.4	on Lateral motion.
3-8	9000	10	1.6	0	6.5	29	1000	2400	2.4	
3-9	9000	7	1.6	0	6.5	27	1000	2400	2.4	5-mm shim
3-10	9000	8	1.6	0	6.5	28	1000	2400	2.4	Monitor effect of CG on pitching,
3-11	9000	9	1.6	0	6.5	28.5	1000	2400	2.4	2 CGs will be tested.
3-12	9000	10	1.6	0	6.5	29	1000	2400	2.4	

Test configurations 3-1, 3-2, 3-3, and 3-4 are intended to evaluate the ride quality of the vehicle secondary at four different cruise speeds. Accelerometer readings from the secondary will be used to quantify the ride quality in three directions: vertical, lateral and longitudinal.

Test configurations 3-5, 3-6, 3-7, and 3-8 are intended to measure the lateral displacement during the negotiation of the curve segment of the test track. The two lateral gap sensors, front and

back of the vehicle, will measure the lateral displacements while the vehicle runs the transition and curve sections.

Test configurations 3-9, 3-10, 3-11, and 3-12 are intended to find the effects of center of gravity (CG) on the behavior of the vehicle such as pitching, yawing, etc. This behavior will be investigated at two different CGs and four different cruise speeds. When the vehicle weight is 6500 kg without additional weight, the CG is at the floor level. When the weight is increased to 9000 kg with the water tank, the CG is 1000 mm above the floor, but it may be adjusted to 100 mm above the floor when lead weights are used. For reference, the floor level of the secondary for the test vehicle is similar to floor level of the passenger compartment for a commercial vehicle.

8.0 CONCLUSION

The results obtained from the above described testing will be used to compare to analytical predictions to ensure that our analysis tools accurately predict system performance so that we can confidently proceed with the design of the demonstration and future deployment systems.

This page intentionally left blank

APPENDIX A
COMPONENT TESTS COMPLETED AS PART OF SUPPLEMENTAL #1 AND
SUPPLEMENTAL #2

1. LSM STATIC BENCH TEST

The LSM static bench test was conducted to verify the LSM generated forces. A full-scale LSM model, 2λ in length, was built on a milling machine and the forces were measured using 6-degree load cell. Three DC currents simulating the 3 phase LSM current at the peak thrust condition was applied to the LSM windings. The permanent magnets in two Halbach arrays were mounted on the milling machine base table allowing accurate measurements of test parameters.

These tests were conducted in July 2002, and the results reported during TIM #9. The test results verified the analytical predictions very closely. The test results may be summarized as follows:

Thrust: ~ 50 kN / vehicle @ 1500A(4 turn) and 25 mm gap and no Lateral Displacement

Thrust is linearly proportional to the LSM current

Guidance force: 30 kN / vehicle @ 25 mm lateral displacement

The sample test results are shown in Figures 1 and 2. These measurements represent $1/18^{\text{th}}$ of the value for one vehicle. The test results verified that the LSM would generate the required forces as designed.

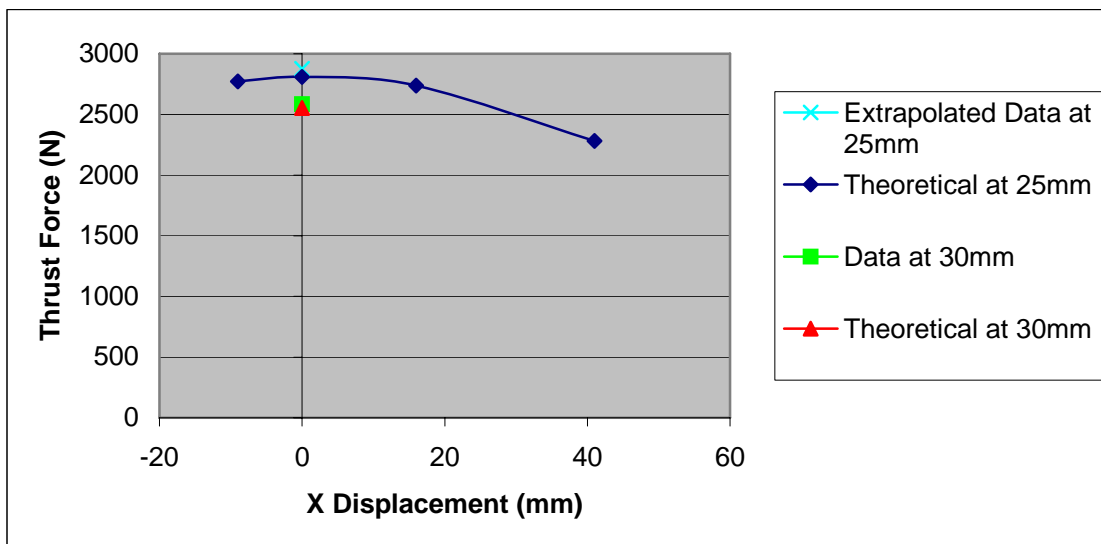


Figure 1. LSM thrust at 1500 A (4-turn winding)

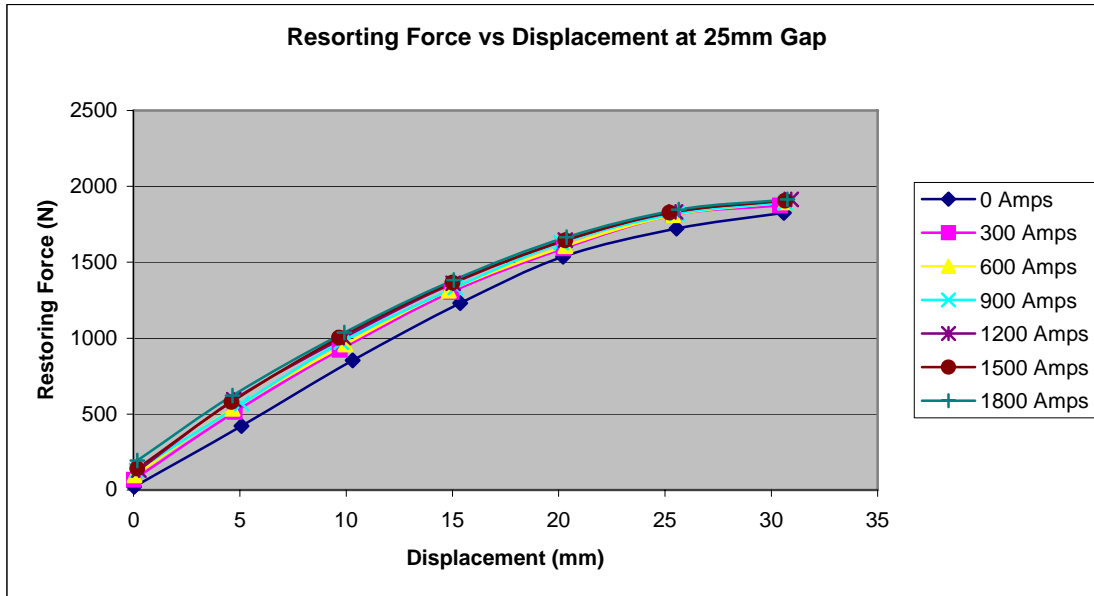


Figure 2. Restoring force at various LSM currents

2. TRACK AND VEHICLE MEASUREMENTS

The following measurements were made with the test vehicle and 1st guideway module:

- Measurement of important physical dimensions
 - Guideway dimensions
 - Chassis dimensions
 - Dimensions after mating of the two
- Measurement of Structural Properties
 - Natural Frequencies of Litz track and Vehicle
 - Static deflections of Litz track due to vehicle weight
- Measurements of magnetic properties
 - Field distribution between magnet arrays
- Measurements of LSM cable electrical parameters
 - Resistance, Inductance, Time Constants, Electrical Insulation
- Static Force measurement

These measurements were reported in prior monthly reports and were used in both the analyses and simulations. A few important measurements are selected and included in this report.

The magnetic field (longitudinal) along the centerline of upper and lower magnet arrays was measured as shown in Figure 3. As shown, the field distribution is sinusoidal and the peak field was predicted to be approximately 0.6 Tesla. The measurement verified the analytical predictions.

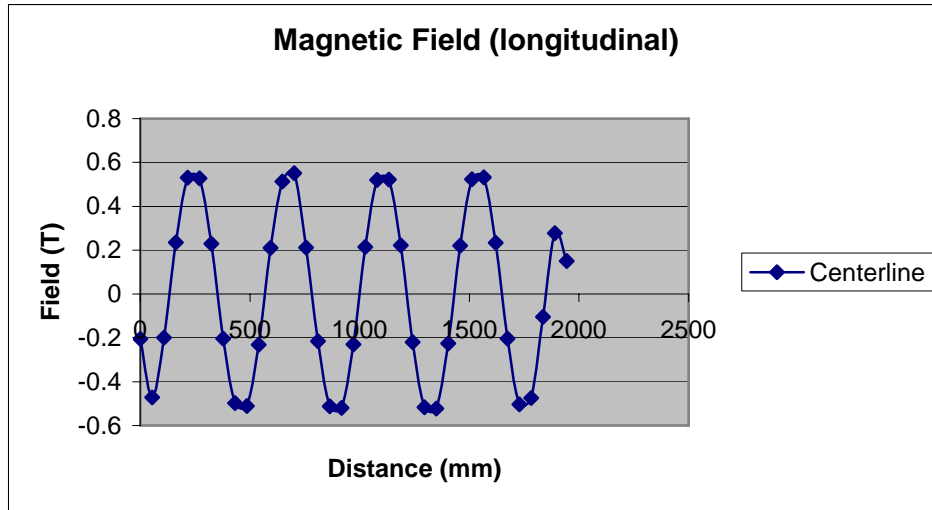


Figure 3. Magnetic field between magnet arrays

The LSM electrical parameters were measured as follows:

- Electrical Resistance 42.4 mΩ/module
- Inductance 600–750 μH/module
- Time Constant, L/R 14.3–17.9 ms
- Hi Pot Over 4000 V

The natural frequencies of the structural components were measured as follows:

- Litz Track (guideway) 50 Hz
- Magnet Cans, Upper 60 Hz
- Lower 44Hz

The excitation frequency of 23 Hz at 10 m/s indicates that there will be no resonance during the test operations up to 10 m/s.

3. SYSTEM LSM STATIC TEST ON TEST TRACK

LSM static thrust for the test vehicle on the test track was measured using two load cells attached to each side of the vehicle and reacted on the test track. The thrust was generated at preset motor angle from 0 to 360° in increments of 30°. The tests were run with no shim and with a 10-mm shim. The results showed very close agreement with the predictions (Figures 4 and 5). For the same propulsion current, the thrust increased by 16% when 10-mm shim was used.

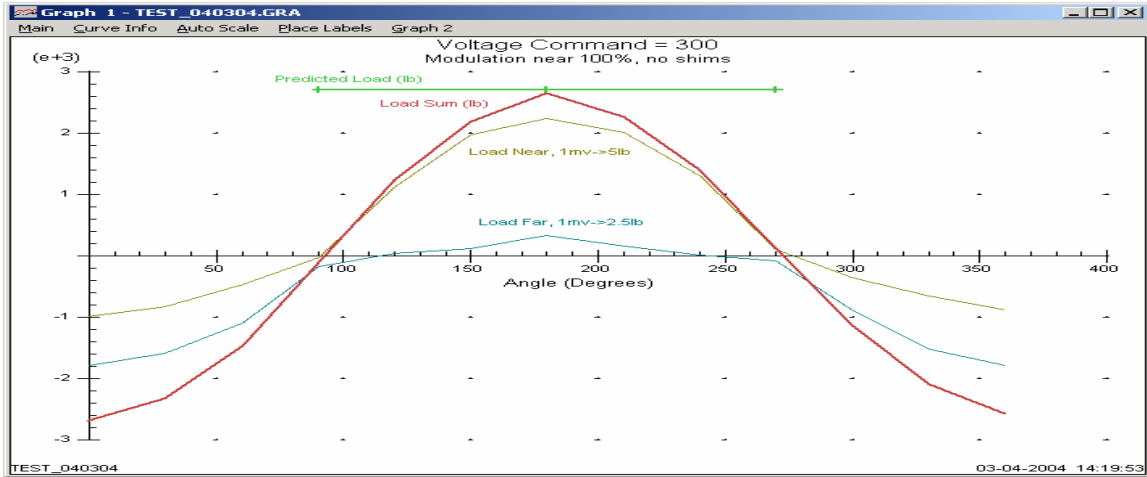


Figure 4. Thrust as function of phase angle — no shim, 1050A

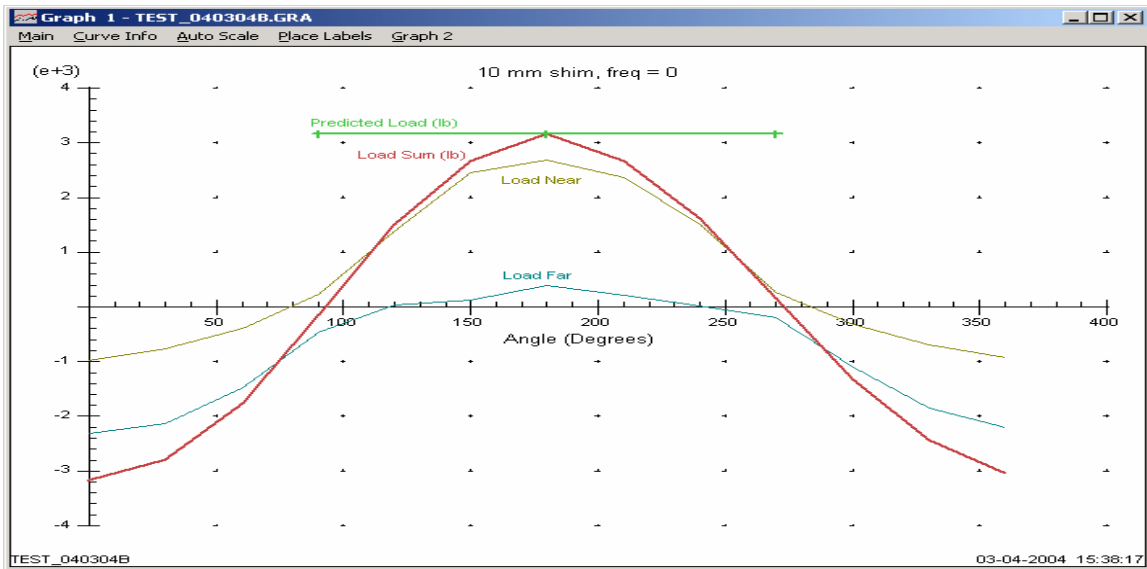


Figure 5. Thrust as a function of phase angle — 10-mm shim, 1050A

4. POSITION DETECTION TEST

An accurate and reliable position detection system is essential for inverter and propulsion control. The original approach for the position detection was use of wiggly wire in the guideway and the vehicle antenna injecting 20 kHz signal on the wiggly wire. The signal from the wiggly wire is to be collected at the wayside. During the development of this technology, printed circuit panels with transpositions spaced at 9 mm, 36 mm and 432 mm were built and extensive tests were conducted at the GA test track. The wiggly wire idea, however, was discarded for the test track because of strong inverter switching noise. The interference between the inverter switching (2 kHz and its harmonics) and injected signal (20 kHz) was noticeable and caused the following problems.

- **False pulses detected at standstill:** Inverter noise signals were interpreted by the position sensor micro controller as vehicle motion, resulting in a varying position indication while the vehicle was at standstill.
- **Corruption of normally detected pulses during vehicle motion:** The software falsely interprets the high frequency ripple components as transpositions, resulting in a higher-than-actual transposition count.

The results of the above are apparent in Figure 6, which shows the (demodulated) input voltage to the wayside processor, as well as the transpositions detected by the processor during vehicle motion:

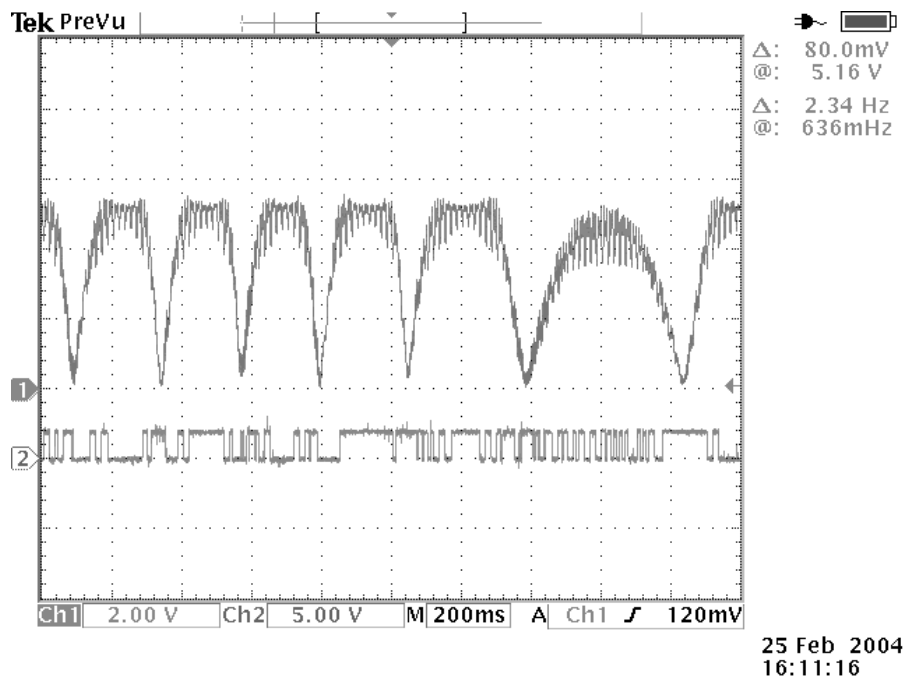


Figure 6. Wiggly wire test data (vehicle moving)

One of the problems was the 20 kHz signal frequency, which is too close to the 10th harmonic of the inverter switching frequency. A few changes have been made and the modified system was tested without satisfactory results. The changes on the modified system includes:

1. Change signal carrier frequency to 19 kHz
2. Stabilize signal carrier frequency by crystal control.
3. Change band pass filter center frequency to 19 kHz.
4. Increase software noise threshold.

These changes did not produce a satisfactory result. Consequently, a new position detection method was adopted for the test track test. The new system employs a laser sensor and optical tape with black and white stripes (18 mm wide) with resetting stripes at 432 mm. The laser signals were not affected by the inverter noise. The new system requires the signal to originate on the vehicle and to be transmitted wirelessly to the wayside. Tests conducted at the GA test track with vehicle in motion, produced clear and reliable signals for 18 mm pulses and 432 mm resettings.

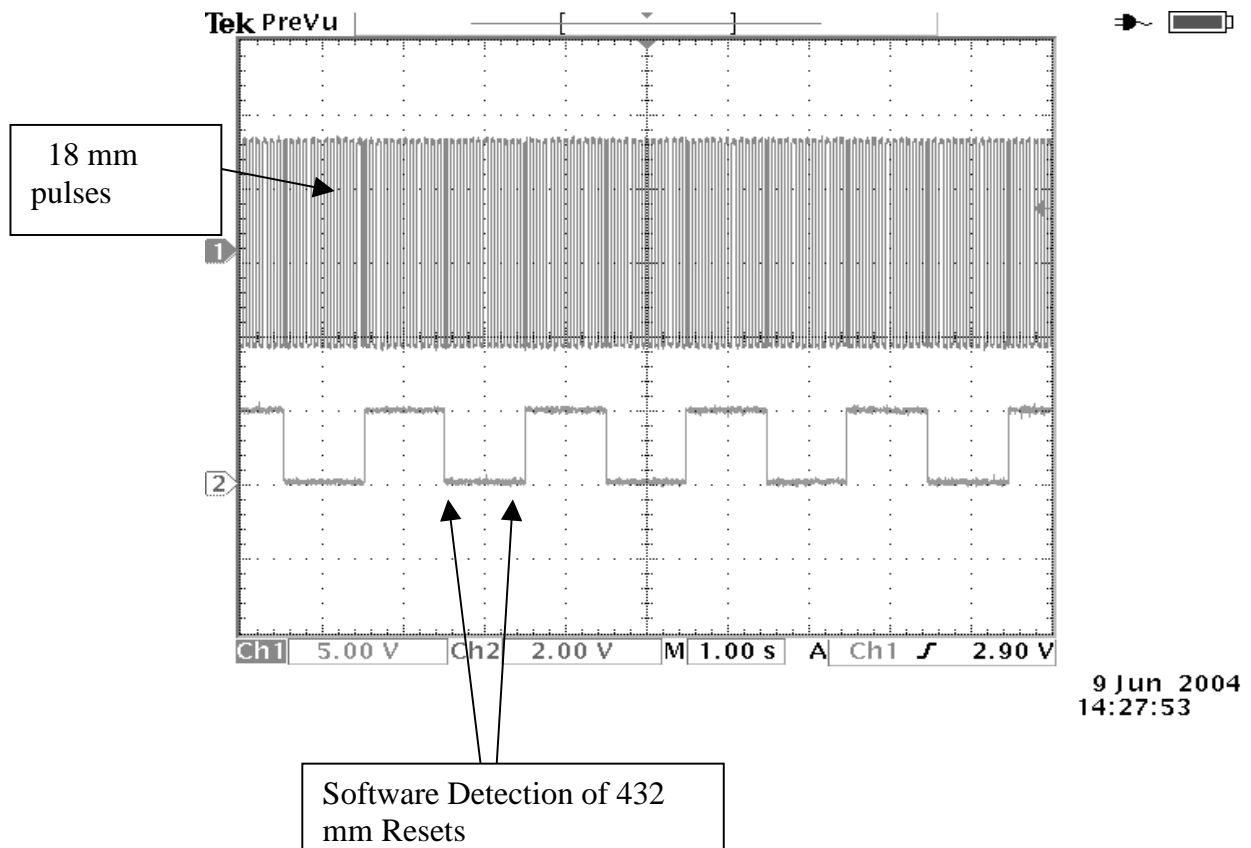


Figure 7. Laser Optical Test Data- vehicle moving

5. LSM STATIC LIFT FORCE MEASUREMENT

The weight of the test vehicle is an important parameter and needs an accurate measurement for the test operations. The vehicle weight is to be measured with strain gages on the eight outboard wheels. A systematic offset was observed in addition to the effect of the static lift. The strain gage readings had to be corrected for the LSM static lift by the relationship:

$$\text{True Vehicle Weight} = \text{Strain Gage Reading} + \text{LSM Static Lift}$$

The static lift force is a function of LSM gap. The static lift was measured by three different methods and compared with analytical prediction. There was some data scatter ($\pm 20\%$) but the results validated the calculation.

The vehicle weight may be calculated from the air bag pressure also. The air pressure allows us to calculate the secondary mass above the air bags. The primary weight is known and does not change.

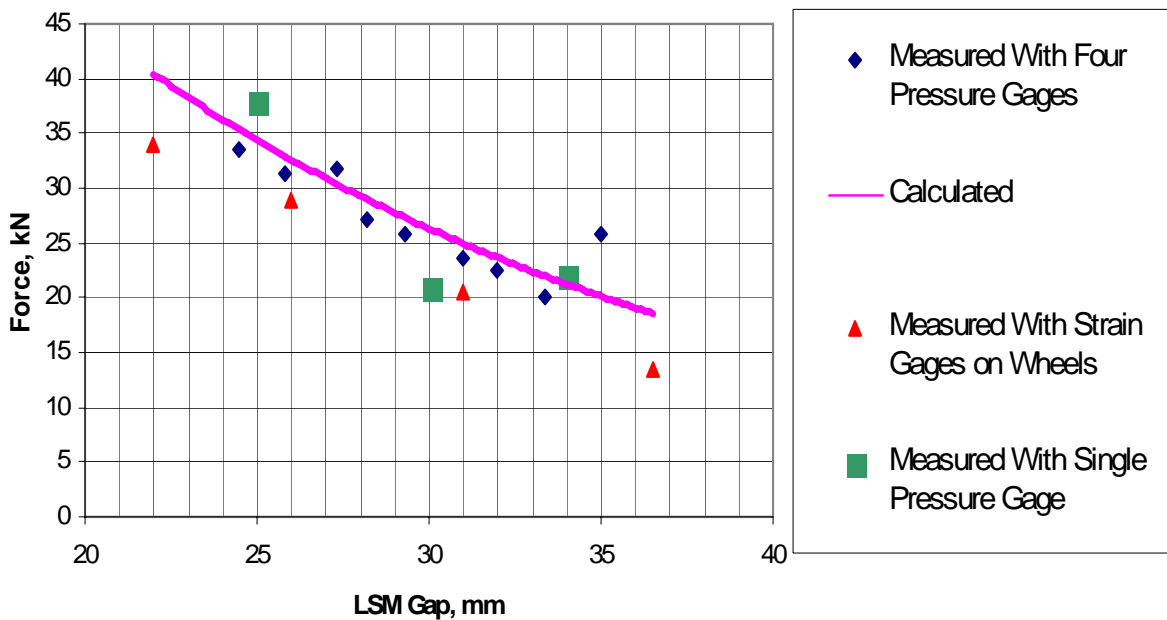


Figure 8. LSM static lift

6. DATA ACQUISITION SYSTEM TEST

The data acquisition system was assembled and tested under a condition similar to the real situation while vehicle was moving with LSM power. The goals of the tests were:

- Verify functionality of data acquisition system
- Demonstrate ability of DAQ system to acquire, store, wireless transmission, and
- Real time display of the data
- Gain better understanding of sensor wiring and signal processing concerns
- Acquire useful initial data from vehicle tests.

The test proved that the system is working and all the test goals were achieved. However, only six data signals were available and real-time display of only one signal at a time was possible during the test. Further testing will be conducted with all assigned data signals and with improved capability to display up to ten signals simultaneously. Figures 9 and 10 show the test data on the data acquisition monitor in control room.

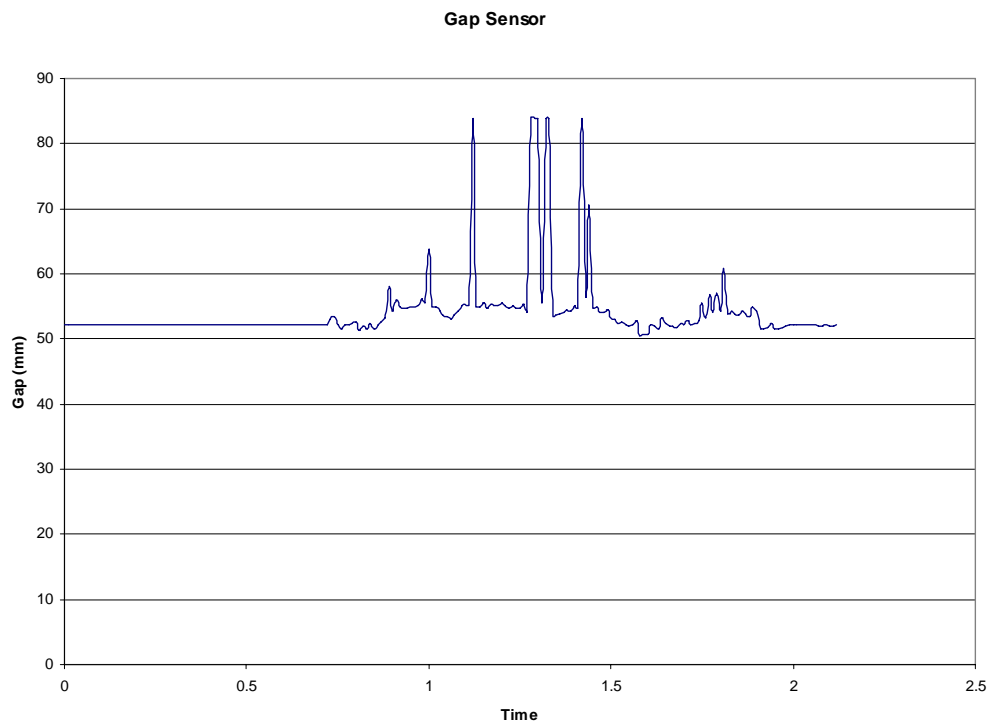


Figure 9. Gap signal displayed on data acquisition computer

The large spikes in the gap signal shown on Figure 9. occurred when the laser beam was directed to the gaps between Litz wire stainless support tubes.

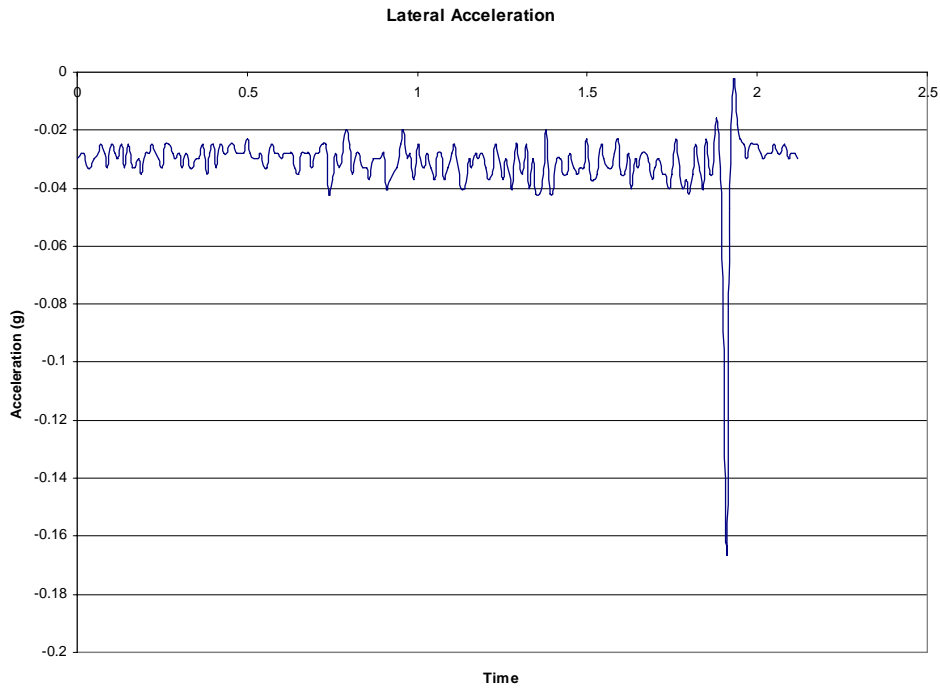


Figure 10. Acceleration signals displayed on data acquisition computer

The large spike of (approximately 0.14g) in the lateral acceleration, at the end of the test, indicates jerking motion that was observed during stopping.

APPENDIX B
CHECKLISTS FOR MAGLEV TEST SYSTEM OPERATION

CHECKLIST FOR STARTUP OF THE MAGLEV TEST SYSTEM

- _____ Visual inspection of the test track for any abnormality and foreign objects on the guideway before start of test (inspection by walking along the track)
- _____ Switches and keys in 37-138 are off and secured
- _____ Rectifier #1 service disconnect is off and secured
- _____ Rectifier #2 service disconnect is off and secured
- _____ Rectifier #1 is set to remote, local off
- _____ Check for Foreign Object Damage (FOD) or other problems in inverter
- _____ Remove ground clips
- _____ Remove ground sticks
- _____ Instrument power (120V) on
- _____ All LEDs are correct, reset if needed
- _____ Turn inverter cooling fan on
- _____ Close inverter door
- _____ Control computer is on (blue)
- _____ Control box is on (gold)
- _____ Interface computer is on
- _____ Verify control computer communicate with inverter (ST/CD/ST/CD/ST)
- _____ All LEDs correct
- _____ Inverter ready
- _____ Ground sticks on interlock hooks
- _____ All personnel ready (a minimum of 3 persons in the room)
 - Test director
 - Test conductor
 - Test support
- _____ Test equipment ready (turn on switches on the vehicle)
 - Turn on DAQ
 - Turn on position device
 - Turn on load leveling
 - Turn on brakes
- _____ Track is secured and marked
- _____ Track red light on
- _____ **“At this point the track is considered energized”**
 - _____ Rectifier #1 service disconnect turned on
 - _____ Rectifier #2 service disconnect turned on
- _____ **“At this point the inverter room is considered energized”**
 - _____ Three keys in room 37-138 to enable position
 - 15 kV breakers on
 - CB#1 on
 - CB#2 on

At this point, it is ready for the test to start”

CHECK LIST FOR SYSTEM SHUTDOWN

a) Standard Shutdown after a Series of Tests

- _____ Test data retrieved from PXI and properly logged
- _____ Turn off inverter control (EI) and verify it (ST) –from control computer
- _____ Turn off rectifiers (ER) and verify it (ST) –from control computer
- _____ Turn off transformer with emergency switch #1 and verify it by checking three red flash lights on the circuit breakers
- _____ Turn on cap dump (cd) and verify buss link voltage is zero (st)
- “At this point the track and inverter is de-energized**
- _____ Open inverter room door
- _____ Open and lock rectifier #1 service disconnect
- _____ Open and lock rectifier #2 service disconnect
- Walk to room 37-138”
- _____ Turn off three switches in 37-138
- _____ Remove and secure three keys (15 kV, CB#1, CB#2)
- “At this point the inverter room is de-energized”**

b) Emergency Shutdown During a Test Run

- _____ Push emergency switch #2: The following actions will take place
 - Rectifier turn off
 - Cap dump
 - Mechanical brake engage
- _____ Turn off inverter control (EI) and verify it (ST) – from control computer
- _____ Verify rectifier turn off (ST) – from control computer
- _____ Verify cap dump (ST) – from control computer
- _____ Open inverter room door
- _____ Open and lock rectifier #1 service disconnect
- _____ Open and lock rectifier #2 service disconnect
- _____ Turn off three switches in room 37-138
- _____ Remove and secure three keys (15kV, CB#1, CB#2)

Legend:

EI – Enable Inverter
 ER – Enable Rectifier
 CD - Cap Dump
 ST – Status (Refers to either Inverter, Rectifier, or Cap Dump)

This page intentionally left blank

Appendix B

*Presented at the Maglev 2004 Conference, Shanghai, PRC and
reproduced in this appendix in its entirety*

LINEAR SYNCHRONOUS MOTOR CONTROL FOR AN URBAN MAGLEV

David W. Doll, *Robert Kratz, **Michael J. Newman

*** Allan B. Plunkett **** Robert D. Blevins

* General Atomics, 3550 General Atomics Court, San Diego, CA 92186, USA,
858 455 3888, david.doll@gat.com,

*858 455 2198, robert.kratz@gat.com,

**858 455 3477, michael.newman@gat.com

*** AC Drives Technology, 26280 S.W. Baker Road, Sherwood, OR 97140 USA

Tel: 503 625 5555 bmwalker@gte.net

**** Consultant, 3818 Pringle St., San Diego, CA 92103, USA

619 297 3827, rdblevins@aol.com

Keywords

Electro-dynamic Suspension (EDS), Urban MagLev, Linear Synchronous Motor (LSM),
Permanent Magnet (PM), Pulse Width Modulation (PWM)

Abstract

A new concept in Urban Maglev transportation design is in the testing phase. The vehicle uses permanent magnets (PM) for both the electro-dynamic suspension (EDS) and linear synchronous motor (LSM) propulsion. Because of the 3D coupled non-linear velocity-dependent magnetic levitation, the LSM must provide stabilizing forces to the vehicle. To do this, Vector Control is used to modulate the inverter voltage, frequency and angle. The inverter angle is adjusted to maintain vertical stability. The controls architecture was developed and tested in a 2D simulation and verified in a 3D six dof dynamic model of the vehicle and guideway; the same magnetic levitation and LSM propulsion algorithms were used in both with the 2D simulation model providing the common control system. Control programming was implemented in C-code, which talks to the inverter pulse width modulation (PWM) card via an intermediate control box. The 2D simulation architecture provided the basis for implementing the control software design. Results from preliminary testing are discussed.

1 Background

The Urban MagLev system (low speed vehicles for inner-city service) now under development at General Atomics relies on an attraction assisted EDS for levitation and a LSM for propulsion. Both the on-board levitation and propulsion magnets are made from high-field NdFeB. This presents a challenge to the control system designer in that all six degrees of freedom (dof) are magnetically and dynamically coupled and are also coupled to the LSM propulsion. At stake is

not only the basic operation of a vehicle but, because it is directed toward public transportation, the ride quality is of paramount importance [1].

The GA Urban MagLev uses simplified algorithms developed from 3D magnetic models (OPERA by Vector Fields) of the geometry in order to describe the forces and Simulink/Mathworks, and MSC Nastran Motion [2] to model the 2D and 3D dynamic operation, respectively. This paper describes the approach taken and includes a sample of the test vehicle simulation results. Included are results from static tests run in February 2004; dynamic operation started in September 2004 and is in progress at this time.

2. System Design

A description of the Urban Maglev is essential in understanding the controls design. A brief summary is presented, and a more complete description can be found in reference [3] and [4].

2.1 Full-Scale Commercial Vehicle and Guideway

Although the GA Urban Maglev is still in the prototype testing stage, a first deployment is in the planning stages at California University of Pennsylvania. The key feature of the attraction-assisted EDS is the use of PMs for both levitation and propulsion. The system is driverless, lending to central control. Vehicles may be operated singly or in trains. The guideway is elevated leaving full access to the space beneath for cross-traffic. Power systems are distributed along the wayside at intervals appropriate for block-switching, which keeps the LSM power demands to a minimum. A 2 minute headway ensures that the LSM duty factor is low with allowance made at stations for higher starting power demands. Figure 1 is an artist's concept of one fully deployed vehicle.

The levitation and propulsion components are located on either side of the guideway and are mechanically interlocked (Figure 2) with the LSMs directly above and in line with the levitation PM Halbach arrays and ladder track. Table 1 provides a summary of the key parameters for the fully deployed Urban MagLev system and test vehicle.



Figure 1. Urban Maglev Vehicle and Guideway

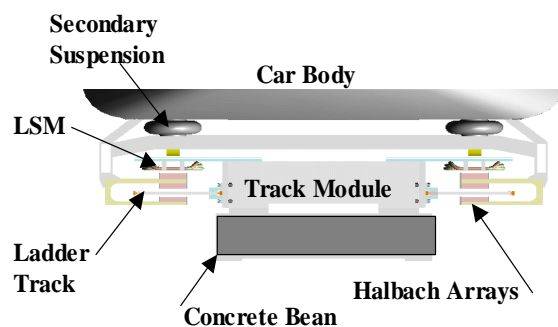


Figure 2. Vehicle-to-Guideway Arrangement

Table 1 Urban Maglev Specifications

System Parameter	Value for Full-Size Vehicle	Value for Test Vehicle
Levitation	PM Halbach array	PM Halbach array
Propulsion	PM LSM	PM LSM
Guidance	Attraction to LSM iron	Attraction to LSM iron
Permanent Magnets	NbFeB; Br=1.4 T; 50 mm sq	NbFeB; Br=1.4 T; 50 mm sq
Halbach Wave Length,	0.432 m	0.432 m
Number of PMs/	M=8; 45 deg	M=8; 45 deg
Operation/safety	ATC (driverless)	ATC (driverless)
DC magnetic field to passengers	<1 Gauss	Measured
Speed/acceleration, maximum	160 km/hr (100 mph)	36 km/hr (22.5 mph)
Speed, average	50 km/hr (31 mph)	36 km/hr (22.5 mph)
Vehicle size	12 m x 2.6 m x 3 m	4 m x 2.6 m x 3 m
Vehicle weight	18 tonnes (100 passengers)	6–11.5 tonnes (no passengers)
Acceleration, max	1.6 m/s ²	1.6 m/s ²
Jerk, max	2.5 m/s ³	2.5 m/s ³
Grade	7% (design >10%)	Zero
Turn radius, minimum	25 m	50 m
Ride quality	ISO 2631 (1987)	Measured

2.2 Test Vehicle

A test vehicle has been built that duplicates without scaling half the actual vehicle described. Figure 3 shows the vehicle as it was installed onto the first guideway module. Preliminary checkout took place on this 15 m section of guideway, and went into full dynamic operation in September 2004 on a 120 m long track, which provides capability to accelerate to 10 m/s at 1.6 m/s². A 50 m radius was introduced midway of the track length in order to test the dynamics and control around a curve. Levitation, propulsion and guidance will validate the overall operation and control



Figure 3. Urban Maglev Test Vehicle

2.3 Test Facility Power Systems

Propulsion power is supplied to the LSM from an inverter specifically designed by GA to handle the high peak current encountered as the vehicle accelerates through the drag peak encountered at 3 to 4 m/s. The inverter is three-phase five level and utilizes four half-bridges. Since the power is delivered into LSM load is voltage-limited, both a series delta and parallel Y connections will be tested to identify the lowest impedance and most scalable arrangement.

3. Dynamic Simulations Modeling

3.1 2D Simulation Description

Because of the coupled nature of the magnetics, it was necessary to construct a simulation of the Urban Maglev test system. Simulink/Matlab was selected as the computing platform. The simulation was developed for the test vehicle to meet that system’s specific requirements, but modifications to scale to the full-sized commercialized system accounting for alignment features (grades, turns and station stops) are straightforward.

Four separate subsystems were used to describe the simulation: Control, Inverter, LSM and Vehicle. Each contains the particular algorithms best describing the hardware and software; Figure 4 shows the primary dependencies. A brief description of each subsystem follows.

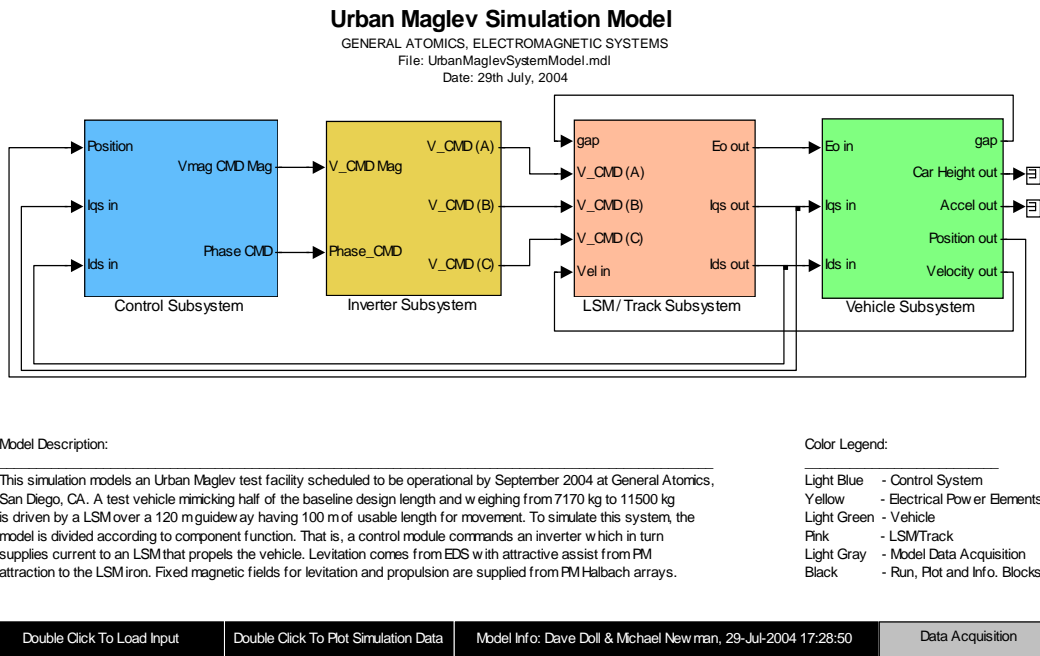


Figure 4. Matlab Simulink Model of the Urban Maglev Test Track System with the Control Highlighted

Vehicle: The vertical force components are EDS levitation, LSM iron/PM attraction and LSM d-axis current, I_{ds} , attraction/repulsion. For a given PM strength (nominally $B_r = 1.4$ T) and geometry, EDS levitation forces depend on forward velocity and gap. PM/LSM iron attraction is exponential with gap and varies weakly with lateral displacement from centreline; d-axis current depends on motor angle. Thrust is derived from the q-axis current, which is sent with the d-axis current from the LSM.

LSM: This block calculates the current in the direct I_d and quadrature I_q axes by vector transformations from the three phase voltages created by the inverter.

Inverter: The inverter takes the voltage magnitude and phase command coming from the Controls and converts them into three phases, A, B and C.

Controls: Vector control [5] is used for commanding the LSM drive currents. Unlike most PM LSMs, damping plates are not used to suppress oscillations. Instead, the voltage magnitude and angle are controlled to both suppress oscillations and provide a vertical force balancing mechanism to augment or suppress the attractive and levitating forces. Processing of the

feedback signals is necessary before they are applied to the functions that generate the control signals to control to inverter, and thus the vehicle. This is done with filters.

3.2 3D Simulation Description

A 6 dof numerical simulation in NASTRAN Motion, a 3D modeling platform for solid body dynamics was used to model the MagLev test system. It included all the coupled magnetic forces derived for the 2D model plus the coupled dynamic forces in 6 dof, plus the lateral and vertical limiting guidance wheels that allow up to ± 0.02 m travel. In order to test the simulated control system, the 3D NASTRAN simulation was coupled to the 2D Simulink controls simulation and run interactively. This gave the nearest approximation of the actual system practicable.

3.3 Magnetic Force Models

EDS lift and drag were calculated with a 3D current sheet model of the PM's B-field and verified against 3D calculations using OPERA. The interactions with the ladder track follows from Faraday's law. These calculations were performed for a series of gaps and velocities and subsequently subjected to a curve fit.

The form of the fit functions, i.e., the dependence on gap and velocity was taken from simple 2D theory. The fit coefficients adjust these functions to the three dimensional model. These coefficients incorporate the transition velocity and accounts for the footprint area, the track geometry and the 3D nature of the generating fields.

$$F_L(g_1, v) = N_{ski} (a_1 e^{-2k g_1} - a_2 e^{2k g_1}) \cdot \frac{1}{1 + \left(\frac{a_3}{v}\right)^2} \text{EQ1}$$

$$F_D(g_1, v) = N_{ski} (b_1 e^{-k g_1} - b_2 e^{k g_1})^2 \cdot \frac{\frac{b_3}{v}}{1 + \left(\frac{b_3}{v}\right)^2} \text{EQ2}$$

$$k_s(g_1, v) = N_{ski} 2k (a_1 e^{-2k g_1} + a_2 e^{2k g_1}) \cdot \frac{1}{1 + \left(\frac{a_3}{v}\right)^2} \text{EQ3}$$

Coefficient	Value	Units	Error
a1	114.328	kN	0.04%
a2	7.335	kN	0.16%
a3	3.717	m/s	0.07%
b1	-10.889	sqrt(kN)	0.04%
b2	-2.740	sqrt(kN)	0.10%
b3	3.719	m/s	0.06%
Variable	Value	Units	Definition
k	14.544	1/m	2pi/Lambda
Lambda	4.320E-01	m	Wave length
FL		kN	EM Lift force
Fd		kN	EM Drag force
ks		kN/mm	Spring constant
g1		m	Mag. Levit. gap
v		m/s	Forward velocity

The LSM coupling to the propulsion Halbach arrays was more complicated. An attractive force exists between the PMs and the iron rails supporting the LSM coils which varies exponentially with the gap between them. Also, LSM operation off of a 90^0 motor angle produces an upward or downward force that varies with current, angle and exponentially with the LSM gap.

The coupled non-linear relationship describing the magnetic interaction between the LSM current and the Halbach arrays was also modelled in 3D OPERA (Vector Fields). Algorithms of the forces based on the linear dependence on current, exponential dependence on LSM gap and sinusoidal dependence on wave number were derived by curve fitting to 3D plots. This approach

permitted calculating the dynamic forces in a simulation environment otherwise unapproachable if attempted completely in 3D.

The functions and coefficients for thrust force, guidance force (active and passive) and lift forces (active and passive) are:

$$Th(d, g_3, \alpha) = \frac{N_{ski}}{4} (a_0 + a_2 \cdot d^2) \cdot \exp(a_g \cdot g_3) \cdot \frac{I_{peak}}{I_{norm}} \cdot \cos(\alpha) \quad \text{EQ4}$$

$$Ga(d, g_3, \alpha) = \frac{N_{ski}}{4} (ba_1 \cdot d + ba_3 \cdot d^3) \cdot \exp(ba_g \cdot g_3) \cdot \frac{I_{peak}}{I_{norm}} \cdot \sin(\alpha) \quad \text{EQ5}$$

$$Gp(d, g_3, \alpha) = \frac{N_{ski}}{4} (bp_1 \cdot d + bp_3 \cdot d^3) \cdot \exp(bp_g \cdot g_3) \quad \text{EQ6}$$

$$La(d, g_3, \alpha) = \frac{N_{ski}}{4} (ca_0 + ca_2 \cdot d^2) \cdot \exp(ca_g \cdot g_3) \cdot \frac{I_{peak}}{I_{norm}} \cdot \sin(\alpha) \quad \text{EQ7}$$

$$Lp(d, g_3, \alpha) = \frac{N_{ski}}{4} (cp_0 + cp_2 \cdot d^2) \cdot \exp(cp_g \cdot g_3) \quad \text{EQ8}$$

$$\alpha = \frac{x}{\lambda} \cdot 2\pi = x \cdot k \quad \text{EQ9}$$

Coefficient	Value	Unit
a0=	61.1509	kN
a2=	-0.0032	kN/mm ²
ag=	-0.0152	1/mm
cp0=	200.1756	kN
cp2=	-0.0747	kN/mm ²
cpg=	-0.0425	1/mm
ca0=	-66.9098	kN
ca2=	0.0088	kN/mm ²
cag=	-0.0138	1/mm
bp1=	-4.9915	kN/mm
bp3=	0.0022	kN/mm ³
bpg=	-0.0636	1/mm
ba1=	0.9485	kN/mm
ba3=	-0.0003	kN/mm ³
bag=	-0.0321	1/mm

Variable Definitions

Th = Thrust

Ga = Guidance – active

Gp = Guidance – passive attraction

La = Lift – active

Lp = Lift – passive attraction

d = Lateral displacement

g₃ = LSM gap

α = Phase angle

3.4 Position Sensing

Position sensing emerged as a significant challenge. This was because the motor angle had to be controlled accurately, something not common in commercial train control. Simulations indicated the position had to be resolved within 18 mm in order to maintain stable operation. The vehicle vertical and lateral positions relative to the guideway are also monitored with laser position sensors in order to evaluate the 6 dof dynamic performance and validate the simulation models. The forward position sensing system provides the angle information showing the absolute position of the magnets on the vehicle within a resolution determined by the position sensor resolution. Two resolutions used are 18 mm and 432 mm (motor wave length). This latter position resets the computer to avoid error build up.

3.5 Simulation Results

3.5.1 2D Simulation

Simulations were run for the full range of operating parameters with a focus on the effects of changes in the vehicle mass. The test vehicle mass can be varied from 6000 kg to 11500 kg with a primary mass of 4137 kg and the remainder in secondary structure and water ballast. Because of the 120 m track length and 50 m radius of the single curve, the velocity had to be limited to 10 m/s with a maximum acceleration of 1.6 m/s^2 . The velocity profile used allowed full use of the track and was blended by limiting the jerk, set as an input parameter ($1-1.6 \text{ m/s}^3$). The baseline for testing the simulation was chosen as 9000 kg since it lies midway between the weight limits. The test vehicle simulation parameters were: initial rest LSM gap $g_3 = 36.1 \text{ mm}$ and corresponding levitation gap $g_1 = 17 - 18 \text{ mm}$. The initial gap g_1 can be modified by starting on 5 mm or 10 mm shim beneath the start-off wheels.

Figure 5 shows the vehicle response to the baseline velocity profile (middle graph) and mass. The levitation gap in the upper graph shows lift-off delayed to later than it would otherwise be due to the use a shim beneath the start-off wheels. This was done to minimize the current draw while the vehicle passes through the magnetic drag peak at 3-4 m/s. The second line (violet) shows the response of the secondary or suspended part of the vehicle mass. It follows the primary closely but softens the dynamics for passenger comfort. The sudden lift-off occurs when the lift forces exceed the vehicle mass, and the resulting gap change reduces the magnetic drag correspondingly. As the vehicle slows and returns to its wheels, it does so in the same sudden manner. Wheels modeled with a high spring rate respond to the impact at their characteristic high frequency. Control was maintained through these rapid transients by a combination of the position observer and PI controllers in the control system.

The bottom graph in Figure 5 shows the vertical force balance through the 20 s simulation. At all times during levitation the sum of the lift forces must equal the vehicle mass. The LSM active vertical force is preset by the operator based on the vehicle mass and modulated to maintain the resultant force. A 9000 kg vehicle mass needs no downward or upward force to balance the forces for this gap.

The effect of position error on the thrust and normal force is indicated in the Figure 6. Note that changes in the motor thrust are small for relatively large position errors. However, the effect of a position error on the normal force is more significant as the normal force could oscillate from a minus to plus value while the position jitters about zero.

The current, voltage and power show the effects of the magnetic drag. The force command increases the current in response the increased drag until the peak is reached. Thereafter, the current falls off until the vehicle reaches maximum speed. In the case of the test vehicle, this is limited by the track to 10 m/s. Time at this high current is only about 4 s, well within the inverter’s transient capability and not a significant impact on the overall average power. Slow-down is dominated by the increased drag with reducing gap and added power required to maintain the 1.6 m/s deceleration rate.

3.5.2 3D Simulation

Simulation results showed stable operation over 120 m of straight track, but some difficulty through the 50 m turn. It was found that there is sufficient magnetic lateral guidance to maintain the Test Vehicle in a flat turn.

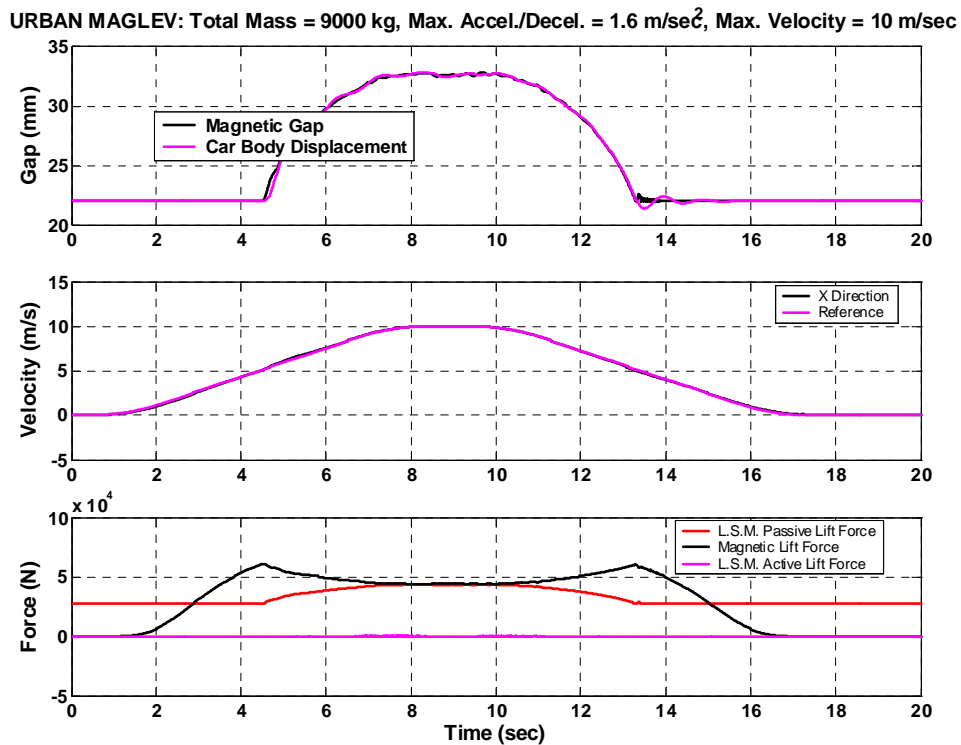


Figure 5. Gap and Force – Start-off Gap Raised to 27 mm with 5 mm Shim

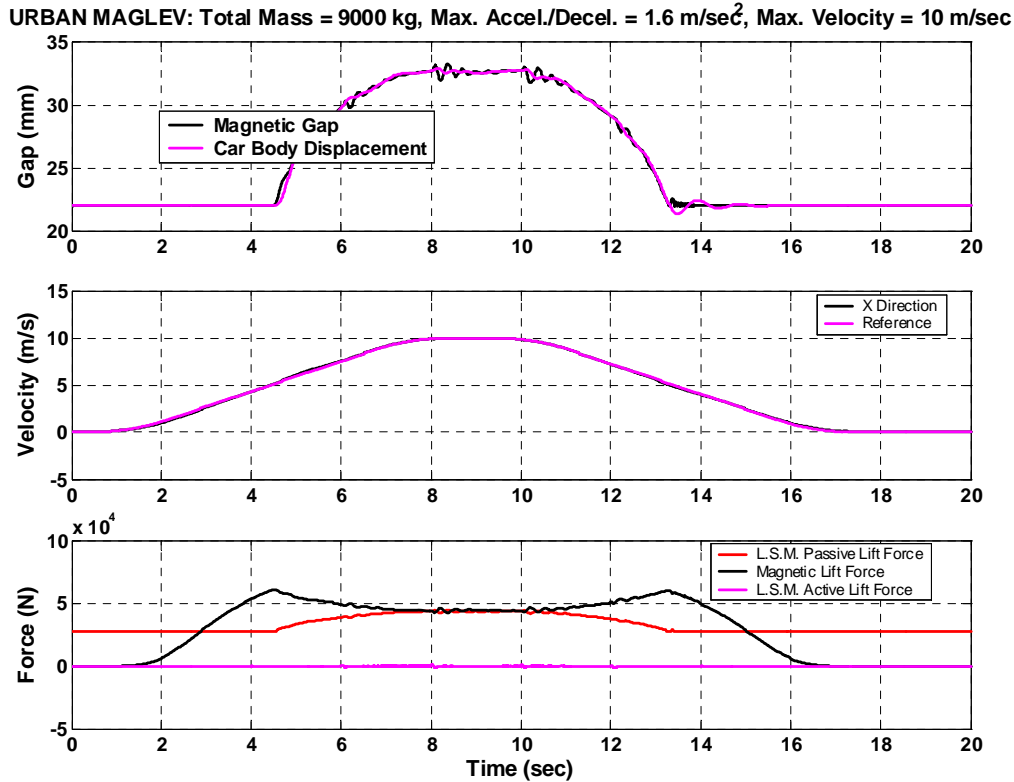


Figure 6. Simulation of Missing Position Location Pulses Every 2 seconds. Error Size: 20mm, offset duration: 50 ms, V_{\max} : 10 m/s, $accel_{\max}$: 1.6 m/s², mass: 9000 kg

4. Controls Design

Once the simulation was completed and satisfactory results obtained, the control logic and algorithms from it were reduced to C-code for implementation into the test facility power and sensing systems. The controls architecture used to construct the simulation also served to guide the implementation. The challenge was to implement only what was necessary without compromising the overall performance.

4.1 Architecture

The overall control architecture used in both the control simulation and implementation is shown in Figure 7. The process begins with the current command to the inverter, which comes from an initial magnetic gap estimate and the thrust requirement. These are summed with the measured I_d and I_q to create the regulated current I_{reg} . From this, the voltages are calculated in the d and q axes, and the corresponding command angle calculated. This angle is summed with the motor angle to command the inverter via the PWM card. The V_d is adjusted by the vehicle weight to match a particular desired gap and the angle adjusted to achieve this gap. The key feedback data comes both from the inverter output and the position sensor. Current feedback is processed to create I_{dmeas} and I_{qmeas} ; the position sensor establishes velocity, acceleration and angle to the PWM via a position estimator that weights the estimates by a thrust/mass/acceleration comparison. The estimated velocity is then compared with the desired velocity to produce the thrust command via the I_qCMD .

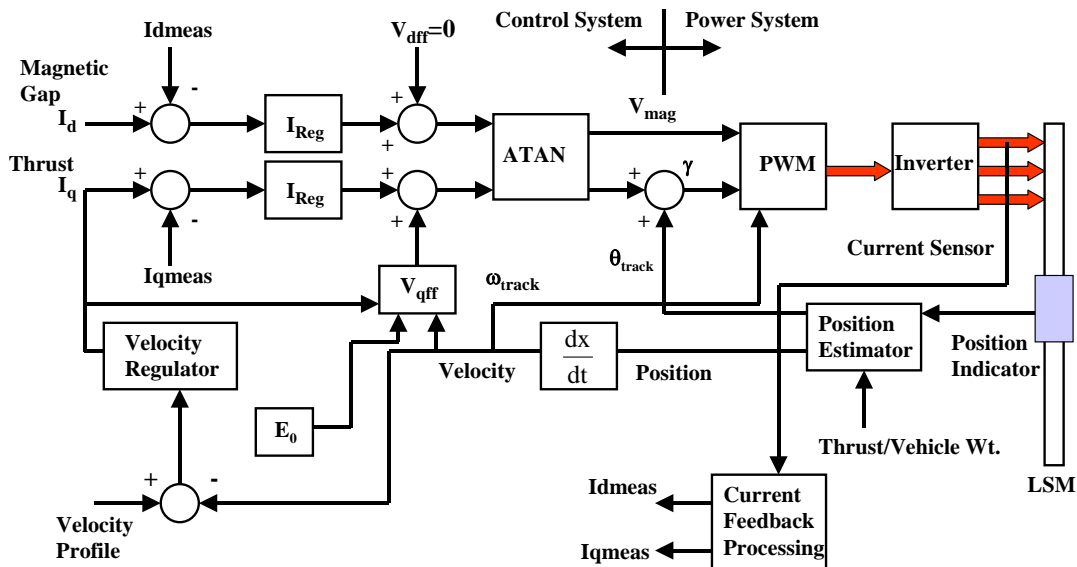


Figure 7. UML Control System Schematic

4.2 Approach to Implementation

Each of the function blocks that made up the simulated controls was reduced to an implementable form. This included processing of inverter voltages, currents and position data. The input signals to the control all require processing before being applied to the functions that generate the control signals to control the inverter, and thus the vehicle. The input signals consist of, inverter voltages and currents and the position sensor data. The data from the position sensor is transmitted to the control box using a serial fiber optic link. The actual data consists of steps in position. To make the position data useable in the control, the data is processed through a digital filter circuit, which provides smoothed data for position and velocity. The position signal and velocity signals are estimates, which will have some lag with respect to the actual data.

5. Test Results

Two sets of static tests were conducted on the vehicle. The first test measured the magnetic attraction of the PMs to the motor iron. Figure 8 shows the test results and the predicted values using equation EQ8. This agreement validated the static lift algorithm used in the controls.

“Locked rotor” tests were run to validate the LSM thrust force algorithms. With the vehicle anchored solidly to the guideway, the inverter was commanded to apply a fixed current at motor angles from 0 to 360° every 30°. The thrust was measured with load cells mounted along the thrust axis parallel to the track. Two levitation gaps were tested, 17 mm with no shim and 27 mm with a 10 mm shim beneath the start-off wheels. Figures 9 and 10 show the measured q-axis force with the calculated maximum values. These results showed excellent agreement with the predicted values calculated from EQ4.

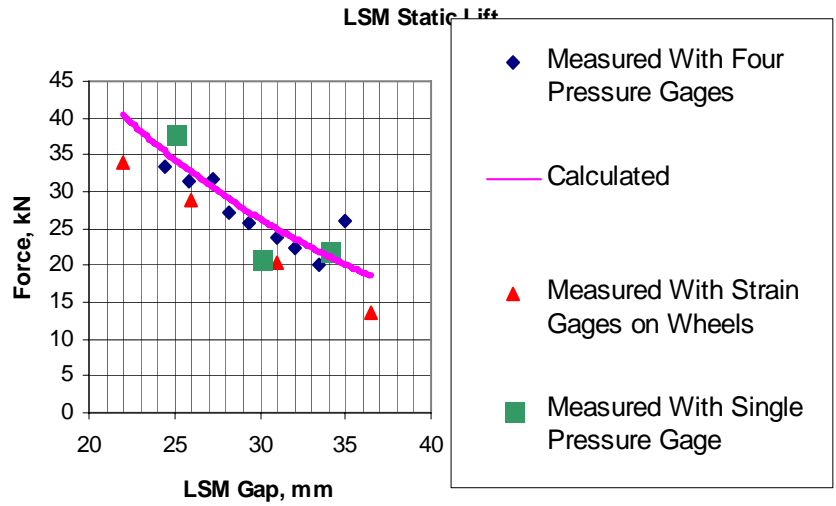


Figure 8. Static Lift Due to Attraction Between LSM Iron and PMs in the Halbach Arrays

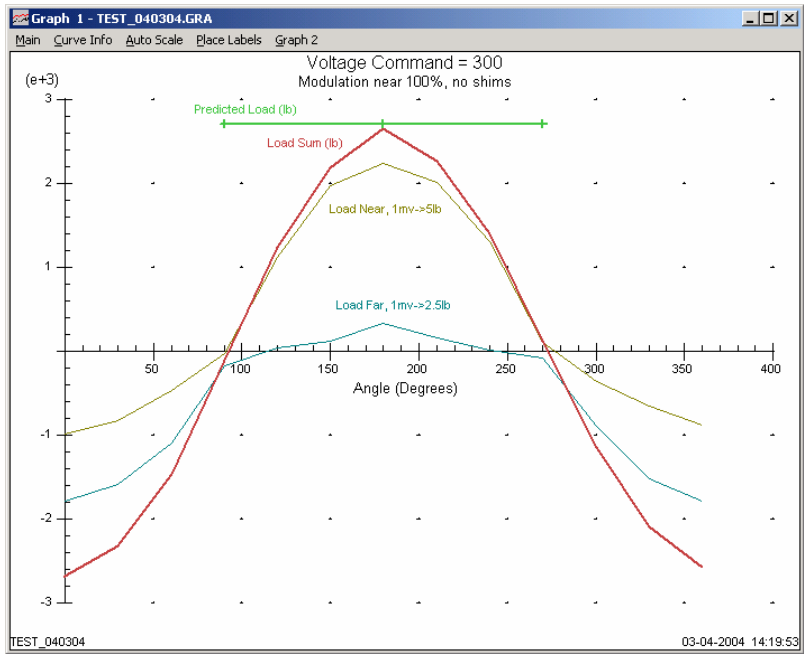


Figure 9. Locked-Rotor Test Results of the Maglev Vehicle with No Shims Under Start-off Wheels (17 mm Levitation Gap)

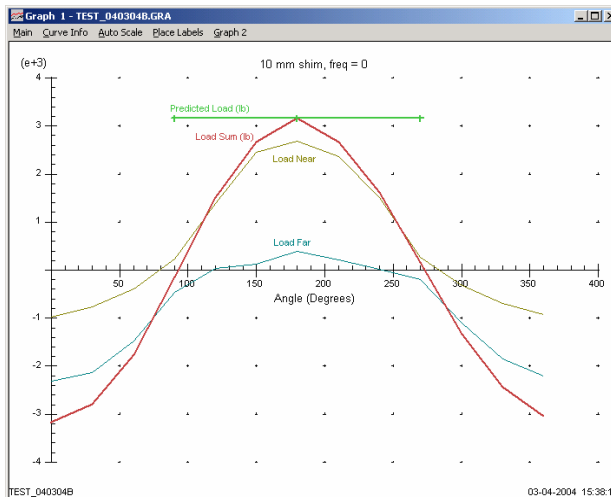


Figure 10. Locked-Rotor Test Results of the Maglev Test Vehicle with 10 mm Shims Under Start-off Wheels (27 mm Levitation Gap)

6. Conclusions

A control system has been developed for General Atomics' Urban Maglev test facility that can be scaled to apply to any alignment. Although the architecture used is fairly standard for transportation systems, the 6 dof coupled behavior required special algorithms describing the levitation, propulsion and guidance. These algorithms reduced the highly complicated 3D magnetics to a form usable in the control system. This understanding of the unique attraction assisted magnetic levitation gives confidence that the Urban Maglev will be successful in the remaining tests leading ultimately to commercialization.

7. Acknowledgements

This paper presents the results of a research effort undertaken by General Atomics under Cooperative Agreement No. CA-26-7025 to the Office of Research, Demonstration, and Innovation, Federal Transit Administration.

8. References

1. D. Doll, et al., "Ride Dynamics of General Atomics' Urban Maglev", Maglev 2002, Lausanne, Switzerland, September 4–8, 2002
2. MSC VISUAL NASTRAN, version 6.2, MSC software, Los Angeles, CA, 2000
3. Sam Gurol, Bob Baldi, and Richard L. Post, "Overview of the General Atomics Urban Maglev Program," Maglev 2002, Lausanne, Switzerland, September 4–8, 2002
4. Sam Gurol, Bob Baldi, "Status of the General Atomics Urban Maglev Program," Maglev 2004, Shanghai, China, October 24–29, 2004
5. D.W. Novotny and T.A. Lipo, "Vector Control and Dynamics of AC Drives", Oxford University Press, Great Clarendon Street, Oxford ox2 6dp, 2000

Appendix C

*Presented at the Maglev 2004 Conference, Shanghai, PRC and
reproduced in this appendix in its entirety*

A Laminated Track for the Inductrack System: Theory and Experiment

J. F. Hoburg, Carnegie Mellon University, Pittsburgh, PA 15213, USA
412-268-2473, hoburg@ece.cmu.edu

R. F. Post, Lawrence Livermore National Laboratory, Livermore, CA USA
925-422-9853, post3@llnl.gov

Keywords

Halbach arrays
Inductrack
Laminated track
Litz cable track
Urban maglev

Abstract

This paper describes work on alternative technologies associated with an urban maglev system that employs Halbach arrays of permanent magnets onboard a moving vehicle to induce levitating currents in a stationary “track”. A laminated structure, composed of stacks of thin conducting sheets, has several advantages over a litz-cable ladder as the track. Modeling and experimental results for the laminated track are described and evaluated in this paper.

1 Introduction

As a part of the development of a generic urban maglev system based on the Inductrack approach, studies have been underway at Carnegie-Mellon University and at the Lawrence Livermore National Laboratory on a new kind of maglev track design – the “laminated track”. The laminated track configuration, as its name implies, is composed of a multi-layer laminate made up of thin conducting sheets of copper or aluminum that are slotted transversely, with a slot width that is less than the total width of the sheet. The pattern thus produced can be visualized as a close-packed configuration of shorted electrical circuits within which currents are induced by the passage of the Halbach arrays of the Inductrack maglev configuration. The advantages of the laminated track over the presently employed ladder-like litz-cable

design are the higher conductor "packing fraction" that can be achieved, its potentially lower fabrication cost, and the track's long-time durability (no solder-joints are required in manufacturing the track).

The particular studies reported here are aimed at evaluating the levitation and drag forces of a laminated track. Two approaches to the analysis are discussed: (1) an approach based on 2-D analytic approximations to the 3-D fields of the Halbach arrays, plus a "circuit-based" analysis of the track electromagnetic parameters (R. F. Post), and (2) a "fields-based" approach (J. F. Hoburg) employing Maxwell's equations, with Fourier analysis of the 3-D field structure and retention of only the first Fourier component. Both approaches were compared to the results of experiments performed on the "Laminated Track Test Rig" constructed at Livermore. Good agreement was found, both between the computed results from the two methods of analysis, and with the results from the test rig.

2 Circuit-based Analytic Description

2.1 Calculation of Induced currents, lift and drag

For the purpose of developing a fast-computing Inductrack levitation code, based on a 2-D analytic formulation, we have developed a code, using the Mathematica® platform, that calculates the lift and drag of a laminated track configuration coupling to an Inductrack II double Halbach array levitating system. In writing the code several approximations were made, and it is important to determine the level of error to be expected in the use of these approximations. Our checkpoints include: (1) a "fields-based" description covered in Section 4 of this paper, (2) separate 3-D Halbach array magnetic field calculations based on the Biot-Savart Law and Amperian currents, and (3) experimental results from a "Laminated Track Test Rig" built at the Lawrence Livermore National Laboratory for the express purpose of benchmarking the code. As will be shown, the results from the simple 2-D code track well with results from the Laminated Track Test Rig and with the results of the fields-based treatment in regimes that are of practical interest.

The starting points for the 2-D analysis and code development are the 2-D equations for the vertical (y) and horizontal (x) components of the magnetic field from a single-sided Halbach array, as defined by Halbach in his published work [1]. These are as follows:

$$B_x = B_0 \text{Sin}[kx] \text{Exp}[-k(y_1 - y)] \quad (1)$$

$$B_y = B_0 \text{Cos}[kx] \text{Exp}[-k(y_1 - y)] \quad (2)$$

$$B_0 = B_r [1 - \text{Exp}(-kd)] \frac{\text{Sin}(\pi/M)}{\pi/M} \quad (3)$$

Here, in Equations 1 and 2, $k = 2\pi/\lambda$, where λ (m) is the wavelength of the Halbach array, y_1 (m) is the distance between the surface of the Halbach array and the location of a surface current in the track. In Equation 3, B_r (Tesla) is the remanent field of the magnetic material in the Halbach array, d (m) is the vertical thickness of the array magnets, and M is the number of magnet bars per wavelength in the Halbach array.

The magnetic field components (in 2-D approximation) from a dual-Halbach-array (Inductrack II) configuration are simply the superposition of the width-truncated 2-D fields of an upper and lower array, with width and/or thickness dimensions reflecting the particular configuration being considered. In this paper we will be mainly discussing a particular array, the so-called “(5 x 3)” array. That is, a dual array in which the upper array is 5 units wide and the lower array is 3 units wide, with both arrays having the same thickness in the vertical direction. The reason for the unequal widths of the upper and lower arrays is that in this way one achieves a partial nulling of the vertical field component so as to reduce the amount of current induced in the track (relative to the levitating (horizontal) field component when the midplane of the laminated track conductors is located midway between the upper and lower arrays, better to optimize the lift-to-drag ratio at urban speeds. At the same time the magnitude of the horizontal field is increased by the presence of the lower array, thus reducing the amount of current required to levitate a given mass per unit area.

Using Equations (1) and (2) the resultant field components for an Inductrack II magnet configuration with unequal widths of the upper and lower arrays are given by Equations 4, 5, 6, and 7. Here w_U (m) is the width of the upper array in the z direction, w_L (m) is the width of the lower array, and v (m/sec) is the velocity of the moving Halbach array.

Domain: $-(w_L/2) < z < (w_L/2)$:

$$\Sigma B_{y1} = -B_0 \{ \text{Exp}[-k(y_1 - y)] - \text{Exp}[-k(y_1 + y)] \} \text{Cos}[k(x - vt)] \quad (4)$$

$$\Sigma B_{x1} = B_0 \{ \text{Exp}[-k(y_1 - y)] - \text{Exp}[-k(y_1 + y)] \} \text{Sin}[k(x - vt)] \quad (5)$$

Domain: $-(w_U/2) < -(w_U/2)$ or $(w_L/2) < (w_U/2)$:

$$\Sigma B_{y2} = -B_0 \text{Exp}[-k(y_1 - y)] \text{Cos}[k(x - vt)] \quad (6)$$

$$\Sigma B_{x2} = B_0 \text{Exp}[-k(y_1 - y)] \text{Sin}[k(x - vt)] \quad (7)$$

Equations 4 and 5 may now be used to calculate the flux through an area equal to that of an elementary circuit of the laminated track at vertical position y_1 , and from this flux the current induced in that circuit may be determined. The equation for the time-varying flux is given by Equation 8. In this circuit-based analysis an “elementary circuit” consists of two infinitesimal-width transverse conducting strips separated by a half-wavelength and shorted at their ends by shorting means of “zero” resistance and inductance. The laminated track then consists of a stack of planar sheets, each such sheet being made up these elementary circuits so as to form the slotted surface that characterizes the laminated track

$$\begin{aligned} \phi(t) &= - \left(\frac{2B_0}{k} \right) \{ [(w_U - w_L) \text{Exp}[-k(y_1 - y)] - w_L(\text{Exp}[-k(y_1 - y)] - \text{Exp}[-k(y_1 + y)])] \} \text{Sin}[\omega t] \quad (8) \\ &= \phi_0 \text{Sin}(\omega t) \end{aligned}$$

Here $\omega = kv$ is the angular frequency of the flux generated by the moving Halbach array.

The time-varying current induced in an elementary circuit of the laminated track, given by Equation 9, is calculated from circuit theory.

$$I(t) = \frac{\phi_0}{L_c} \left[\frac{1}{1 + (R_c / \omega L_c)^2} \right] \left[\text{Sin}(\omega t) + \left(\frac{R_c}{\omega L_c} \right) \text{Cos}(\omega t) \right] \quad (9)$$

Here L_c (henrys) and R_c (ohms) are the inductance and resistance of the elementary circuit defined above.

The levitation force at $x = 0$ on an elementary circuit, F_y (Newtons), equal to the product of the x component of the magnetic field and the current, is given by Equation 10.

$$F_y = \left[(w_U - w_L) \sum B_{x2}(x = 0, y) + w_L \sum B_{x1}(x = 0, y) \right] I(t) \quad (10)$$

Similarly, the drag force, F_x (Newtons) at $x = 0$ associated with the induced current, $I(t)$, is given by the product of the y component of the magnetic field and the current as shown in Equation 11. (The additional drag force component associated with parasitic eddy currents in the conducting strips of the laminated track will be considered later.)

$$F_x = \left[(w_U - w_L) \sum B_{y2}(x = 0, y) + w_L \sum B_{y1}(x = 0, y) \right] I(t) \quad (11)$$

Inserting the definitions of the above quantities and performing a time average yields equations for the steady-state lift and drag forces on an elementary circuit. If we now consider a single sheet of the laminated track made up of these elementary circuits, with a spacing d_c (m) between the center lines of each conducting strip, we then can obtain, after some algebraic simplifications, expressions for the lift and drag forces per unit area (i.e. per m^2) on such a sheet, as given by Equations 12 and 13.

$$\frac{\langle F_y \rangle}{\text{Area}} = \frac{B_0^2 w_U}{k L_c d_c} \left[\frac{1}{1 + (R_c / \omega L_c)^2} \right] \text{Exp}[-2k(y_1 - y)] \{1 - (w_L / w_U)^2 \text{Exp}(-4ky)\} \quad (12)$$

$$\frac{\langle F_x \rangle}{\text{Area}} = \frac{B_0^2 w_U}{k L_c d_c} \left[\frac{(R_c / \omega L_c)}{1 + (R_c / \omega L_c)^2} \right] \text{Exp}[-2k(y_1 - y)] \{1 - (w_L / w_U) \text{Exp}(-2ky)\}^2 \quad (13)$$

Thus far the only significant approximation that has been made is the use of the truncated 2-D Halbach array field equations in calculating the lift and drag forces. We have also thus far left undefined the resistance and inductance terms. For the inductance of an elementary circuit embedded in an array of other circuits so as to form a sheet of the laminated track we will employ a definition of the “distributed inductance”, L_d (Henrys), as derived by Ryutov [3], employing a theoretical model based on surface currents. Thus for each leg of an elementary circuit we will assign the value given by Equation (14).

$$L_d = \frac{\mu_0 w_c}{2k d_c} \quad \text{henrys} \quad (14)$$

Here $\mu_0 = 4\pi \cdot 10^{-7}$ henrys/meter, and w_c (m) = length of the strip conductor of the elementary circuit. The total inductance of an elementary circuit is thus twice the value of L_d . When this definition is inserted into Equations 12 and 13 there results the expressions for the lift and drag forces given by Equations 15 and 16.

$$\frac{\langle F_y \rangle}{\text{Area}} = \frac{B_0^2 w_U}{\mu_0 w_c} \left[\frac{1}{1 + (R_c / \omega L_c)^2} \right] \text{Exp}[-2k(y_1 - y)] \{1 - (w_L / w_U)^2 \text{Exp}(-4ky)\} \quad (15)$$

$$\frac{\langle F_x \rangle}{\text{Area}} = \frac{B_0^2 w_U}{\mu_0 w_c} \left[\frac{(R_c / \omega L_c)}{1 + (R_c / \omega L_c)^2} \right] \text{Exp}[-2k(y_1 - y)] \{1 - (w_L / w_U) \text{Exp}(-2ky)\}^2 \quad (16)$$

We are now ready to introduce the next important approximation used to obtain the final expressions for the lift and drag forces, the equations that will be used to program the levitation code used at Livermore for modeling Inductrack II systems and to be bench-marked against the experimental results from the Laminated Track Test Rig.

To determine a value for the total lift and drag forces (except for the drag from parasitic eddy currents, to be discussed later) arising from a laminated track composed of many thin slotted sheets we will introduce the "equivalent conductor" concept. In employing this concept we first visualize a single sheet conductor located at a specific value of y within the upper and lower boundaries of the stack of laminations. The circuit inductance of this sheet is calculated using Equation 14 and its circuit resistance is the resistance value one would obtain from conductors whose width is d_c and whose thickness in the vertical direction is equal to the thickness of the laminate stack. In this way we determine lift and drag forces associated with the particular value of y that has been chosen, when exposed to the vertical flux component given by Equation 8. We then conceptually place this "equivalent conductor" at all the values of y within the laminate stack and perform an (numerical) integral-average of these values. The end result is a calculation of the total lift and drag forces that would be exerted under the assumption that the incident fields at a given y value are not appreciably perturbed by the currents induced in adjacent sheets.

The latter approximation clearly needs justification as to its domain of validity. First, if the conducting strips of each lamination are very narrow compared to a skin depth, and their thickness is also very small compared to a skin depth the presence of parasitic eddy currents in one sheet will make a negligible perturbation to the flux from the Halbach arrays passing through an adjacent sheet. Second, if the length of the conducting strips, w_c , is much greater than the widest dimension of the Halbach array, w_U , then the inductance of each elementary circuit will so limit the induced current that there will be a negligible

perturbation of the flux incident on a given lamination caused by the currents induced in laminate sheets above or below that sheet.

As it turns out, for track and Halbach array parameters of interest, and in particular for the parameters employed in the Laminated Track Test Rig, the “equivalent conductor” approximation gives results that are in good agreement with the experiment. Certainly one must always be aware of the domain restrictions on the approximations that have been made, using the more rigorous “fields-based” treatment described in other parts of this paper as a check. Nevertheless, and particularly for scoping designs and for inter-comparison of options, the fast-computing code that we have developed employing these approximations has proved to be a valuable tool.

2.2 Parasitic eddy-current losses

To complete the discussion of the 2-D levitation code as applied to the laminated track the effect of parasitic eddy-current losses in the conducting strips of the track needs to be considered. A simple derivation can be used to show that the two sources of drag losses (levitating currents and parasitic eddy currents) can be considered independently and then summed to determine the total drag.

Parasitic eddy current losses arise owing the incidence of a time-varying magnetic field normal to the surface of a conducting strip. The effect is to create a pattern of counter-flowing currents in the strip, but no net current. The eddy current losses are thus simply the ohmic losses in the conductor associated with these parasitic currents. These losses scale down rapidly (as the cube) with the width of the conducting strip in the direction normal to the field, so that this scaling provides a means for limiting the eddy current losses so that they are acceptably small.

The expression for the parasitic eddy current losses in Watts/meter length of a conducting strip with a width $w(m)$, a thickness, $t(m)$ and a resistivity, ρ (ohm-meters), when exposed to a time varying magnetic field, B , incident normal to the “ w ” face is given by Equation (17).

$$\frac{P}{\text{length}} = \frac{1}{24} \frac{\omega^2 B^2 t w^3}{\rho} \quad \text{Watts/meter} \quad (17)$$

This expression was programmed into the Laminated Track Levitation Code, using the same truncated 2-D fields employed to calculate lift and drag. The (weaker) perpendicular field is, of course, incident normally on the conducting strips of the track, while the (stronger) horizontal field component is incident on the thickness dimension of the strip, which is therefore made much thinner than the width of the conducting strips.

2.3 Check of the validity of the use of truncated 2-D fields in the levitation code

In order to estimate the errors associated with the use of truncated analytic 2-D functions for the representation of the real 3-D fields from the Halbach arrays another code was written, again using the Mathematica® platform. The ability of that platform to handle complicated double integrals analytically allowed the programming, analytically, of the magnetic field components of a rectangular bar magnet

polarized at an arbitrary angle transverse to a reference face, and located at an arbitrary position on a reference plane. Then using this analytic representation a Halbach array of arbitrary order and physical dimensions can be built up. The end result: a very fast-computing code that can be used to determine the field components, at an arbitrary location, from Inductrack I or Inductrack II configurations. Other than the assumption of fixed Amperian currents to represent the permanent-magnet bar fields and the use of the Biot-Savart law in calculating the fields from the bars no simplifications or approximations were used.

In exercising the 3-D field code and comparing its computed fields with those determined using the 2-D analytic formulation of Halbach there were some pleasant surprises. In the context of an Inductrack system that uses a laminated track that is wider than the width of the Halbach array (as would be the case in most practical applications), the effect of the “fringing fields” produced by the Amperian currents flowing transversely at the ends of each Halbach array bar is to compensate, very nearly, for the fall-off of the field occurring upon approaching the edges of the Halbach arrays that are perpendicular to the direction of motion down the track. Also, the decrease in field (relative to the truncated 2-D analytic field) observed in the front and back ends of the array is relatively small. Figure 1 illustrates this latter point, a plot of B_z vs x , at a distance of .0225 m. from the upper array, for an $M=8$, “(5 x 3),” dual Halbach array with the following magnet parameters:

Remanent field	1.4 Tesla
Number of magnet bars per array	25
Length of upper magnet bars	0.25 m.
Length of lower magnet bars	0.15 m
Height of bars	0.025 m.
Width of bars	0.025 m.
Wavelength of $M=8$ Halbach arrays	0.4 m

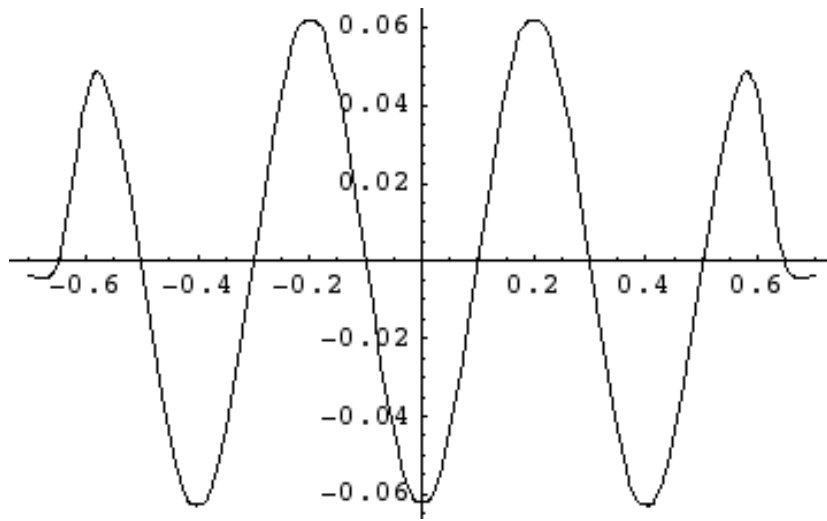


Figure 1: Plot of calculated B_z as a function of x for $z = 0$ and gap (y) = .035 m.

Note that of the seven maxima in B_z , five of the maxima have essentially full amplitude. Also note that the array that was calculated is shorter in the longitudinal (x) direction than arrays, such as those used in the General Atomics designs [2] so that in those designs these end effects would be even further reduced.

When a “(5 x 3)” configuration was modeled the 3-D code yielded very useful information on the question: How well does the 2-D levitation code model reality? A test of this reality is to compare the value of the integrals, in the transverse direction, of the peak B_z and peak B_x values, and then compare these values with those calculated by multiplying the 2-D component by the width of the Halbach arrays. To take into account the (here) helpful effect of the 3-D fringing fields the integrations are carried out for a distance on each side of the Halbach array equal to 50 percent of the transverse width of the array. It is to be expected that in most applications of the laminated track the slots will be at least as wide as the width over which the integrations were performed. Table I summarizes the comparisons just described.

Table I

Integral of B_z (peak) <u>vs</u> z , for $-w < z < w$:	0.1068 Tesla-meters
Product of B_z (2-D, peak) and w	0.1071
Integral of B_x (peak) <u>vs</u> z , for $-w < z < w$	0.1044
Product of B_x (2-D, peak) and w	0.1071

As can be seen from the table these pairs of evaluations (which are representative of the inducing flux and the levitating force) differ by only a percent or two. Also encouraging is the fact that the peak fields themselves, i.e. those located midway between the sides of the array and at a maximum in the x direction, differ by less than a percent from the 2-D-calculated value.

To illustrate the type of detail that the 3-D is capable of providing, Figure 2 is a 3-D plot produced by the code showing the magnitude of the B_z field component midway between the upper and lower Halbach arrays of a “(5 x 3)” Inductrack II, $M = 8$, configuration made up of magnet bars with the dimensions given above.

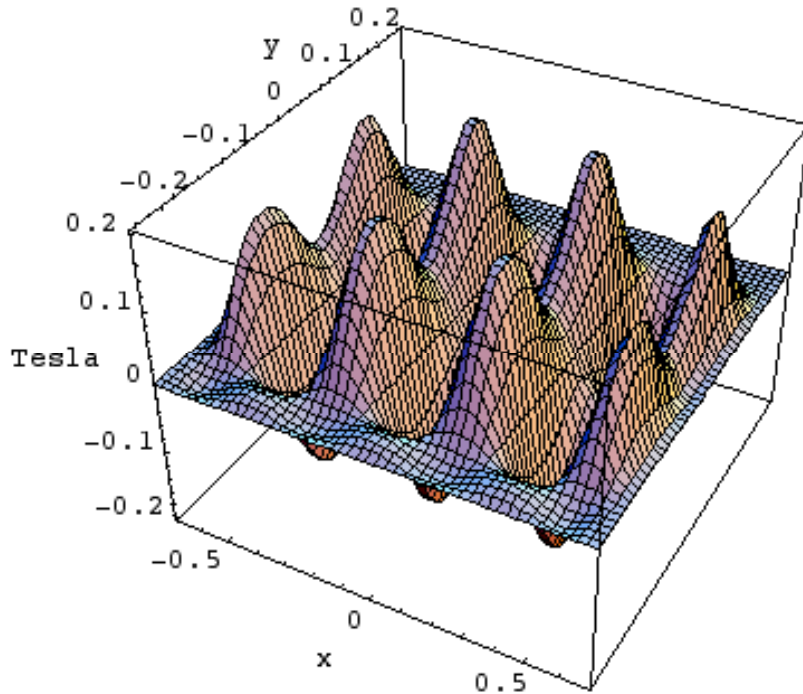


Figure 2: 3-D plot of magnitude of B_z at midplane of a $M=8$, “5 x 3” Inductrack II array

We conclude, based on the comparisons given above, that as far as the integrated magnetic fields are concerned, the lift and drag forces calculated using the 2-D truncated values should differ little, in typical cases, from the 3-D values calculated from first principles.

3 Laminated Track Test Rig

The Livermore Laminated Track Test Rig was designed and built to provide an experimental check on the laminated-track computer code calculations and to help build a data base for designing a laminated track system. The use of this rig enables making measurements, as a function of velocity, of the lift, drag, and stiffness coefficients of a laminated track interacting with both single (Inductrack I) and double Halbach array (Inductrack II) configurations. In the test rig a section of laminated track is pulled (on precision guide rails) through a Halbach array assembly and mount that is instrumented to measure the lift and the drag forces. The critical dimensions of the test rig, i.e., wavelength of the Halbach arrays, and the thickness of the laminated track, are scaled down by a factor of four from a full-size system. As a result the data that are taken can be extrapolated to a full-size system by using known scaling laws. By moving the track instead of the Halbach arrays, and by using pressure sensors with near-zero displacement under

load, all inertial and displacement-sensitive corrections to the forces are eliminated, simplifying data reduction and improving the experimental accuracy.



Figure 3: Test rig

Figure 3 is a photograph of the test rig, showing the assembly that holds the Halbach array and the vertical force sensor, together with the carrier for the laminated track elements, propelled through the Halbach arrays by a gravity-driven pulley-and-weight system (not shown).

The track itself is made up of a stack of 0.5 mm thick copper sheets. The sheets are 20 cm. wide and the slots in the sheet are 15 cm. wide, leaving “shorting” strips at each end that are 2.5 cm. in width. The slots, made by chemical etching, using printed circuit techniques, are 0.5 mm wide, and the thus-formed strip conductors between them are 2.5 mm. wide. For the measurements reported here the laminate stack was 10 sheets thick. Longitudinally the track was made of three such stacks, each approximately 75 cm. long. The stacks were butted together at their ends but no provision was made for longitudinal electrical conduction continuity of the track at the butt joints.

The stacks were mounted on a carrier “cart” that was equipped with v-grooved rollers that were captured between precision-ground guide rails, insuring accurate vertical and horizontal positioning of the cart. Since the peak forces exerted by the Halbach arrays on the track were large (100 kilograms or more) the rollers were spaced at many locations along the cart and additional support against vertical displacements was provided by rubber-tired rollers located so as to engage the cart as it passed through the Halbach-array mounting structure. Even with these precautions local deflections of a fraction of a millimeter occurred in some situations, leading to measurement errors that were, however, deemed to be acceptably small upon analysis of the data and the computer-code results.

As previously noted, the choice to move the track under stationary Halbach arrays rather than vice-versa was based on the consideration that the force measurements could be made without any influence from inertial effects, since “zero-displacement” force sensors could be used. Based on previous experience our choice was to use spring-loaded hydraulic pistons equipped with solid-state pressure sensors for the force measurements. To measure the velocity of the track as it moved through the Halbach array assembly we employed a tachometer generator attached to a rubber-edged wheel that engaged the edge of the cart as it moved by. Both systems worked well in the experiments.

The track was propelled through the Halbach arrays by a flexible stainless-steel cable that was tensioned by a gravity-driven pulley-and-weight system. The design of the drive system was based on a simple analytical formula for such systems. In order to achieve adequate acceleration, i.e., to accelerate the cart (weight about 50 kilograms), to velocities of order 10 meters/second in the available distance of 4 meters, accelerations of order 1.0 g are required. As the analysis showed, accelerations this high can only be obtained in a gravity-driven system by using a multi-cable system, in our case a four-pulley, four-cable system. The driver weight consisted of a stack of lead bricks loaded onto a carrier attached to the end of the steel cable.

The equation governing the velocity achieved by the load mass, M_L after an acceleration distance of s_L (meters) is the familiar one given by Equation (18).

$$v_s = \sqrt{2a_L s_L} \quad \text{meters / sec ond} \quad (18)$$

The acceleration term, a_L (m/sec.^2) is determined by the driving mass, M_d , the load mass, M_L , and the number of supporting cables, N , of the pulley and weight system. Defining the ratio $M_d/M_L = K$, the acceleration is given by Equation (19).

$$a_L = \frac{K / N}{1 + K / N^2} g \quad \text{meters / sec.}^2 \quad (19)$$

In setting up the system a calibration run was made to compare the measured cart velocities with those predicted by Equations (18) and (19). Figure 4 is a plot of the results of this run, showing good agreement between the theory and the measured velocity.

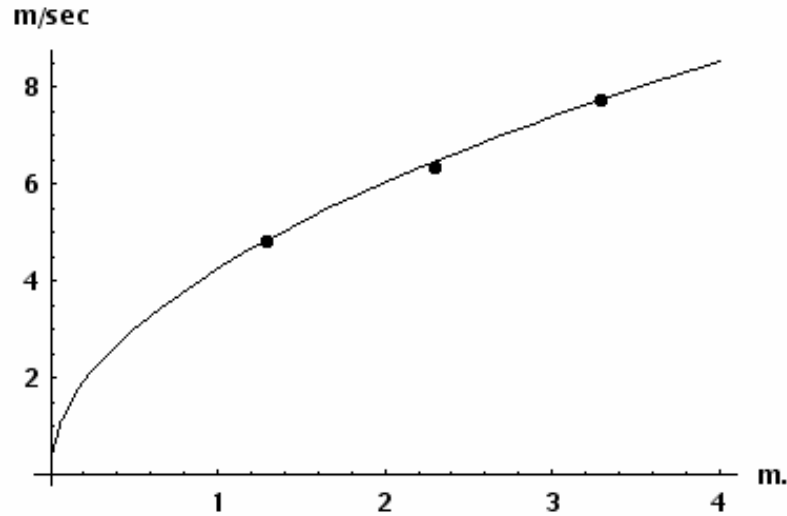


Figure 4: Comparison between theoretically predicted cart velocity and tachometer-wheel velocity measurements. Cart mass = 45 kg., driver mass = 220 kg. ($K = 4.9$). Axes: x (starting point in meters); y (velocity, m/sec).

We report here the results of measurement of a "(5 x 3)," $M = 4$, array made up of blocks of NdFeB magnet material ($B_r = 1.2$ Tesla) with dimensions 2.5 cm x 2.5 cm x 1.25 cm. The wavelength of the Halbach arrays was 10 cm. and the length of the array in the x direction was 4.0 wavelengths (plus a slight overhang at each end to partially compensate for end effects).. The width of the upper array was 5.0 cm and that of the lower array was 3.0 cm. The gap between the upper and lower arrays was 3.5 cm.

Figure 5 and 6 show comparison plots between the lift and drag force as calculated by the Livermore levitation code (based on the 2-D and other approximations discussed above) and the results from the Laminated Track Test Rig. In the plots the upper and lower curves shown bracketing the middle plotted curve represent the effect of a displacement of 1.0 mm up or down relative to the nominal gap position. The plots pointed are the results of measurements taken at different speeds of transit of the track through the Inductrack II dual Halbach array. The scatter of data observed, corresponding to a fraction of a mm of displacement, are of the order of that reasonably could be expected to arise from vibrational displacements and track fabrication inaccuracies.

On the basis of the above comparisons, and others made with different Halbach array configurations (to be reported at a later time), we conclude that the 2-D-based code is capable of giving predictions that can be employed in performing design studies of full-scale laminated track systems. The code should therefore be useful for such purposes when backed up by calculations made using the rigorous treatment described in Section 4 of this paper.

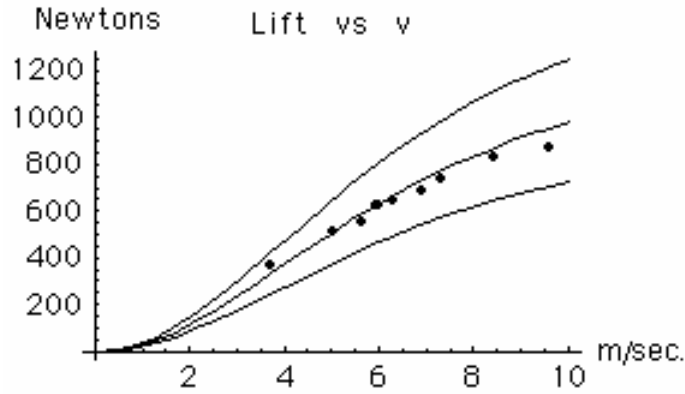


Figure 5: Comparison between lift force predictions of the Livermore 2-D levitation code and measurements made with the Livermore Laminated Track Test Rig performed on a 5 x3 Inductrack II Halbach array configuration.

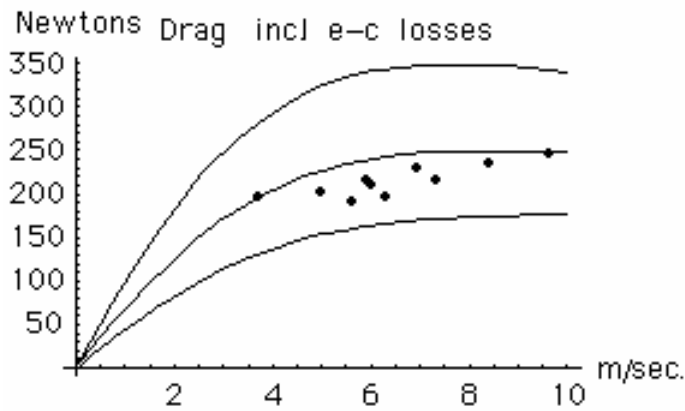


Figure 6: Comparison between drag force predictions of the Livermore 2-D levitation code and measurements made with the Livermore Laminated Track Test Rig that were performed on a 5 x3 Inductrack II Halbach array configuration.

4 Fields-based analytic description

We describe here an analytic model that, in contrast to the “circuits-based” description of Section 2, is developed directly in terms of the 3-D fields of the permanent magnets, along with 2-D fields from the induced currents in the individual laminations of the track. This model differs from the circuits-based model in two ways: (1) it uses a Fourier analysis of the 3-D source fields in the direction of vehicle motion, with retention of the first Fourier component, to explicitly determine the nature of the “2 ½ -D” approximation, and (2) it accounts directly for the mutual coupling between the laminations by including contributions to the fields that penetrate and interact with each lamination in the matrix equation that governs the induced currents.

The fields-based model shown in Figure 7 describes the mutual coupling between upper and lower Halbach arrays and any number (3 are shown in the figure) of passive conducting layers between the two sources.

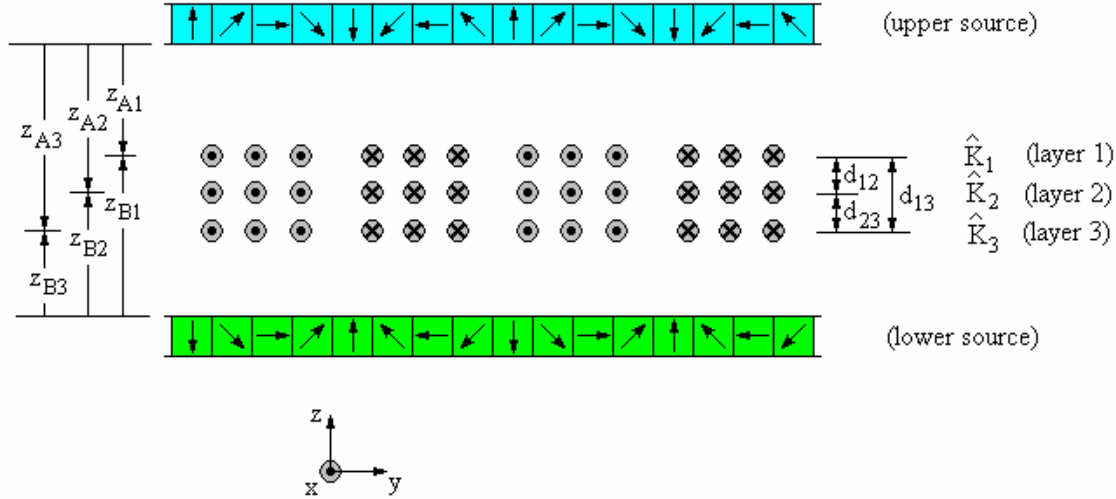


Figure 7: A model that accounts for 2-dimensional induced currents in laminations, including mutual coupling, and 3-dimensional source fields.

In a simple 2-dimensional model, the source fields as well as the fields due to induced currents in the laminations take the form of traveling waves. However, in order to account for the transverse (3-dimensional) structure of the source fields, we use the fundamental Fourier component of the source fields at each transverse (x) position, and integrate these Fourier components over the track width to find the total source flux that passes through each lamination.

Figure 8 shows longitudinal (y) and vertical (z) components of the source magnetic flux density over a plane within one lamination for the double Halbach array that is 5 magnets wide in the upper array and 3 magnets wide in the lower array, as described in Section 2. The components on the left in Figure 8 are calculated on the basis of superimposing contributions from individual magnet cubes in the arrays, using either a magnetization current or magnetization charge methodology [4]. The components on the right are based upon retaining only the first term in a Fourier series representation of the fields at each widthwise (x) position. The first Fourier component provides a relatively accurate description of the source field structure, including widthwise variations, in a form that is amenable to a sinusoidal steady state phasor analysis of the resultant induced currents in the laminations.

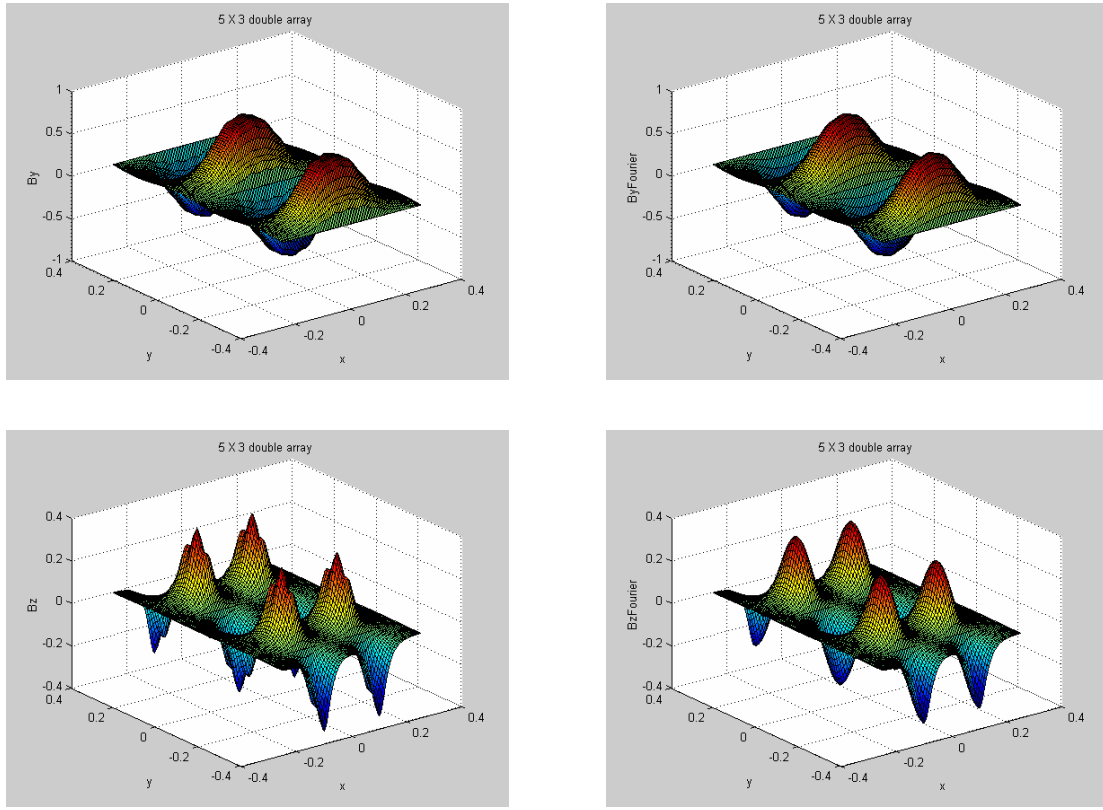


Figure 8: Longitudinal (top) and vertical (bottom) magnetic field components as calculated from individual magnet cube contributions (left) and only first Fourier component at each widthwise position (right).

A self-consistent description of the induced currents in the laminations, including mutual coupling, is accomplished as follows:

With the source wavelength denoted λ and with the velocity of the source relative to the track denoted v , the induced current in each layer is described by as a surface current that takes the form of a traveling wave:

$$\bar{K} = \bar{i}_x \operatorname{Re} \left\{ \hat{K} \exp \left[j \frac{2\pi}{\lambda} (vt - y) \right] \right\}. \quad (20)$$

Each lamination contributes fields above and below itself that have a Laplacian character, with exponential decays in the vertical direction based upon wavelength in the longitudinal direction.

The 2-dimensional descriptions of currents and fields are quite accurate, because the thin, slotted laminations force induced currents to take this form over most of their widths – it is only at the outside edges of the laminations beyond the slots that the current paths become more complicated, and even there, they have no vertical components.

Faraday’s Law governs induced currents in each lamination, and is written for a rectangular contour that is one-half wavelength long. In the sinusoidal steady state, the following complex amplitudes describe the coupling between physical variables at the vertical position of any one lamination:

- \hat{E}_x : widthwise induced electric field
- $\hat{\Lambda}_A$: total flux from upper array that passes through contour
- $\hat{\Lambda}_B$: total flux from lower array that passes through contour
- $\hat{\Lambda}_{self}$: total flux from induced current in lamination being described
- $\sum \hat{\Lambda}_a$: total flux from laminations above lamination being described
- $\sum \hat{\Lambda}_b$: total flux from laminations below lamination being described

Using ℓ to denote the width over which induced currents circulate and p to denote the “packing fraction” in the longitudinal direction of conducting strips with interspersed slots in each lamination, we write Faraday’s Law:

$$2\ell\hat{E}_x = -j\omega\left[\hat{\Lambda}_A + \hat{\Lambda}_B + p\left(\hat{\Lambda}_{self} + \sum \hat{\Lambda}_a + \sum \hat{\Lambda}_b\right)\right] \quad (21)$$

where, for laminations with conductivity σ and thickness Δ , the complex amplitudes of induced electric field and surface current density are related by:

$$\hat{E}_x = \frac{\hat{K}_x}{\sigma\Delta} \quad (22)$$

Writing the fluxes through each rectangular loop in terms of the surface currents that serve as their sources, we form a system of self-consistent equations that determine the induced surface current densities, with source terms that are based upon integrals over the track width of the array field complex

amplitudes. The solution involves the product of the source frequency $\omega = 2\pi\frac{v}{\lambda}$, based upon the

vehicle velocity and wavelength, with a magnetic diffusion time defined by $\tau_m = \frac{\mu_0\sigma\Delta\lambda}{4\pi}$.

The system of equations takes the form:

$$\begin{bmatrix}
\left(1 + \frac{1}{j\omega p \tau_m}\right) & e^{-kd_{12}} & e^{-kd_{13}} & \dots \\
e^{-kd_{12}} & \left(1 + \frac{1}{j\omega p \tau_m}\right) & e^{-kd_{23}} & \dots \\
e^{-kd_{13}} & e^{-kd_{23}} & \left(1 + \frac{1}{j\omega p \tau_m}\right) & \dots \\
\dots & \dots & \dots & \dots
\end{bmatrix}
\begin{bmatrix}
\hat{K}_1 \\
\hat{K}_2 \\
\hat{K}_3 \\
\dots
\end{bmatrix}
= \frac{j2}{p\ell}
\begin{bmatrix}
\int_{-\ell/2}^{\ell/2} \hat{H}_z^A(x, z_{A1}) dx + \int_{-\ell/2}^{\ell/2} \hat{H}_z^B(x, z_{B1}) dx \\
\int_{-\ell/2}^{\ell/2} \hat{H}_z^A(x, z_{A2}) dx + \int_{-\ell/2}^{\ell/2} \hat{H}_z^B(x, z_{B2}) dx \\
\int_{-\ell/2}^{\ell/2} \hat{H}_z^A(x, z_{A3}) dx + \int_{-\ell/2}^{\ell/2} \hat{H}_z^B(x, z_{B3}) dx \\
\dots
\end{bmatrix}
\equiv \frac{j2}{p\ell}
\begin{bmatrix}
\hat{I}_z^1 \\
\hat{I}_z^2 \\
\hat{I}_z^3 \\
\dots
\end{bmatrix}
\quad (23)$$

After the induced currents are determined by solving these matrix equations, the time-averaged forces on the sources are computed.

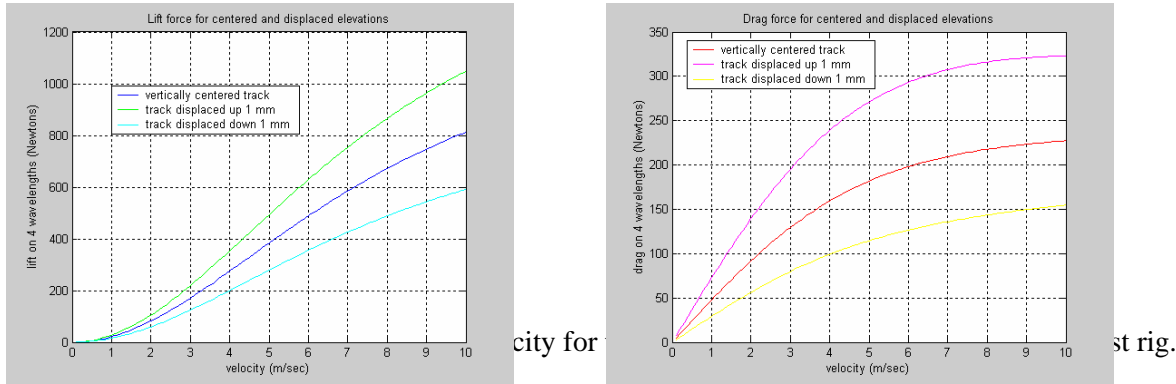
The time-averaged lift force per wavelength is:

$$L_\lambda = -\frac{\mu_0 \lambda p}{2} \sum_i \operatorname{Re} \left\{ \int_{-\ell/2}^{\ell/2} \hat{K}_i^* \left[\hat{H}_y^A(x, z_{Ai}) + \hat{H}_y^B(x, z_{Bi}) \right] dx \right\} \equiv -\frac{\mu_0 \lambda p}{2} \sum_i \operatorname{Re} \left\{ \hat{K}_i^* \hat{I}_y^i \right\} \quad (24)$$

and the time-averaged drag force per wavelength is:

$$D_\lambda = -\frac{\mu_0 \lambda p}{2} \sum_i \operatorname{Re} \left\{ \int_{-\ell/2}^{\ell/2} \hat{K}_i^* \left[\hat{H}_z^A(x, z_{Ai}) + \hat{H}_z^B(x, z_{Bi}) \right] dx \right\} \equiv -\frac{\mu_0 \lambda p}{2} \sum_i \operatorname{Re} \left\{ \hat{K}_i^* \hat{I}_z^i \right\} \quad (25)$$

Application of this methodology to the LLNL laminated track test rig produces lift and drag as functions of vehicle velocity as shown in Figure 9 for track positions that are centered and displaced by 1 mm up and down with respect to the upper and lower portions of a “5 X 3” double Halbach array. The curves are in excellent agreement with the LLNL experimental measurements, and with the LLNL “circuits based” model.



5 Acknowledgements

The work of one of the authors (RFP) was performed under the auspices of the U. S. Department of Energy at the University of California Lawrence Livermore National Laboratory under contract W-7405-Eng-48.

This work was supported in part by the U.S. Department of Transportation, Federal Transit Administration Office of Technology, through General Atomics, under Cooperative Agreement No. CA-26-7025.

6 References

- [1] K. Halbach, Nucl. Inst. and Methods, **187**, 109 (1981)
- [2] S. Gurol, B. Baldi, R. F. Post, “Overview of the General Atomics Low Speed Urban Maglev Technology Development Program,” Proceedings of 17th International Conference on Magnetically Levitated Systems and Drives – “Maglev 2002,” Sept. 3-5, 2002, Lausanne, Switzerland
- [3] R. F. Post, D. D. Ryutov, “The Inductrack Concept: A New Approach to Magnetic Levitation,” Lawrence Livermore National Laboratory report UCRL-ID-124115. May 1996.
- [4] J. F. Hoburg, “Modeling Maglev Passenger Compartment Static Magnetic Fields from Linear Halbach Permanent Magnet Arrays,” *IEEE Transactions on Magnetics*, **40**, 1, January, 2004.

Appendix D

ATP and Speed/Position Sensing System

Overall System Architecture

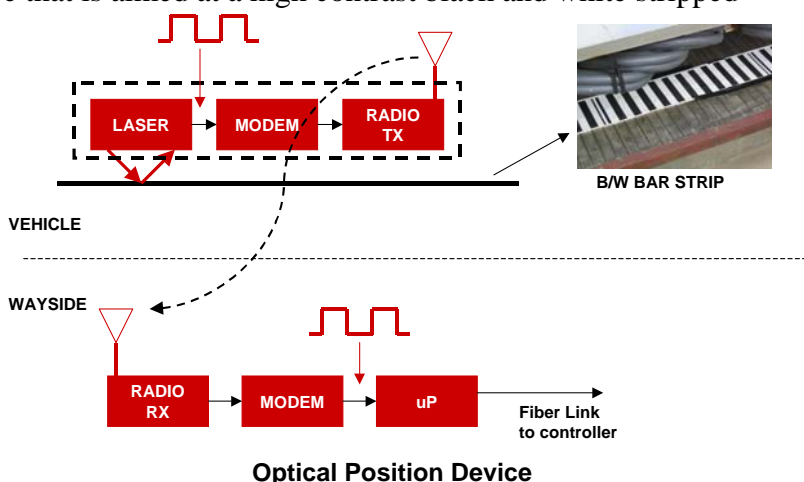
US&S supplied the Speed/Position Sensing System and Automatic Train Protection (ATP) for the test track located at General Atomics. This document reviews these two subsystems.

Speed/Position Sensing System

This subsystem consists of two major components: Vehicle and Wayside. The vehicle accommodates a LASER device that is aimed at a high contrast black and white striped tape located on the Litz-wire levitation track.

The LASER monitors the black and white transitions of the optical tape.

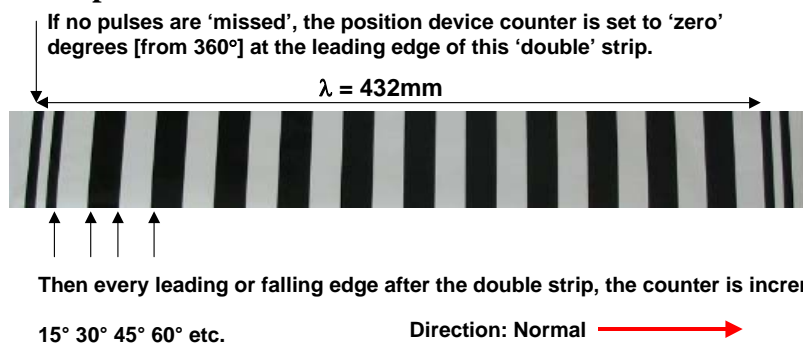
These transitions are transmitted back to the central control room via a modulated 450 MHz, NBFM radio.



Optical Position Device

In the control room, a special controller counts these pulses and processes them. The information calculated represents angle and location, using the leading edge of the lead magnet as a reference point. This information is passed on to the Inverter Controller by a high-speed optical serial link.

The Optical Tape



The 'double markers' are also detected to indicate the start of each wavelength (432 mm) associated with the magnets. The width of each black and white strip is 18 mm.

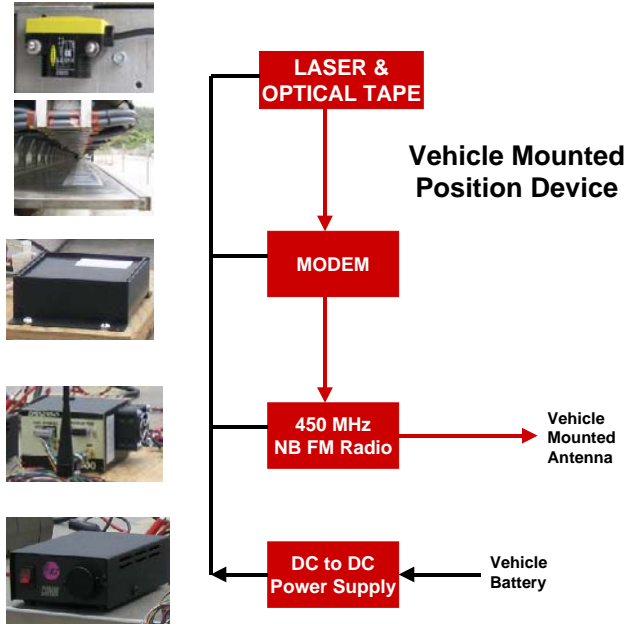
Vehicle's Components

The Vehicle components of the position device are shown in the figure to the right.

The LASER is mounted on the structure that houses the vehicle's levitation magnets. The output of the LASER is a variable frequency square wave that is fed to the input of a MODEM.

The output of the MODEM is fed to the input of the digital radio and modulates the NBFM, 450 MHz digital signal.

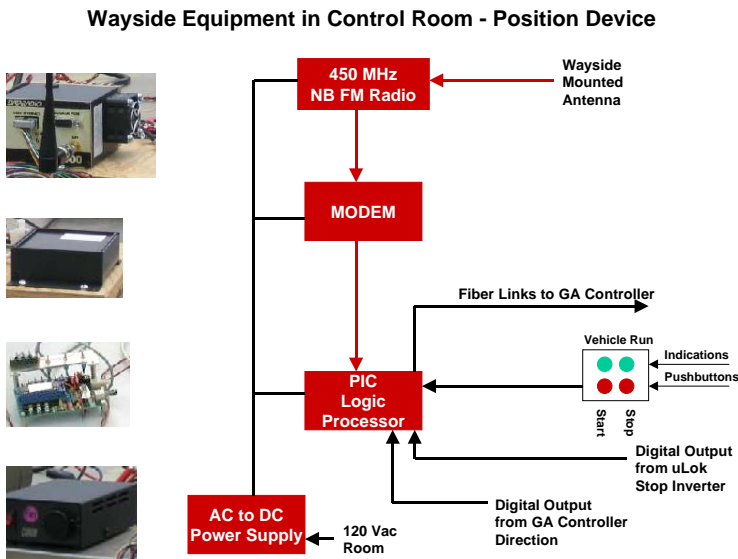
The vertical differential range over which the LASER can respond is 30 mm.



A DC to DC converter is employed to supply the power for the LASER, MODEM and digital radio.

Wayside Components

The figure below is a block diagram of the wayside components of the position device.



The data transmitted from the vehicle is received in the control room via the 450 MHz data radio. The output of data radio is an input to a MODEM.

The output of the MODEM is then fed to the input of the PIC processor device.

The PIC processor performs the calculations associated with the data and passes the results to

the inverter controller.

To take advantage of the serial link, special digital inputs are sensed by the PIC's physical I/O (i.e. start and stop the inverter). These digital data bits are passed onto the inverter controller via the PIC processor.

Position Device Summary

The position sensor is fully functional and satisfies the performance requirements agreed upon by US&S and General Atomics. The position sensor was tested as part of the closed-loop inverter control system. As a result of this testing, it has been determined that the 18 mm resolution afforded by the existing optical tape layout is sufficient for stable vehicle startup and levitation. The minimum resolution (maximum tape segment width) for satisfactory operation is not known at this time, but will be evaluated as part of ongoing testing conducted by General Atomics.

Automatic Train Protection (ATP)

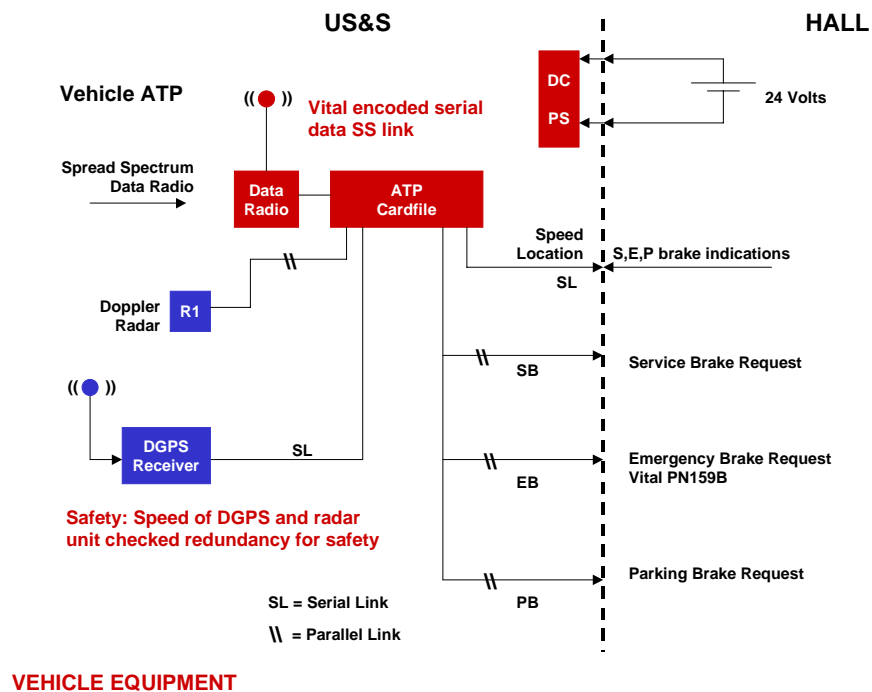
This subsystem consists of two major components: The Vehicle and the wayside.

Vehicle

The figure to the right is a block diagram of the vehicle's ATP subsystem.

The primary function of the ATP is to request emergency braking if the vehicle violates a fixed maximum speed or location profile on the test track.

The ATP interfaces to the vehicles emergency and service braking devices.



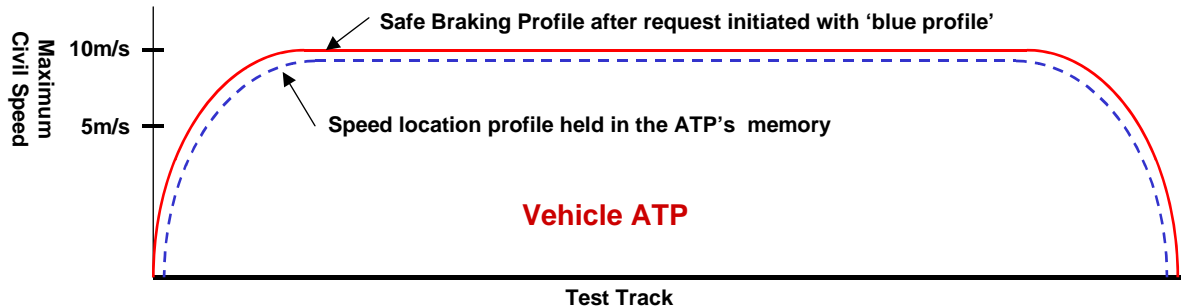
The ATP, using a Doppler Radar unit, calculates the speed of the vehicle. The ATP, using data from the radar unit, calculates the location of the vehicle.

The ATP initializes its location on the test track using a differential global positioning system (DGPS). This DGPS receiver together with a digital map stored in the memory of the ATP, together with the Doppler Radar unit determines if the vehicle is below the maximum permitted speed-location profile.

The vehicle ATP transmits its location and speed to the Microlok wayside unit via a Spread Spectrum data radio. In addition, the ATP unit can process a request from the central control room for an emergency brake application.

Summary of Profile

The diagram below summarizes the maximum civil speed profile.



The Carborne ATP would have this maximum civil speed profile in its memory. If at any time the vehicle 'bumps' the maximum speed profile (blue curve), emergency brakes are requested and a message is sent to Microlok (via SDR) to 'power down' the inverter. Microlok in turn request the inverter shut down via the position device.

As long as the speed of the vehicle is below the maximum civil speed profile, the vehicle's ATP would not request emergency braking or the inverter to be shut down.

The ATP communicates its speed and location to the wayside Microlok unit via the SS data radio. If this data link is interrupted for more than 2 seconds, the ATP requests emergency braking.

Note: The 'time/distance' displacement of the 'blue and red curve' is a function of the response time of the Carborne ATP, error associated with the DGPS, time response of the request for emergency braking, and the 'net deceleration' generated.

The Carborne ATP knows its speed via the Doppler Radar unit and DGPS. The ATP calculates its location using the pulses from the radar. The speed and distance measurement system of the ATP is independent of the wayside position device. The ATP communicates its speed and location to the wayside Microlok unit via the SS data radio.

The ATP employs a DGPS to know its location on the guideway at all times.

Initial Power UP of the vehicle: With the initial vehicle power up, the Carborne ATP does not know where it is on the guideway. It obtains its initial position after several seconds via the DGPS receiver. Once the location is known by the ATP, emergency brakes are released.

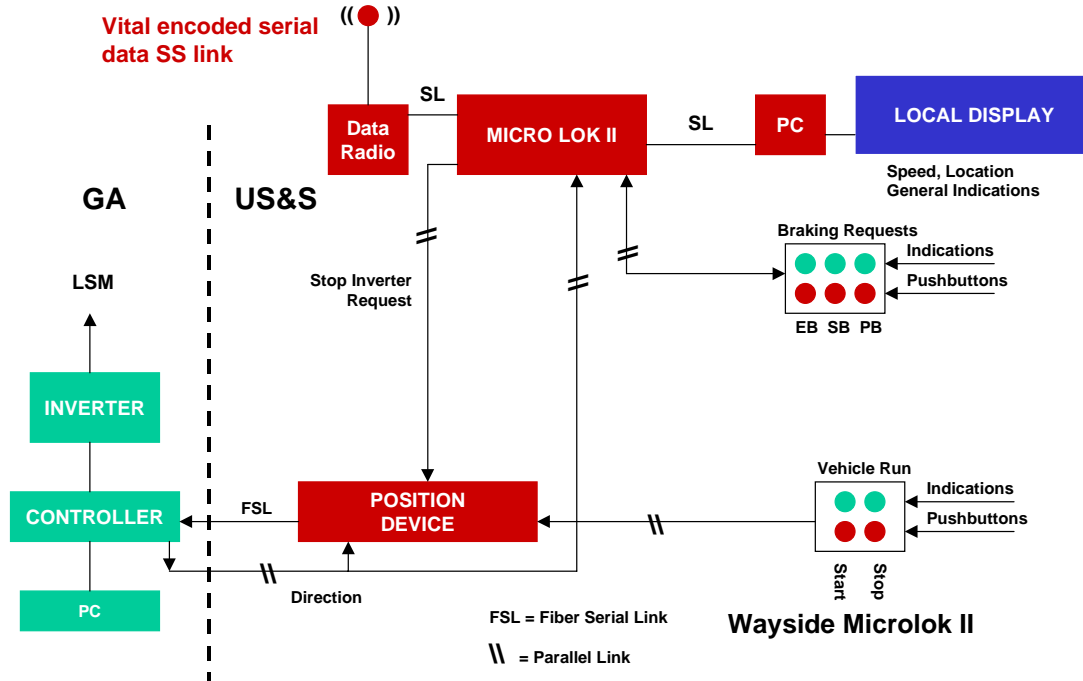
If power is removed from the ATP unit, the ATP unit fails, etc, the ATP removes energy from the emergency brake relay. This in turn opens the contacts of this relay and requests emergency brakes. The Carborne ATP must be re-initiated in terms of location.

Direction of movement is obtained from Microlok II via the SS data radio

From the Control Room, requests for emergency, Service and/or Parking brake applications can be initiated. This request information is via the SS data radio.

Wayside

The figure below illustrates the block diagram of the wayside ATP equipment located in the central control room.



Microlok II is a Vital Certified Safety Processor for Logic Control

The chart below illustrates a summary of the functionality of the wayside ATP subsystem.

Wayside Microlok II Summary

The speed and location of the vehicle is known to Microlok II because of the data radio link between the vehicle's ATP and Microlok II. The speed and location of the vehicle is displayed on the local control room's flat panel display.

Microlok II requests that the inverter be shut down via the interface between Microlok II and the Position Device. This request to shut down the inverter is initiated via the ATP Carborne unit.

Microlok II also interfaces to the three push buttons in the control room that request the vehicle's service brake, parking brake and emergency brake be applied.

Microlok II interfaces to the position device to pass information concerning the direction to the Carborne ATP via the SDR.